Experimental and Theoretical Analyses of the Load Sequence Effects on Fatigue Crack Growth Resistance

Final Progress Report

Prepared for

Office of Naval Research
800 North Quincy Street
Arlington, VA 22217-5660
Attn: Dr. A.K. Vasudevan

By

D. Kujawski, Ph.D., D.Sc. (Professor)
V. Goswami (Graduate student)
Western Michigan University
Department of Mechanical and Aeronautical Engineering
Kalamazoo, MI 49008

DISTRIBUTION STATEMENT A
Approved for Public Release
Distribution Unlimited

December 2004

20050112 060

REPORT DOCUMENTATION PAGE

Form Approved
OMB No. 0704-0188

The public reporting burden for this collection of information is estimated to average 1 hour per response, including the time for reviewing instructions, searching existing data sources, gathering and maintaining the data needed, and completing and reviewing the collection of information. Send comments regarding this burden estimate or any other aspect of this collection of information, including suggestions for reducing the burden, to Department of Defense, Washington Headquarters Services, Directorate for Information Operations and Reports (0704-0188), 1215 Jefferson Davis Highway, Suite 1204, Arlington, VA 22202-4302. Respondents should be aware that notwithstanding any other provision of law, no person shall be subject to any penalty for failing to comply with a collection of information if it does not display a currently valid OMB control number.
PLEASE DO NOT RETURN YOUR FORM TO THE ABOVE ADDRESS.

1. REPORT DATE *(DD-MM-YYYY)*	2. REPORT TYPE	3. DATES COVERED *(From - To)*
14-12-2004	Final	July 1, 2001- Sept. 30, 2004

4. TITLE AND SUBTITLE
Experimental and Theoretical Analyses of the Load Sequence Effects on Fatigue Crack Growth Resistance

5a. CONTRACT NUMBER
N00014-01-1-0952

5b. GRANT NUMBER

5c. PROGRAM ELEMENT NUMBER

6. AUTHOR(S)
Kujawski, Daniel and Goswami, Virender.

5d. PROJECT NUMBER

5e. TASK NUMBER

5f. WORK UNIT NUMBER

7. PERFORMING ORGANIZATION NAME(S) AND ADDRESS(ES)
Western Michigan University
1903 W Michigan Ave
Kalamazoo, MI 49008

8. PERFORMING ORGANIZATION REPORT NUMBER

9. SPONSORING/MONITORING AGENCY NAME(S) AND ADDRESS(ES)
Dr. Asuri K. Vasudevan (Technical Representative)
Office of Naval Research
Ballston Centre Tower One
800North Quincy Street
Arlington VA 22217-5660

10. SPONSOR/MONITOR'S ACRONYM(S)

11. SPONSOR/MONITOR'S REPORT NUMBER(S)

12. DISTRIBUTION/AVAILABILITY STATEMENT

DISTRIBUTION STATEMENT A
Approved for Public Release
Distribution Unlimited

13. SUPPLEMENTARY NOTES

14. ABSTRACT

Modeling of the fatigue crack propagation based on damage accumulation process ahead of the crack tip has been developed, which utilizes stress and strain distribution ahead of the crack tip, estimated using Rice and elastic solutions. The methodology is based on the use of both Kmax and DK as contributing parameters to the driving force and damage accumulation. Weight function approach has been adopted to determine the Kres profile. Load interaction and overload effects have been modeled by the effect of Kres on the Kmax and DK. The predictions of the present approach have been compared to experimental data and reasonable agreement has been found.

15. SUBJECT TERMS
Crack propagation, damage accumulation, load ratio effects, overload, load interaction effects, residual stresses.

16. SECURITY CLASSIFICATION OF:			17. LIMITATION OF ABSTRACT	18. NUMBER OF PAGES	19a. NAME OF RESPONSIBLE PERSON
a. REPORT	b. ABSTRACT	c. THIS PAGE			19b. TELEPHONE NUMBER *(Include area code)*
UU	SAR			149	

EXPERIMENTAL AND THEORETICAL ANALYSES OF THE LOAD SEQUENCE EFFECTS ON FATIGUE CRACK GROWTH RESISTANCE

Summary

Modeling of the fatigue crack propagation based on damage accumulation process ahead of the crack tip has been developed, which utilizes stress and strain distribution ahead of the crack tip, estimated using Rice and elastic solutions. The methodology is based on the use of both K_{max} and ΔK as contributing parameters to the driving force and damage accumulation. Weight function approach has been adopted to determine the K_{res} profile. Load interaction and overload effects have been modeled by the effect of K_{res} on the K_{max} and ΔK. The predictions of the present approach have been compared to experimental data and reasonable agreement has been found.

TABLE OF CONTENTS

LIST OF TABLES vi

LIST OF FIGURES vii

1.0 INTRODUCTION 1

1.1. CHARACTERISTICS OF FATIGUE. 3

1.2. PHYSICAL NATURE OF FATIGUE DAMAGE. 4

1.3. FEATURES OF A FATIGUE CRACKED SURFACE 5

1.4. STRESS FIELDS AHEAD OF CRACK TIP 7

1.5. MEASUREMENT OF FATIGUE BEHAVIOR OF MATERIALS 9

1.6. CRACK GROWTH RATE CURVE 11

2.0 LITERATURE REVIEW 13

2.1. CRACK-TIP FAILURE CRITERIONS 15

2.2. DAMAGE ACCUMULATION 20

2.3. EFFECT OF APPLIED R-RATIO ON FATIGUE CRACK GROWTH 23

2.4. CONCEPTS FOR CORRELATION OF R-RATIO EFFECTS 25

2.5. DRAWBACKS OF THE CRACK CLOSURE METHODOLOGY 29

2.6. TWO PARAMETER (K_{max} and ΔK) UNIFIED APPROACH 35

Table of Contents-Continued

3.0 SCOPE OF THE WORK 37

4.0 STRESS AND STRAIN DISTRIBUTION AHEAD OF THE CRACK TIP 39

5.0 FAILURE CRITERION FOR SMOOTH SPECIMEN 46

5.1. SMITH-WATSON-TOPPER (SWT) PARAMETER. 47

5.2. MORROW EQUATION 50

6.0 RELATION BETWEEN SWT AND K* PARAMETER 54

7.0 DETERMINATION OF THE CRACK-TIP ELEMENT SIZE, ρ^* 62

8.0 ACCUMULATION OF DAMAGE AHEAD OF CRACK-TIP ... 65

9.0 CALCULATION OF THE CRACK GROWTH RATE 68

10.0 OVERLOAD EFFECTS ON CRACK GROWTH RATE 72

10.1. MODELING RESIDUAL/INTERNAL STRESSES 74

10.2. WEIGHT FUNCTION PROCEDURE 81

10.3. RESIDUAL STRESS PROFILE MODELING 93

10.4. PREDICTIONS WITH THE MODEL 95

11.0 PREDICTION OF THE R-RATIO EFFECT WITH THE MODEL 104

12.0 CONCLUSIONS 107

13.0 RECOMMENDATIONS FOR FUTURE WORK 109

14.0 REFERENCES 110

Table of Contents-Continued

APPENDICES

A. KNEE-POINT DETERMINATION TO FIND ρ^* AND CONSTANT R-RATIO PREDICTIONS FOR DIFFERENT MATERIALS 115

B. WEIGHT FUNCTION CONSTANTS FOR DIFFERENT GEOMETRIES 130

C. MATLAB SUBROUTINES 133

LIST OF TABLES

1. Mechanical properties of 4140 and 4340 steel [15,46,47]..... 45

2. Mechanical properties of 2324-T39 and 7475 Al. alloy [59]..... 45

3. Mechanical properties of A533-B1 and C-Mn steel [15]. 49

LIST OF FIGURES

1. Different phases of the fatigue crack growth [2] 2

2. A simple representation of different crack growth cases [2]..... 3

3. Fracture surface showing fatigue crack growth and final brittle failure in 18 Mn. Steel 5

4.(a)Beach marks and the crack initiation sites on a fractured surface [4] 6

4.(b)Fatigue striations on a highly magnified fracture surface [4].... 6

5.(a)Illustration of the elastic stress field ahead of the crack, and the redistribution of stress due to plastic zone formation..... 8

5.(b)Different zones ahead of the crack tip under cyclic load 9

6. S-N curve for an unnotched A517 steel specimen [5]..... 10

7. Illustration of fatigue crack growth rate curve 12

8. Cyclic stress-strain hysteresis curve showing area under curve equivalent to the energy absorbed till failure, W_c..... 19

9. Long crack fatigue data for 2024-T351 Al. alloy [26]..... 23

10. Load cycle diagram for R=0.1 and R=0.5..... 26

11. Illustration of point by point basis Harter-T method..... 27

12. Illustration of typical crack growth data for R=0.7 and R=0.1 31

13. Expected theoretical correlation using the K_{eff} method 32

14. Correlation obtained using crack closure methodology 32

15. Load vs. displacement curve showing compliance change..... 33

List of Figures–Continued

16. Stress distribution ahead of the crack tip for the 4140 steel at two applied ΔK values for R=0.1 43

17. Stress distribution ahead of the crack tip for the 4140 steel at two applied ΔK values for R=0.5 44

18. Representation showing the elements ahead of the crack tip considered as smooth specimens 47

19. The plot of the modified SWT curve for 4140 steel 48

20. The plot of the modified SWT curve for A533-B1 steel 49

21. Mean stress data for AISI 4340 Steel, plotted vs. N* according to the Morrow equation 51

22. Family of strain life curves for 4340 Steel plotted vs. N_f according to the Morrow equation 52

23. Mean stress data for AISI 4340 Steel, plotted vs. N_f according to the SWT parameter 53

24. Schematic of the specimen divided into elements of width ρ^* 55

25. The relation between the elastic region of SWT and the near threshold region of the crack growth curve 60

26. The relation between the plastic region of SWT and the Paris region of the crack growth curve 61

27. Best-fit line approach to determine the knee-point for the ρ^* determination 63

28. Accumulated damage distribution in elements for 4140 steel (linear scale) 66

29. Accumulated damage distribution in elements for 4140 steel (log-log scale) 67

List of Figures–Continued

30. Predicted vs. Experimental crack growth data for 4340 steel, at R =0.1 and $\rho^* = 1.56e^{-5}$ 70

31. Predicted vs. Experimental crack growth data for 4140 steel, at R =0.1 and $\rho^* = 2.05e^{-6}$ 71

32. Residual stress profiles measured by x-ray diffraction in 1020 Steel before and after the overload [49] 75

33. Residual stress profiles after overload and after crack extension of 0.054 inches past point of overload [49] 76

34. Residual stress profiles after crack extensions of 0.054 and 0.111 inches past the point of overload [49] 77

35. Residual stress profiles measured by Allison [52], before and after the application of overload 78

36. Residual stress profiles after the overload and after a crack extension of 1.04 mm [52] 79

37. Illustration of integration method based on piecewise linearization of the stress function (a) Weight function m(x, a).(b) Piecewise stress function 88

38. Typical residual stress profiles ahead of the crack tip 90

39. Comparison of S.I.F calculation for the stress profiles by Matlab procedure and Glinka's FALPR05 90

40. Residual stresses ahead of the crack tip after application of a spike overload at interior and surface of the centre crack specimen 91

41. S.I.F calculation by FALPR05 and Matlab procedure for the residual stress profiles in a centre crack specimen after a spike overload 92

42. Residual stresses, experimental vs. modeled, before and after the overload application. 93

43. Stress profiles ahead of the crack tip at base load and after overload for 4140 steel 95

44. K residual profile calculated from the modeled residual stress in the material, after the overload application by using weight function approach 96

45. Effect of overload modeled for 4140 steel data from Holtz [46], using the K_{res} calculated by weight function method 97

46. Residual stress profile obtained from difference between the residual stress at overload and minimum stress at base load 98

47. Crack growth retardation due to overload predicted using the residual K approach for 4140 Steel 99

48. Overload data for 2324 Al. alloy from [59], predicted using K_{res} approach 100

49. Constant R-ratio data fitted to find the knee point and the constants 'b' and 'c' for 2324-T39 Al. alloy at R=0.1 101

50. Constant R-ratio data fitted with a slope of 11.4 in the near threshold region to see the sensitivity on the prediction 102

51. Sensitivity of the model to the slope in the threshold region to predict the crack growth rate in overload affected region 103

52. Experimental and predicted crack growth rate data for 4340 steel, R =0.1 and 0.5 104

53. Local R-ratio in the elements ahead of the crack tip 105

54. Crack growth rate predicted for R=0.1 and 0.5 for 4340 steel using different ρ^* value for each R-ratio 106

1. INTRODUCTION

Fatigue is a process by which a component is weakened by repeated loading. The stress can be much below the ultimate strength or even the yield stress of the material. However, over a large number of cycles the results can be catastrophic. Fatigue has to be considered as an important problem based on the economy and safety of components and structures. Effective control of the fatigue failures starts from the design phase, the material and the processes to be used for manufacturing a component should aim towards the fatigue tolerant design. The fatigue failure still might occur in a well designed component, reasons for which can be severe utilization, accidental loads, aggressive environment, poor maintenance and inspection. As a result the user's fatigue problems are more associated with maintenance, inspections and non-destructive testing techniques. The main concerns for the user can be: where the crack will originate, how fast will the crack grow and what is the critical size of the crack?

Forest [1] in his studies showed that crack nucleation starts early in the fatigue life but most of the fatigue life is spent in the micro range. For convenience sake it is termed as the nucleation phase or period of the micro-crack growth.

The different phases of growth of fatigue crack from inception to final fracture are illustrated in the Fig.1.

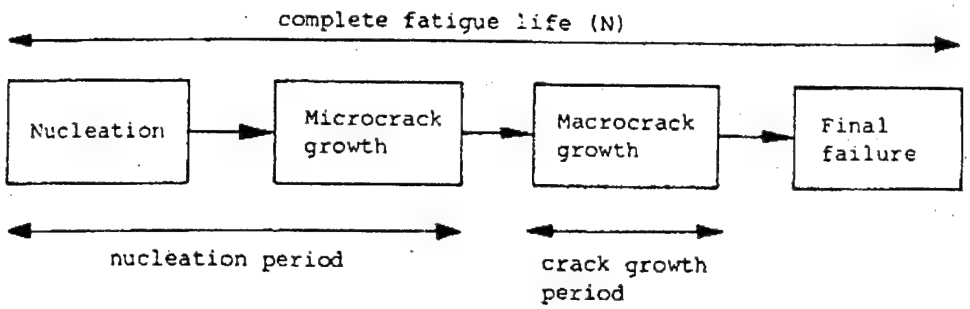

Figure 1. Different phases of the fatigue crack growth [2].

The crack is termed as a macro-crack when it is large enough to be seen by the naked eye according to the classical definition. According to another definition the crack is considered as a macro-crack when it has sufficient depth or length at which the local conditions for the crack nucleation no longer affect the crack growth. In other words the crack growth will depend on the bulk properties of the material. Another definition which is very important to the context of the study is that "a crack is a macro-crack as soon as fracture mechanics is applicable". It is rephrased as "A crack is a macro-crack as soon as the stress intensity factor K has a real meaning for describing its growth" Schijve [2]. Depending upon the design and the function of the component, the percentage of the fatigue life spent in different phases may vary. A simple representation of few such cases is shown in the Fig.2.

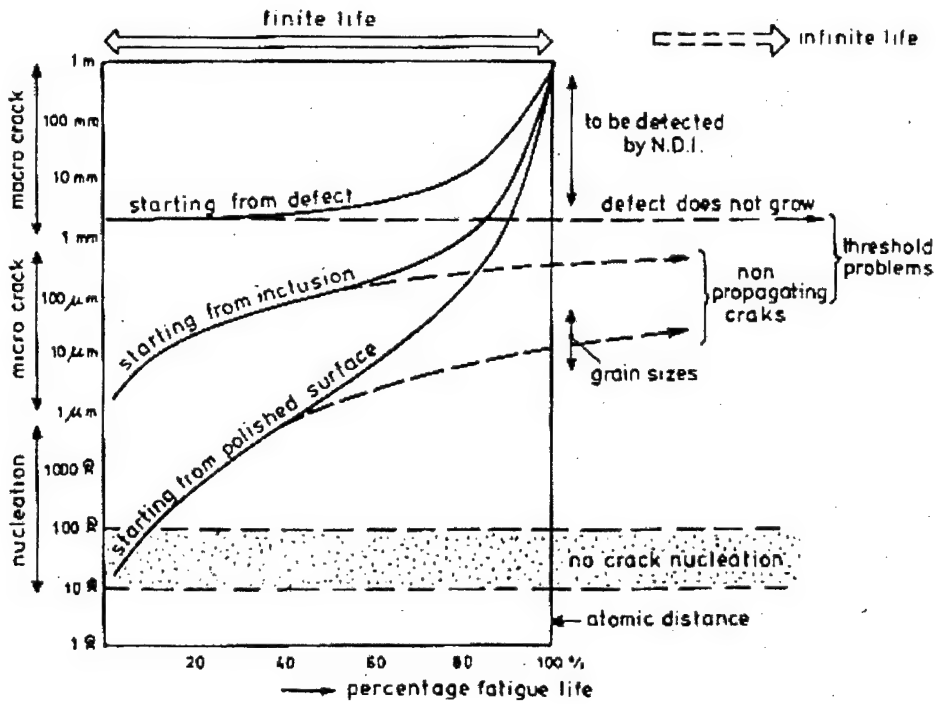

Figure 2. A simple representation of different crack growth cases [2]

1.1 CHARACTERISTICS OF FATIGUE

The following characteristics are common to fatigue in all materials:

(a) The fatigue process starts with a microscopic crack, called the initiation site, which then grows with each subsequent movement, which can be analyzed by fracture mechanics.

(b) Fatigue crack grows as a result of cumulative damage, and the material does not recover when rested. The greater the applied stress, the shorter the life.

(c) Fatigue life is affected by various factors such as temperature, environment, mean stress, loading mode, surface finish etc.

(d) Some materials like steel and titanium exhibit a fatigue limit, a stress below which there is no fatigue crack growth due to repeated loading.

1.2 PHYSICAL NATURE OF FATIGUE DAMAGE

At microstructure level all materials are anisotropic. Within the grains there is anisotropy along the crystal planes. So when viewed at sufficiently small size the non uniform microstructure or inclusions result in non-uniform distribution of stresses. Regions where the stresses are severe are usually the points where the fatigue damage starts.

For ductile engineering metals, grains that have unfavorable orientation relative to the applied stress first develop the slip bands. Individual slip bands become more severe and some develop into cracks within grains, which spread to other grains, joining with other similar cracks to grow into a large crack which can propagate to failure.

For the hard and brittle materials with somewhat limited ductility, the damage due to slip bands or within grains is very less. Damage is more concentrated around the defects in the material. A small crack can develop at a void, inclusion, grain boundary or a surface scratch and generally grows in a plane normal to the applied stress.

1.3 FEATURES OF A FATIGUE CRACKED SURFACE

Where a failure is dominated by growth of crack, the resulting fracture surface when viewed microscopically, generally exhibits a smooth area near its origin. The crack growth region is fairly flat and is oriented normal to the applied tensile stress. Rougher surfaces generally indicate a more rapid growth.

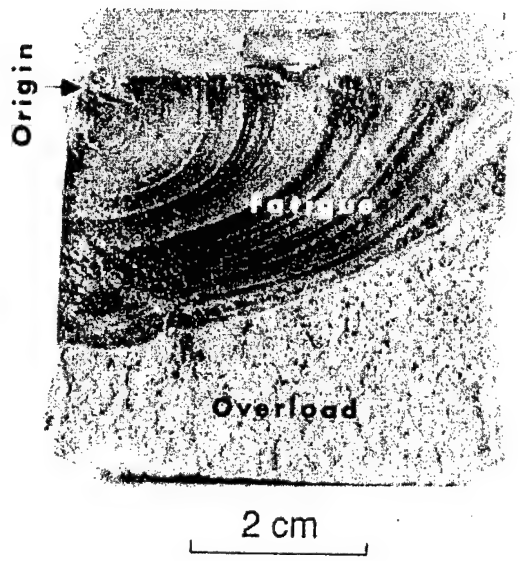

Figure 3. Fracture surface showing fatigue crack growth and final brittle failure in 18 Mn. Steel [3].

Curved lines concentric about the crack origin, called 'beach marks' are often present and mark the progress of crack at various stages. Beach marks indicate changes in the texture of fracture surface as a result of crack being accelerated or retarded, which may occur due to an altered stress level, altered temperature, environment or due to some other cause.

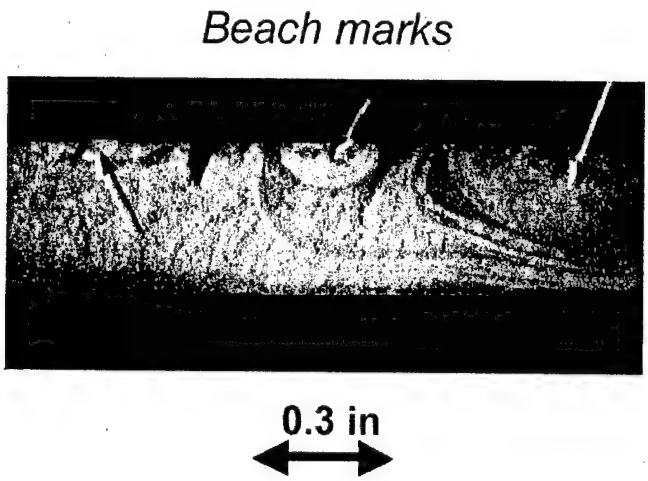

Figure 4(a). Beach marks and the crack initiation sites on a fractured surface [4]

If the fracture surface in a ductile material is viewed at a microscopic level, it often reveals the presence of marks left by the progress of crack with each cycle. These marks are called 'striations' and can be seen in the Fig.4(b).

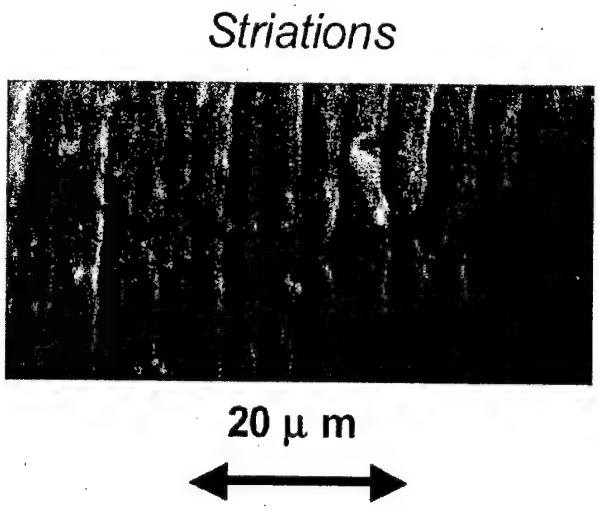

Figure 4(b). Fatigue striations on a highly magnified fracture surface [4]

1.4 STRESS FIELDS AHEAD OF CRACK TIP

If a crack is considered to exist in a material, and a uniform stress, S, is applied remotely. The uniform stress field is altered in the vicinity of the crack; stress rises sharply near the crack and has a maximum value close to the crack tip. A sharp crack causes a severe concentration of stress and is theoretically infinite if the crack is ideally sharp.

From the theory of fracture mechanics, a quantity called "stress intensity factor", K, can be defined that characterizes the severity of crack situation as affected by crack size, stress and geometry. In defining K, the material is assumed to behave in a linear-elastic manner according to Hooke's law, and the approach used is called "linear elastic fracture mechanics", LEFM. K is given by:

$$K = FS\sqrt{2\pi a} \tag{1a}$$

where F is a geometry factor, F=1 for an infinite plate and 'a' is the crack length.

However, an infinite stress cannot exist in a real material. In ductile materials plastic deformations occur in the vicinity of the crack tip. The region within which the material yields is called the plastic zone. Due to this yielding and blunting of the crack tip, the infinite stress is reduced to a finite value close to the crack tip.

In a loading part of the cycle the distance ahead of the crack where material yields is called the monotonic plastic zone, r_m. During the unloading part of the load cycle the elastic material around the monotonic

plastic zone pushes on to the already yielded material, and a small reversed cyclic zone is formed ahead of the crack due to material yielding in compression. This zone is called the cyclic or reversed plastic zone, r_c. An illustration of the typical elastic stress fields ahead of the crack and the formation of the plastic zone are shown in the Fig.5(a) ahead.

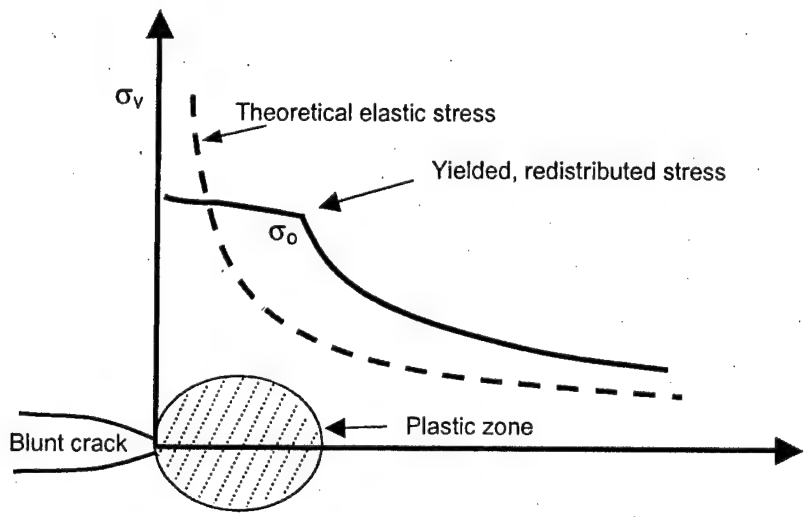

Figure 5(a). Illustration of the elastic stress field ahead of the crack, and the redistribution of stress due to plastic zone formation.

The formation of monotonic and cyclic plastic zones ahead of the crack tip is shown in Fig.5(b). Also, a small region exists ahead of the crack tip where due to crack tip blunting the stress and strain are approximately constant. This small region is called process zone, ρ^*.

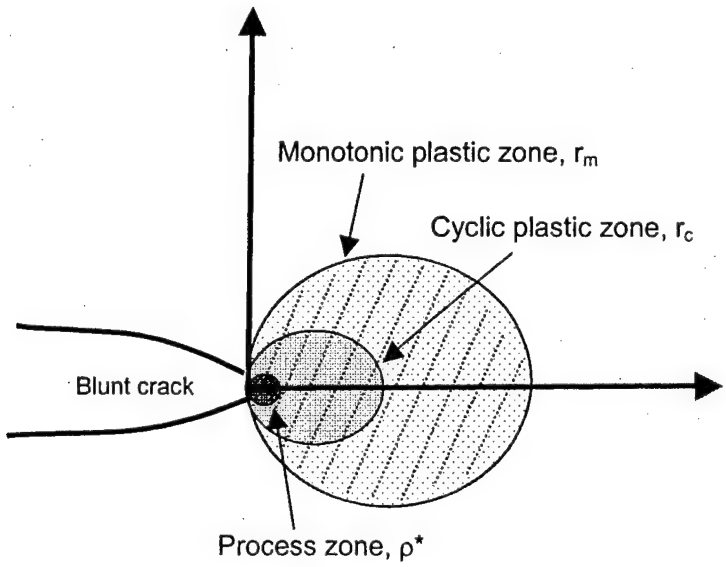

Figure 5(b). Different zones ahead of the crack tip under cyclic load.

1.5 MEASUREMENT OF FATIGUE BEHAVIOR OF MATERIALS

To measure the fatigue resistance of materials, a cyclic load is applied to a specimen until it breaks. The number of cycles to failure, called the fatigue life, N_f, is recorded. The logarithm of this life is plotted against the stress (or the log of stress) to develop an S-N curve (stress versus number of cycles to failure) as shown in Fig.6. This curve defines the fatigue resistance of a material.

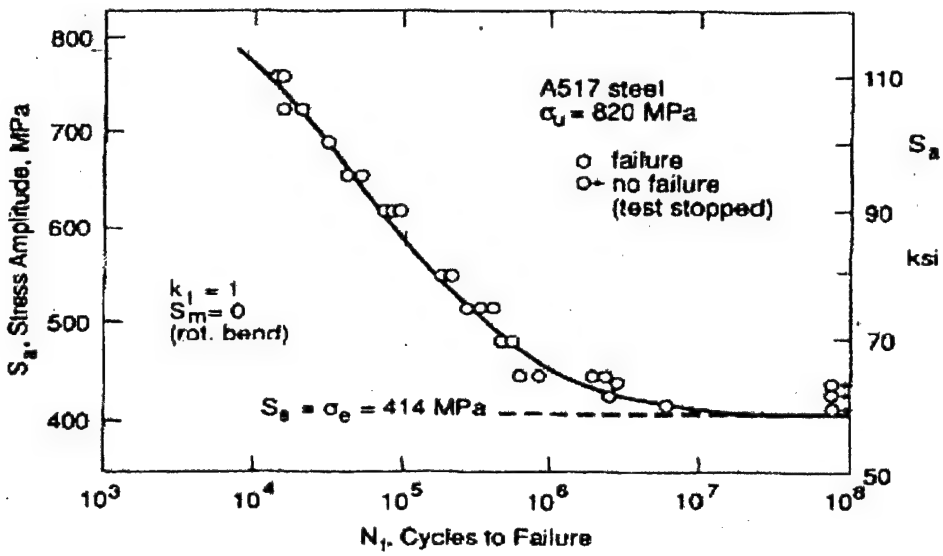

Figure 6. S-N curve for an unnotched A517 steel specimen [5]

As can be seen in Fig.6, there is a great deal of scatter in the fatigue life. Consequently, a large number of tests have to be run in order to determine the fatigue resistance.

For some materials, such as steel, there is a stress below which no fatigue failure is observed. This is called the 'endurance stress' or the 'endurance limit', in terms of the stress or the number of cycles to failure, respectively. The endurance limit is typically on the order of 10^7 cycles. Other nonferrous materials, such as Al and Al-alloys, do not have a true endurance limit. In other words, the S-N curve is never horizontal. For these materials, an artificial endurance limit is defined as the stress that will cause fatigue failure in a given number of cycles, usually10^7 or 10^8 cycles.

1.6 CRACK GROWTH RATE CURVE

Fracture mechanics is important in life prediction of components that are subjected to time dependent crack growth mechanism such as fatigue or stress corrosion cracking.

Crack growth can be caused by a cyclic loading behavior called fatigue crack growth. The rate of cracking is an important parameter to quantify the time required before the material will fail. The rate of cracking is usually called the crack growth rate, da/dN, represents the crack extension per cycle.

Paris et al. [6] proposed a relation to describe crack growth in metals with respect to the applied stress intensity range of the following type:

$$da/dN = C(\Delta K)^m \tag{1b}$$

where da/dN is the crack growth per cycle, ΔK is the SIF range; C and m are the material constants.

The crack growth behavior for a material can be described on a log-log plot as shown in the Fig.7.

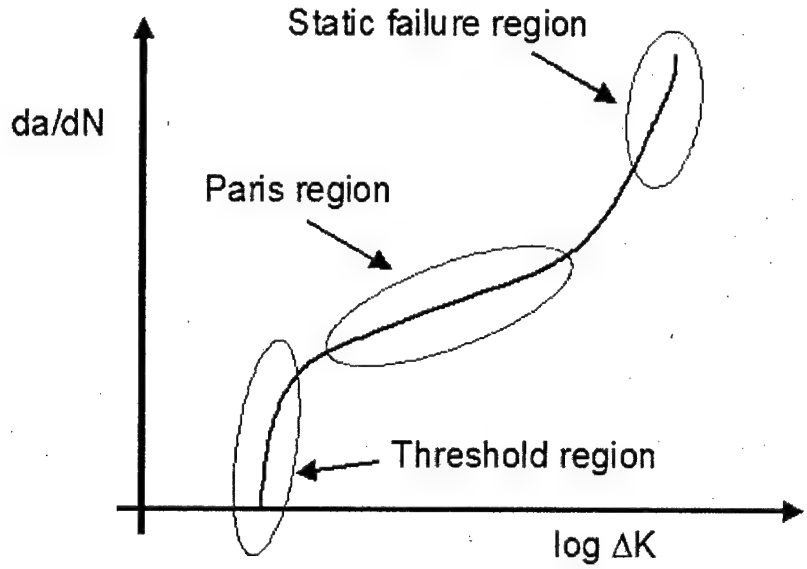

Figure 7. Illustration of fatigue crack growth rate curve.

At low growth rates i.e. in the near threshold region the curve generally becomes steep and appears to approach a vertical asymptote, denoted by ΔK_{th} which is called the threshold SIF range. ΔK_{th} is usually interpreted as a lower limiting value of ΔK below which the crack growth is assumed to be zero.

In the intermediate region of the curve, the crack growth rate follows almost a straight line plot in log-log scale. This region is called the 'Paris Region' where there is a stable crack growth and can be defined by Eq.1. At high crack growth rates above the Paris region there is rapid unstable cracking and the curve again becomes steep just prior to the final failure when the material reaches the critical value of K called the "fracture toughness", K_c. This is called the static failure region of the curve.

2. LITERATURE REVIEW

In order to have damage tolerant design, it is important to know the crack growth behavior of a material, so that the component can be changed or repaired before the crack reaches a critical size. For this, it is necessary to determine the rate of crack growth with as much reliability and accuracy as possible. During the last thirty years or so, considerable attention has been devoted to investigations into crack propagation relationships under cyclic loading. Most of these studies attempt to relate the crack propagation rates with some function of stress intensity factor range, ΔK, based upon experimental data. Although the models are applicable for a particular set of conditions for which they were derived, they lack generality and require experimental determination of coefficients and exponents which are not related to the basic material properties. There are many crack growth softwares available, which use different fatigue crack growth models to predict the failure life, but none has the desired predicting accuracy. Either these require extensive experimental data or some kind of special fitting, coupled with lots of fatigue experience to predict the crack growth behavior. To develop a better predictive model and to shed some light on the damage accumulation process, various fatigue crack propagation models have been studied, a review of these models will be presented in the following discussion.

Fatigue crack growth is a phenomenon of damage and separation of the material ahead of a crack under cyclic loading. It has been reported [7,8] that plastic strains are the cause of damage accumulation at all levels of loading, and that the significant damage takes place when the plastic strain exceeds a threshold value for the material enveloped by the reversed or cyclic plastic zone. Many researchers [7-20] support the fact that the greatest damage in the material is done in a small region ahead of the crack tip, called the 'process zone'. The material in this zone undergoes high plastic deformation that damages the material, As soon as this accumulated damage reaches a critical level, the material element fails.

In the case of small scale yielding i.e. where the plastic zone ahead of the crack tip is small as compared to the component size, represents most crack growth situations. Plastic zone is surrounded by a much larger volume of elastically deformed material. The plastic strains in the monotonic and reversed plastic zones are controlled by the surrounding elastic deformation fields, which in turn are related to the stress intensity factor, K.

Rice [7] traced the deformation history of a material element after it enters the reversed plastic zone. Dugdale model was used to calculate the total absorbed plastic strain energy, and it was assumed that the fatigue damage is proportional to this energy. He obtained a fatigue crack growth rate, da/dN, proportional to fourth power of ΔK. Due to lack of fully

elastic-plastic solutions of crack tip fields for Mode I loading various assumptions of strain distributions were made in this model. It was also assumed that the deformation fields ahead of the stationary crack and a propagating fatigue crack are identical.

In general a fatigue crack growth law can be formulated by coupling the cyclic stress-strain distribution ahead of the crack with a suitable failure criterion.

2.1 CRACK-TIP FAILURE CRITERIONS

Researchers in the past have used different failure criterion to predict fatigue crack growth, some of which are listed below.

2.1.1 Plastic Strain or Total Strain Ahead of the Crack

In this approach it is assumed that only the strains above the yield strain, ϵ_y, cause the damage in the material. Duggan [9] in his study, has assumed the material to be elastic perfectly plastic, with no strain hardening and no Bauschinger effect. The failure life is calculated from the Coffin-Manson [21] law, $\Delta\epsilon_p N_f^{\alpha} = C$, which assumes that the material will fracture when the cyclic plasticity builds up to a critical value.

Lehr and Liu [10] combine the Coffin-Manson law and Miners rule [22] and consider a volume element being strained with increasing amplitudes while traversing the monotonic plastic zone, r_m.

With a strain distribution

$$\epsilon = \epsilon_y \left[\frac{x}{r_m} \right]^{\beta} \tag{2}$$

where ε_y is the yield strain, x is the distance from the crack tip and β is an exponent. Failure is assumed to occur when the total strain exceeds the fracture strain.

McClintock [23] assumes that for a crack opening in Mode III, the average plastic shear strain in the volume element governs the crack propagation process. Failure being when it equals the plastic fracture strain for Mode I.

2.1.2 Magnitude of the Crack Tip Opening

Some researchers have used the crack extension per load cycle equal to the crack-tip opening displacement, Δu, caused by the cyclic stress and hence equal to the crack growth rate.

Lardner [24] applied the crack-tip opening model developed for the static load by Swinden [27 in 24] to the cyclic loading. But this model does not predict the true shape of the crack growth curve. It can only predict the crack growth in the Paris region, with some fitting.

2.1.3 Energy Based Failure Criterions

In the energy based approaches it is assumed that the absorbed energy during cyclic loading causes the crack initiation and propagation.

Ellyin and Kujawski [17, 18] explain that during cyclic loading, part of the mechanical input energy is rendered irrecoverable. A major part of this irrecoverable energy is converted into heat, and the remaining part is responsible for the crack initiation and growth. This energy is the area of the hysteresis loop and it does not change after the initial few cycles. They calculated this absorbed plastic strain energy per cycle, as:

$$\Delta W = \left(\frac{1-n'}{1+n'}\right)\Delta\sigma\Delta\varepsilon^{p} \tag{3}$$

where n' is the strain hardening exponent, $\Delta\sigma$ is the stress range, $\Delta\varepsilon^{p}$ is the plastic strain range.

Fatigue damage, in general, and crack propagation, in particular can be related to this energy term.

They express the stress range $\Delta\sigma$ and the plastic strain range $\Delta\varepsilon^{p}$, in terms of number of reversals to failure $2N_f$ by

$$\Delta\sigma = 2\sigma'_f\left(2N_f\right)^{c} \text{ and } \Delta\varepsilon^{p} = 2\epsilon'_f\left(2N_f\right)^{b} \tag{4}$$

where b is the fatigue strength exponent, c is the fatigue ductility exponent, σ'_f is the fatigue strength coefficient and ε'_f is the fatigue ductility exponent. Product of these ranges, a measure of the absorbed plastic strain energy density is expressed as:

$$\Delta\sigma\Delta\varepsilon^{p} = 4\sigma'_{f}\,\epsilon'_{f}\left(2N_{f}\right)^{b+c} \tag{5}$$

The "process zone" where the stress and strain ranges have a very low gradient was considered, as a region where this absorbed plastic strain energy will cause failure after a given number of cycles.

In another study by Pandey and Chand [19], the criterion of specific energy 'W_c' used by McEvily [8 in 19], has been modified by using the Rice superposition method for cyclic loading to modify the specific energy term. They consider the entire reversed plastic zone as the area for the plastic energy dissipation, with a premise that irreversible plastic work done within this area is a source of energy dissipation. A 'characteristic length' described as the area divided by the circumferential length of the cyclic plastic zone is used to get the unit increment for crack propagation. The crack advances a unit increment when the energy dissipation in this region equals the area below the cyclic stress-strain hysteresis curve.

A cyclic-stress strain hysteresis curve is shown in Fig.8. Point 'A' corresponds to twice of the cyclic yield stress and strain, and point 'B' is the point corresponding to the stress and strain ranges with $2N_f = 1$. The material behavior is described by Ramberg-Osgood equation. The energy absorbed till failure, W_c, is the area of the cyclic stress-strain range curve.

W_c = Area OABCO = Area OFBEO – Area OABFO – Area CBEC

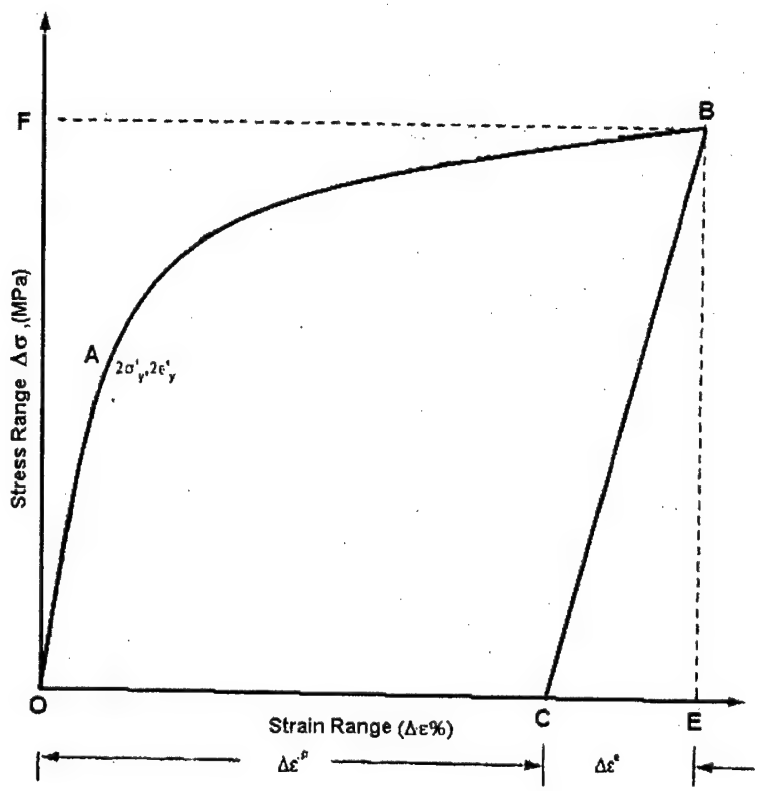

Figure 8. Cyclic stress-strain hysteresis curve showing area under curve equivalent to the energy absorbed till failure, W_c.

It has been noted that the energy-based failure criterions are more suitable than others. One of the explanation being that the energy based criteria use product of the stress and plastic strain range, while in other criteria the intrinsic interplay between the stress and strain ranges is overlooked. Therefore, the criteria that utilize both the stress and plastic strain ranges give better results than only stress or strain criteria.

2.2 DAMAGE ACCUMULATION

From the phenomenological point of view, the fatigue crack growth has been related to the cyclic fatigue damage process of material elements, at the 'process zone' ahead of the crack tip [10-18]. Most of these approaches consider a damage element near the crack tip which is modeled as a uniaxial fatigue specimen.

Plastic strains are the cause of damage accumulation at all levels of loading [7, 8], but when a material element enters the reversed plastic zone it is not subjected to fatigue damage immediately. Fatigue damage accumulates only when the plastic strain range, $\Delta\varepsilon_p$, exceeds a threshold value, $\Delta\varepsilon_o$, for the material. As soon as this accumulated damage reaches a critical level, the material element fails.

Cumulative fatigue damage is an old, but not yet fully resolved problem. There are various theories to calculate the accumulated damage under cyclic loading. These theories are grouped into six main categories by Fatemi and Yang [25] as:

(a) linear damage rules, (b) non-linear damage rule and two-stage linearization approaches, (c) life curve modification methods, (d) approaches based on crack growth concepts, (e) continuum damage mechanics models, and (f) energy based theories.

The linear damage rule cannot account for the load sequence and interaction effects due to its linear nature. Though many damage models have been developed, unfortunately, none of them enjoys universal

acceptance. Each damage model can only account for one or several phenomenological factors, such as load dependence, multiple damage stages, nonlinear damage, load sequence and interaction effects, small amplitude cycles below the fatigue limit, and the mean stress effects. Due to the complexity of the problem, none of the predictive models can encompass all of the factors. The applicability of each model varies from case to case. Consequently, the Palmgren-Miner linear damage rule [22] is still dominantly used in design, in spite of its major shortcomings.

Wu and Cotterell [8] in their approach based on Dugdale model and plastic strain energy failure criterion similar to Rice, model the damage accumulation process according to the Miner's linear damage rule.

Duggan [9] defines the damage zone ahead of the crack, R_d, as the radius from the crack tip to the point corresponding to the endurance strain range. He also assumes that the damage accumulates linearly according to Miner's law.

Glinka [10-12] modeled the fatigue crack growth for steel and aluminum alloys by using local stresses and strains at the crack tip, and the damage accumulation process in the highly strained region 'process zone' in the vicinity of the crack tip.

In one of the most recent of approaches based on the critical plastic strain energy dissipation by Pandey and Chand [19], damage accumulation ahead of the crack tip has been successfully modeled by using the Miner's law.

The results reported in the above studies suggest that the Palmgren-Miner's linear damage rule is the most popular damage accumulation approach, which can be easily used in conjunction with variety of failure criteria.

2.3 EFFECT OF APPLIED R-RATIO ON FAIGUE CRACK GROWTH

The load ratio or R-ratio, is defined as the ratio of S_{min}/S_{max} or K_{min}/K_{max}, where the S is the stress and K is the stress intensity factor.

It is known that an increase in the R-ratio for the cyclic loading at a given ΔK causes the crack growth rate to be higher. This R-ratio effect on fatigue crack growth is shown in Fig.9.

For some metals the R-ratio effect is small or is non existent in the Paris region. The R-ratio effects are more pronounced in the near threshold region and in the rapid unstable crack growth region.

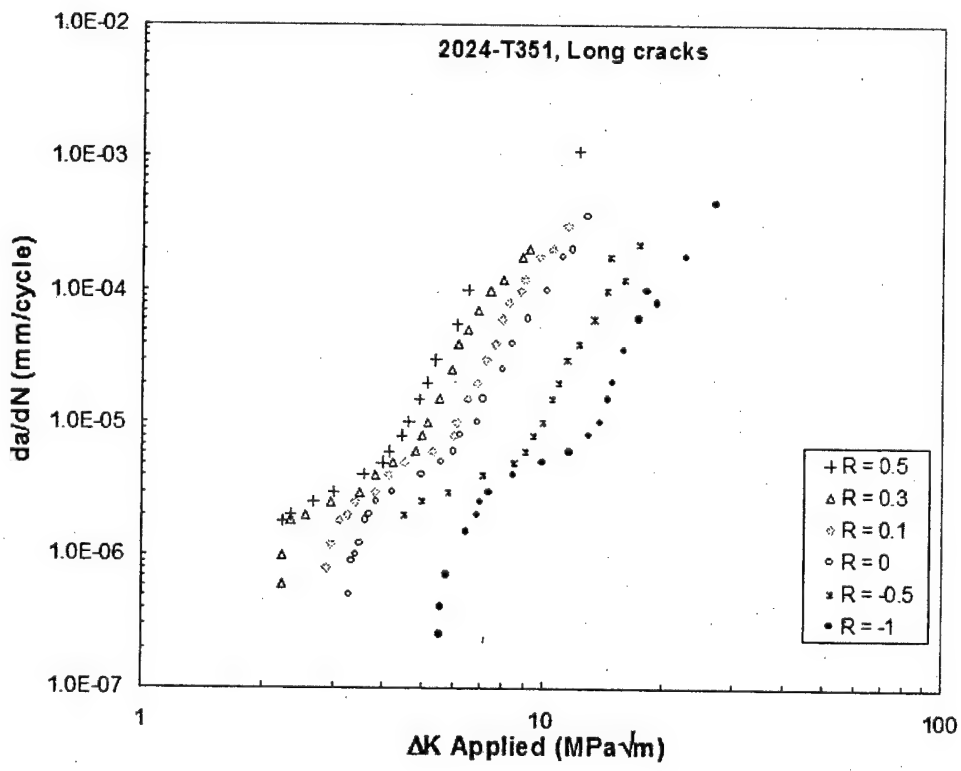

Figure 9. Long crack fatigue data for 2024-T351 Al. alloy [26].

A number of investigators have studied the R-ratio effects on near threshold region in laboratory air and vacuum, in terms of relation between ΔK_{th} and R. The general trend shows that for many materials in air, ΔK_{th} tends to decrease with increasing R, but for some materials and $R > 0.5$, the sensitivity is less. Most experimental results in vacuum indicate that R-ratio effect on the ΔK_{th} is less pronounced or diminished [3].

2.4 CONCEPTS FOR CORRELATION OF R-RATIO EFFECTS

There are several concepts that have been adopted to account for the R-ratio effect, namely a) Crack closure, b) Residual compressive stresses c) Environmental influence. All the approaches tend to calculate an 'effective stress', $\overline{\sigma}$, or 'effective stress intensity factor', $\overline{K}$, to account for the R-ratio effect on the fatigue crack growth.

In 1970 Walker [26] used an effective stress approach

$$\overline{\sigma} = \sigma_{max}^{(1-m)} \Delta\sigma^{m} \tag{6}$$

which was able to correlate effects of R-ratio on the fatigue life for 7075-T6 and 2024-T3 Al alloys.

For the case of fatigue crack growth, the Eq.(6) was modified to the following form

$$\overline{K} = K_{max}^{(1-m)} \Delta K^{m} \tag{7}$$

which correlated the crack growth data for positive R-ratios fairly well. In his approach 'm' was assumed to be a material parameter which was calculated from experimental data.

In 1971 Elber [27] introduced a crack closure concept, in which he stated that the crack is open during only some part of the load cycle. He defined K_{op} as the stress intensity factor at which the crack opens, while cycling from K_{min} to K_{max}. It is assumed that there is no damage ahead of the crack tip for the portion of the cycle in which crack is closed. Therefore, the effective stress intensity factor range, K_{eff} is calculated as:

$$\Delta K_{eff} = K_{max} - K_{op} \tag{8}$$

Fig.10 illustrates the typical relation among K_{max}, K_{min} and K_{op} for load cycles with R = 0.1 and 0.5.

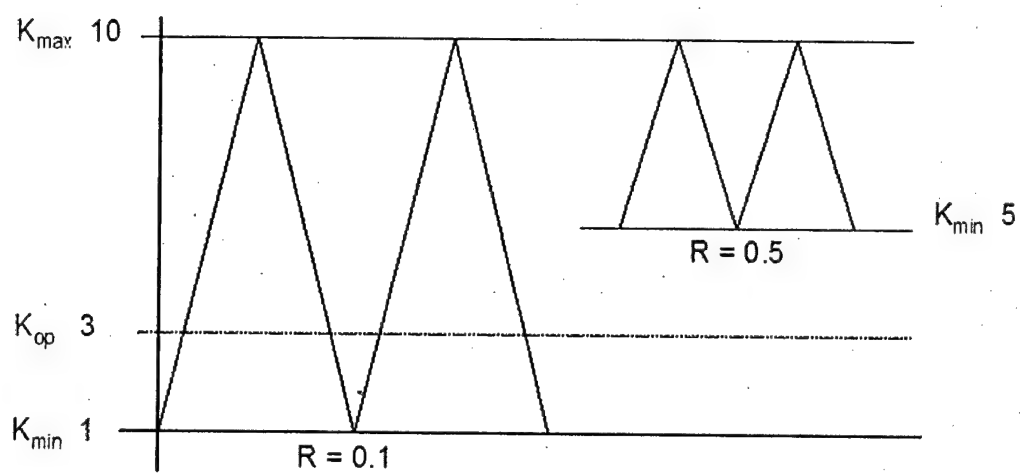

Figure 10. Load cycle diagram for R=0.1 and R=0.5.

The corresponding K_{eff} is calculated as:

For R=0.1 ; $K_{op} > K_{min}$; $\Delta K_{eff} = K_{max} - K_{op} = 7$

For R=0.5 ; $K_{op} < K_{min}$; $\Delta K_{eff} = K_{max} - K_{min} = 5$

Elber suggested that residual tensile displacements left in the wake of the crack tip plastic zone cause the crack to remain closed even when the applied load is positive.

Since then the concept of crack closure has been most widely adopted as a critical mechanism responsible for the R-ratio effects.

Dinda and Kujawski [28] used a fatigue crack driving force parameter similar to Walker's approach, difference being that it is calculated solely

using the positive part of the range of applied stress intensity factor, ΔK^+, and the corresponding maximum value of SIF, K_{max}.

$$\Delta K_D^* = (K_{max})^p (\Delta K^+)^{1-p} \tag{9}$$

Using this approach the R-ratio effects on fatigue crack growth were successfully correlated for a number of materials [28].

Another approach by Harter [29], called the Harter-T method is an adaptation of the Walker equation taken on point-by-point basis. In this implementation 25 da/dN and corresponding ΔK values are used to define the crack growth behavior. The tabular data utilizes the Walker equation on a point-by-point basis (Harter T-Method) to extrapolate/interpolate data for any R value. Illustration in Fig.11 represents the tabular data for two R-ratios which are used in Walker equation, Eq.(7), to determine m.

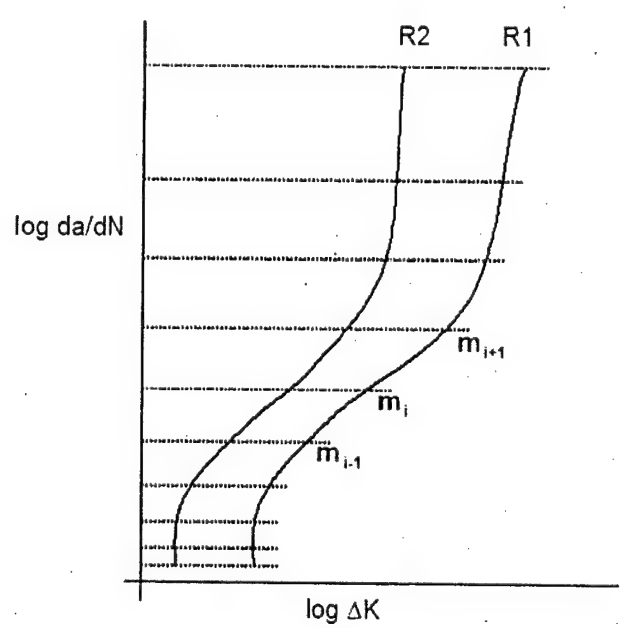

Figure11. Illustration of point by point basis Harter-T method.

Since $da/dN = C[\Delta K(1-R)^{(m-1)}]^n$ (Walker equation)

At a given da/dN, data at any two positive R-values becomes:

$$\Delta K_1(1-R_1)^{(m-1)}=\Delta K_2(1-R_2)^{(m-1)} \tag{10a}$$

$$m=1+\left[\log 10\left(\frac{\Delta K_1}{\Delta K_2}\right)\Big/\log 10\left(\frac{1-R_2}{1-R_1}\right)\right] \tag{10b}$$

When prediction is made for the negative R-ratios, a distinction is made such that K_{max} is used in place of ΔK.

According to Vasudevan and Sadananda [30] the fatigue crack growth is based on two basic fracture mechanics parameters K_{max}, ΔK and the internal stress contribution to K_{max}. They propose that the internal stresses are the missing link that can bridge the gap between four main stages of damage from nucleation to final failure.

2.5 DRAWBACKS OF THE CRACK CLOSURE METHODOLOGY

After Elber [27] proposed the crack closure model, much focus was towards relating the load interaction effects with the plasticity induced crack closure operating in the crack wake. Over the time many researches have shown that other types of crack closure such as a) surface roughness or asperity induced closure, b) fracture surface mismatch induced closure c) fracture surface oxidation induced closure and d) debris related closure have to be considered.

In 1993 Sadananda and Vasudevan [31] reconsidered the plasticity-induced closure and its effects on FCG behavior. They argued that, since the closure occurs behind the crack tip, it has rather limited effect on damage process that takes place in front of the crack. They demonstrated that there is no significant contribution to closure due to plastic stretch in the crack wake. Further, when asperity or roughness induced closure is present, the contribution is small, approximately one quarter of that determined from compliance measurements.

Recently in 2003 Silva [32] showed that the closure concept is inadequate at the negative stress ratios. He conducted experiments at negative stress ratios to focus on the crack tip plasticity and surface roughness effects on closure. Study confirmed that, at negative stress ratios, the closure changes with P_{max} for the same R-ratio. He concluded that the damage accumulation principles or residual stress concepts seem to be more adequate to explain R-ratio effects than the crack closure concept.

Original crack closure concept assumes that the whole crack opens instantly at opening load, P_{op}. Thus, at any load $P<P_{op}$ crack is closed and fully shielded from the damage.

But, for most metals, crack growth in the near threshold region is associated with a single shear mode of crack growth, which gives rise to faceted fracture surfaces and their associated mismatch. Therefore, in near threshold regions the roughness or mismatch dominated closure would be expected.

Donald and Paris [33, 34] modeled this, using so called partial crack closure model, where closure of crack faces only partially shields the crack tip from fatigue damage. They proposed the following modification to the

ΔK_{eff} relation in case of the partial closure in near threshold region

$$\Delta K_{2/PI} = K_{max} - \frac{2}{\pi}K_{op} \quad \text{if} \quad \frac{2}{\pi}K_{op} > K_{min} \tag{11a}$$

$$\Delta K_{2/PI} = K_{max} - K_{min} \quad \text{if} \quad \frac{2}{\pi}K_{op} \leq K_{min} \tag{11b}$$

Usually P_{op} is determined according to the ASTM standard E647 recommendations, which corresponds to the load that causes the 2% deviation in the slope of a load-displacement curve. Then the K_{eff} is calculated from this P_{op} value. However, it is often observed that such calculated K_{eff} for a low stress ratio (e.g. R=0.1) at threshold is lower than the applied ΔK for a high stress ratio (R>0.7 or higher) where crack closure is usually absent.

This contradiction is illustrated by an example below [41]

Fig.12 shows a typical data for crack growth rate (da/dN vs. ΔK) at two stress ratios R=0.7 and 0.1.

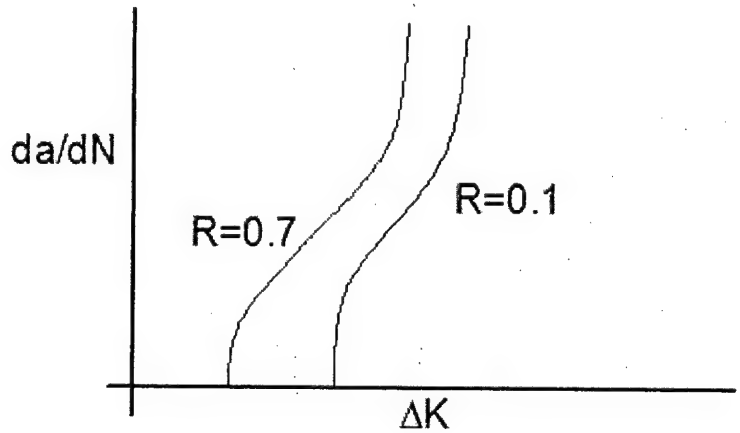

Figure 12. Illustration of typical crack growth data for R=0.7 and R=0.1.

Assuming a similar kind of loading as shown in Fig.10 with K_{op}=6

At load ratio R=0.1; K_{max} =10 and K_{min} =1,

At load ratio R=0.7; K_{max} =10 and K_{min} =7,

and the opening stress intensity factor K_{op} = 6

Therefore using Eqn.(8):

for R=0.1 ; $K_{op} > K_{min}$; $\Delta K_{eff} = K_{max}-K_{op} = 4$

for R=0.7 ; $K_{op} < K_{min}$; $\Delta K_{eff} = K_{max}-K_{min} = 3$

So theoretically the data should correlate as shown in the Fig.13.

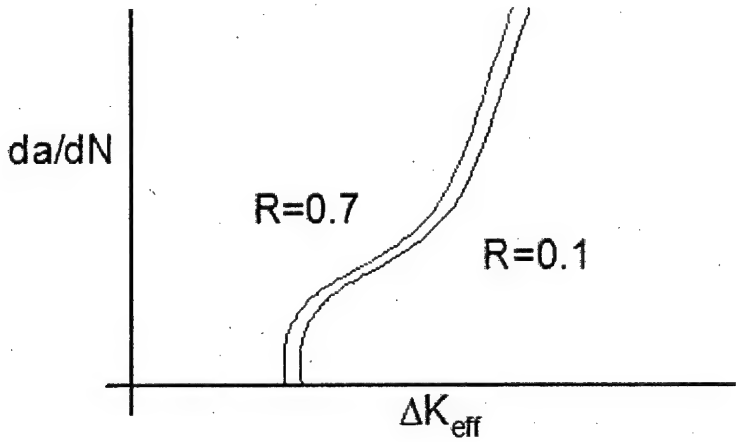

Figure 13. Expected theoretical correlation using the K_{eff} method.

However it has been shown by many authors that using the "crack closure methodology" the correlation shown in Fig.14 is obtained, where the curves for R=0.1 and 0.7 are in reversed order than in Fig.13.
This reverse order of curves indicated that the effective threshold for R=0.1 is smaller than for R=0.7. This contradicts the crack closure concept because, the data for R=0.1 with crack closure has lower threshold than the data for R=0.7 where closure is absent.

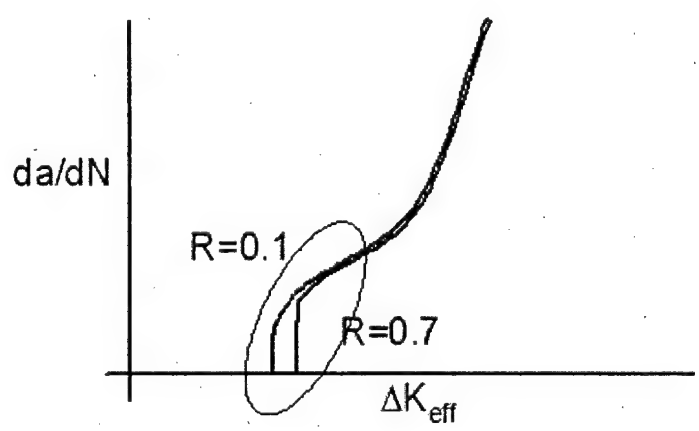

Figure 14. Correlation obtained using crack closure methodology.

The above mentioned contradiction has been observed by many authors and Donald and Paris [33, 34] have explained it on the basis of the partial crack closure phenomenon discussed earlier.

One of the most important drawback of the crack closure methodology is the difficulty of measuring the crack opening load. The crack opening load depends on the measurement location and the technique used. Fig.15 shows a typical load vs. displacement curve which indicates that there is a gradual transition from fully closed to fully open crack.

But the closure method takes a single point as P_{op} below which the crack is fully closed and above it is fully open. To determine this point there are several different methods that can be applied, and each gives a slightly different result [41].

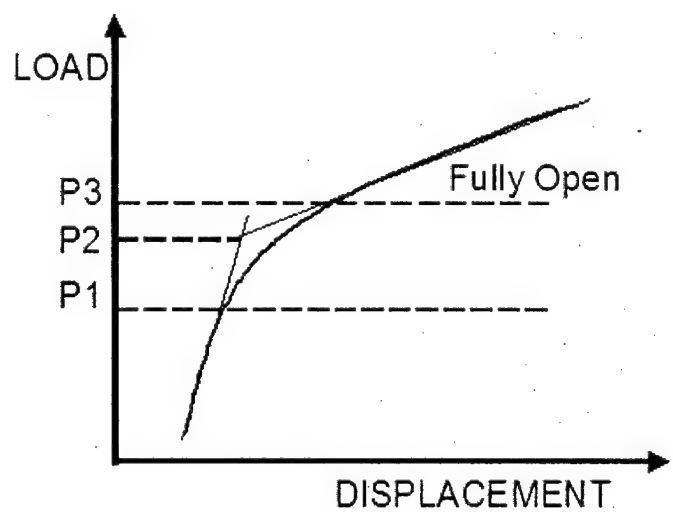

Figure 15. Load vs. displacement curve showing compliance change.

Mc Clung [35] after doing extensive review on crack closure concluded that there are three distinct regimes of crack closure namely a) near threshold, b) Paris region and c) high crack growth region.

Donald [36] also showed that the fatigue crack growth rate is not determined solely by ΔK_{eff} but also depends on the K_{max}.

With all the drawbacks about the crack closure and the conclusions mentioned by different authors it can be inferred that there is a need to develop a fatigue crack growth model that has both the K_{max} and ΔK effects on the crack growth rate. The model should take into account not only what is happening behind the crack tip, but also what is happening ahead of the crack tip.

2.6 TWO PARAMETER (K_{max} and ΔK) UNIFIED APPROACH

In the work done by Vasudevan and Sadananda [37-39], they explain that there are two parameters, ΔK and K_{max}, that are required to describe the crack driving force that controls the fatigue crack growth. This approach has been given the name of 'unified approach' to fatigue crack growth.

In early approaches starting from Paris et al. [6], ΔK and R have been the two parameters to quantify the fatigue crack growth rate. The existence of threshold in terms of ΔK has been considered, as it is a contributing factor to the driving force. Threshold for R is not considered, since it is not a driving force. Hence, the effects of R-ratio on fatigue crack growth have been explained mainly by the crack closure approach.

In contrast, the unified approach considers K_{max} also to be a required parameter to quantify the driving force in addition to ΔK. The existence of the K_{max} threshold has been reported by the authors, which is a definite indication that K_{max} is a crack tip driving force.

Vasudevan et al. [30] have also shown that all deviations from steady state long crack growth behavior can be accounted for by presence of "internal stress" gradients that introduce internal stress intensity factor K_{int}. The K_{int} mainly affects the K_{max} and causes perturbations in it. The value of ΔK is not much affected since K_{int} acts on both K_{max} and K_{min}.

The unified approach suggests the following procedure for fatigue crack growth modeling:

(a) Analytical models must include K_{max}, ΔK and K_{int}.

(b) Understanding and estimating the internal stresses is fundamental to the development of a reliable life prediction model.

(c) Modeling must account for the accumulation of damage from crack nucleation stage to short crack to long crack to final failure.

(d) Physics-based descriptions of fatigue crack nucleation and growth are needed in order to obtain a reliable life prediction model.

3. SCOPE OF THE WORK

The purpose of this study is to develop a mathematical model for the fatigue crack propagation utilizing the stress and strain state near the crack tip region and damage accumulation process. The methodology will be based on the use of both K_{max} and ΔK as the contributing parameters to the driving force and to understand, how these parameters affect the damage accumulation.

Effort will also be made to understand and estimate the internal stresses, and to model the effect of these internal stresses and K_{int} on the applied K_{max}.

This will not only help to predict the crack propagation rates without the experimental determination of empirical parameters, but it would also lead to a better understanding of the effect of these factors on the fatigue crack growth behavior.

The crack tip stress-strain distributions within and beyond the plastic zone will be evaluated adopting Rice [7] and the elastic solution, respectively. It has been widely accepted [8-12, 15-18, 20] that there is a small region ahead of the crack, where due to yielding and crack tip blunting the stress and strain magnitudes are finite, so the singularity at crack tip inherent to these models can be avoided. This small region in front of the crack tip is termed the 'process zone', ρ^*. Subsequently, the damage accumulation in the process zone will be determined and analyzed, in relation to how it governs the progressive growth of the crack. In this

study it will be assumed that the damage accumulates according to the Palmgren-Miner [15] linear damage rule.

The effect of the internal stresses on K_{max} will be modeled by evaluating K_{int} using the weight function methodology proposed by Glinka [54-57]. A graphic user interface (GUI) will also be developed based on the model, which will be programmed in MATLAB. Finally, the model will be verified by comparing the predictions of the model to the data available in literature for a spectrum of materials. The verification of the predictions by the current model will consist of following steps:

(a) Predict the crack growth data for the constant amplitude loading and compare it to the available data published in literature.

(b) Next, the predictions of the weight function subroutine, developed in MATLAB, will be compared to the predictions by Glinka's FALPR application.

(c) Internal stresses ahead of the crack tip for the overload will be utilized to predict the K_{int} profile.

(d) The predictions for the overload effected crack growth data, by K_{int} modeling, will be compared to the data available in the literature.

(e) Predictions for the R-ratio effect by the current model will be compared to the data available in the literature.

4. STRESS AND STRAIN DISTRIBUTION AHEAD OF THE CRACK TIP

Rice [7] analytically solved the stress and strain distribution ahead of the crack tip for a stationary crack in anti-plane shear (mode III loading) under small scale yielding. The corresponding shear stress and shear strain relationship was assumed:

$$\tau = G\gamma \qquad \text{for} \quad \gamma \le \gamma_o, \tau \le \tau_o$$

And (18)

$$\tau = \tau_o \left(\frac{\gamma}{\gamma_o} \right)^n \qquad \text{for} \quad \gamma \ge \gamma_o, \tau \ge \tau_o$$

Where τ_o and γ_o are the yield strength and strain respectively and n is the strain hardening exponent.

The following equations for mode III were derived [7]

$$\tau = \tau_o \left[\frac{K_{III}^2}{(1+n)\pi\tau_o^2 x} \right]^{n/1+n} , \qquad \gamma = \gamma_o \left[\frac{K_{III}^2}{(1+n)\pi\tau_o^2 x} \right]^{1/1+n} \tag{19}$$

A similar analysis for tensile loading (mode I) is not available. However, McClintock [23] had suggested that there is the analogy between mode III and mode I for a case where displacements parallel to the crack are small as compared to those normal to the crack surface.

Assuming the following stress and strain relationship

$$\sigma = E\varepsilon \qquad \text{for} \quad \varepsilon \le \varepsilon_o, \sigma \le \sigma_o$$

And (20)

$$\sigma = \sigma_o \left(\frac{\varepsilon}{\varepsilon_o} \right)^n \qquad \text{for} \quad \varepsilon \ge \varepsilon_o, \sigma \ge \sigma_o$$

The analogous equations for Mode I are

$$\sigma_{max} = \sigma_o \left[\frac{K_{max}^2}{(1+n)\pi\sigma_o^2 x} \right]^{n/1+n}, \quad \varepsilon_{max} = \varepsilon_o \left[\frac{K_{max}^2}{(1+n)\pi\sigma_o^2 x} \right]^{1/1+n}. \tag{21}$$

Assuming that the plastic strain components at each point within the plastic zone remain proportional to each other the following equations can be adopted for unloading

$$\Delta\sigma = 2\sigma_o \left[\frac{\Delta K^2}{4(1+n)\pi\sigma_o^2 x} \right]^{n/1+n}, \quad \Delta\varepsilon = 2\varepsilon_o \left[\frac{\Delta K^2}{4(1+n)\pi\sigma_o^2 x} \right]^{1/1+n}. \tag{22}$$

The product of stress and strain ranges is given by multiplying the above two equations

$$\Delta\sigma\Delta\varepsilon = \frac{\Delta K^2}{(1+n)\pi E x}. \tag{23}$$

The cyclic plastic zone size, r_c, can be approximated by setting $\Delta\sigma = 2\sigma_o, \Delta\varepsilon = 2\varepsilon_o$ in Eq.(23).

$$r_c = \frac{\Delta K^2}{4(1+n)\pi\sigma_o^2}. \tag{24}$$

Similarly, by setting $\sigma = \sigma_0$ in Eq.(23) the monotonic plastic zone, 'r_p' can be approximated as

$$r_p = \frac{K_{max}^2}{(1+n)\pi\sigma_o^2} \tag{25}$$

It has been shown by Kujawski and Ellyin [18] that Eq.(21) and Eq.(22) are only valid inside the monotonic and cyclic plastic zones respectively, whereas the elastic solution outside the plastic zones should be used. Assuming plane stress, the elastic stress and strain and their ranges can be calculated from the elastic solution given by:

$$\sigma_{max} = \frac{K}{\sqrt{2\pi x}}, \qquad \varepsilon_{max} = \frac{K}{E\sqrt{2\pi x}} \tag{26}$$

$$\Delta\sigma = \frac{\Delta K}{\sqrt{2\pi x}}, \qquad \Delta\varepsilon = \frac{\Delta K}{E\sqrt{2\pi x}} \tag{27}$$

While calculating the elastic solution from the Eq.(26) and Eq.(27), the distance 'x' should be offset by approximately half of the monotonic plastic zone size for the loading part, o_m, and by approximately half of the cyclic plastic zone for the unloading part, o_c. This offset is applied to make the prediction to be continuous at the monotonic and cyclic plastic zones.

The exact values of these offsets can be derived as follows:

At $x = r_p$, the value of stress by both the rice solution and elastic solution should be equal to the yield stress, σ_o.

Substituting $\sigma_{max} = \sigma_o$ and solving Eq.(21) for x,

$$x = \frac{K_{max}^2}{(1+n)\pi\sigma_o^2} \tag{28}$$

Solving for $x = x\text{-}o_m$ from elastic solution, Eq.(26) at r_p, with $\sigma_{max} = \sigma_o$

$$x - o_m = \frac{K_{max}^2}{2\pi\sigma_o^2} \tag{29}$$

Now substituting the value of 'x' from Eq.(28) into Eq.(29) and solving

$$o_m = \frac{1}{\pi}\left(\frac{K_{max}}{\sigma_o}\right)^2\left(\frac{1}{1+n} - 0.5\right) \tag{30}$$

Similarly the offset for the unloading part, o_c can be calculated by solving Eq.(22) and Eq.(27) at $x = r_c$.

$$o_c = \frac{1}{4\pi}\left(\frac{\Delta K}{\sigma_o}\right)^2\left(\frac{1}{1+n} - 0.5\right) \tag{31}$$

Once both the loading and the unloading profiles have been calculated, the stress profile for the minimum load is found out by subtracting the solution for unloading from the solution for loading. In this study, the Rice solution within the plastic zone and the elastic solution beyond this zone were adopted for the stress and strain calculation in the direction perpendicular to the crack plane.

Since both solutions exhibit a singularity as $x \rightarrow 0$, there exists a small region ahead of the crack tip called 'process zone' where, due to yielding and crack tip blunting, the stresses and strains have a finite magnitude. The stress and strain gradient in reality is much smaller in this region

than that predicted by analytical solutions. So for the predictions to be very close to the real behavior, the stresses and strains are assumed to be constant in the process zone. Fig.16 illustrates the stress and strain distribution ahead of the crack in mode I loading for 4140 steel for R =0.1 at two different load levels and Fig.17 illustrates the stress and strain distribution ahead of the crack tip for 4140 steel for R=0.5. Both the graphs have been plotted for a distance ahead of the crack tip, equal to twice the monotonic plastic zone size. As it was described above, the stress-strain distributions within and beyond the plastic zone have been evaluated adopting Rice and the elastic solution, respectively.

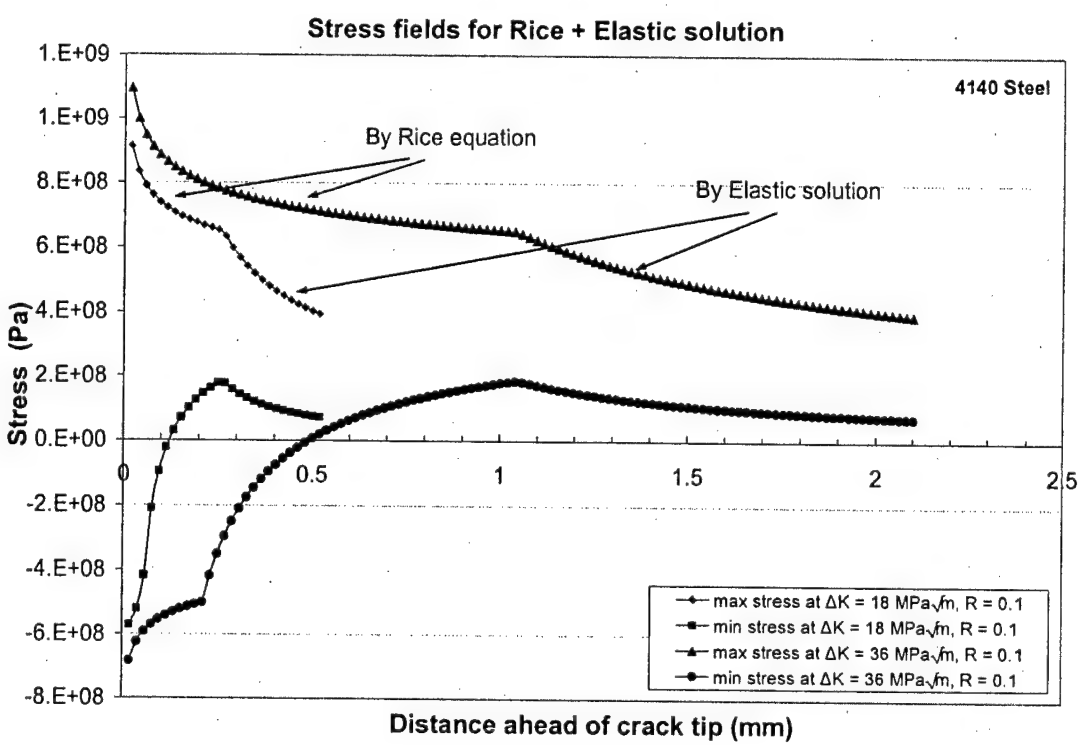

Figure 16. Stress distribution ahead of the crack tip for the 4140 steel at two applied ΔK values for R=0.1.

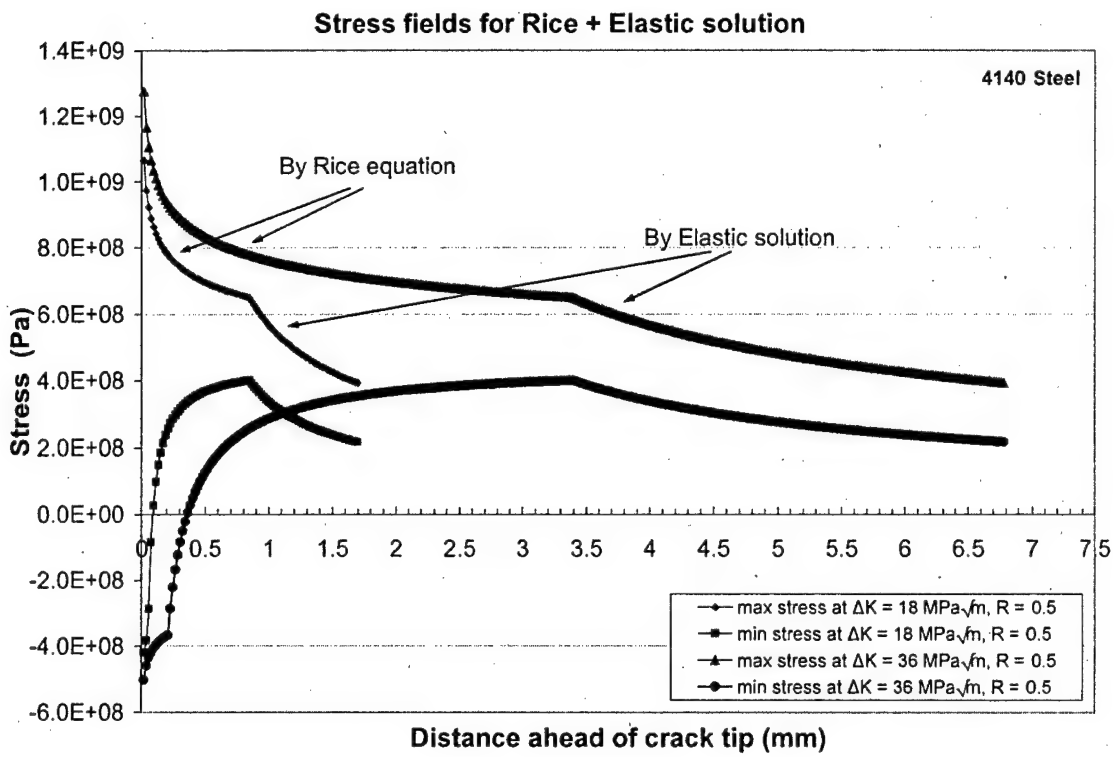

Figure 17. Stress distribution ahead of the crack tip for the 4140 steel at two applied ΔK values for R=0.5.

As it can be seen from the Fig.16 and Fig.17, the change in R-ratio from 0.1 to 0.5 with same ΔK, changes only the loading part of the profile and the monotonic plastic zone size. The unloading part of the profile and the cyclic plastic zone sizes are the same in both cases.

Also to be noted is the fact that very far away from the crack tip the local R-ratio reaches the applied R ratio. The corresponding mechanical properties for 4140 steel are listed in Table 1.

Table 1. Mechanical properties of 4140 and 4340 steel [15, 46, 47]

PROPERTY	SYMBOL	0050A steel	4340 STEEL	UNITS
Young's Modulus	E	205	209	GPa
Yield Stress	σo	645	724	MPa
Cyclic hardening exponent	n'	0.15	0.146	
Cyclic strength coefficient	H'	1640	1720	MPa
Fatigue strength coefficient	σ_f'	1530	1713	MPa
Fatigue ductility coefficient	ϵ_f'	0.65	0.83	
Fatigue strength exponent	b	-0.087	-0.095	
Fatigue ductility exponent	c	-0.6	-0.65	

Table 2. Mechanical properties of 2324-T39 and 7475 Al. alloy [59].

PROPERTY	SYMBOL	2324-T39 Al.	7475 Al.	UNITS
Young's Modulus	E	71	71	GPa
Yield Stress	σo	430	460	MPa
Cyclic hardening exponent	n'	0.106	0.11	
Cyclic strength coefficient	H'	877	977	MPa
Fatigue strength coefficient	σ_f'	927	1466	MPa
Fatigue ductility coefficient	ϵ_f'	0.4	0.262	
Fatigue strength exponent	b	-0.0642	-0.4985	
Fatigue ductility exponent	c	-0.4009	-0.088	

5. FAILURE CRITERION FOR SMOOTH SPECIMEN

Most engineering components and structures experience both alternating stresses 'σ_a' and a mean stress 'σ_m' during service life. Often defects or crack-like flaws, ranging from micro to macro sizes may be present which cause the stress-strain concentration. The local stress-strain field in the neighborhood of the crack governs the damage accumulation [7-13]. To correlate fatigue life, a proper damage parameter is needed that has an appropriate measure of mean stress effect and the applied stress-strain amplitude. The SWT parameter or the Morrow Equation can be used as a failure criterion to predict the failure life of the smooth specimen. In this analysis, the SWT parameter has been adopted to calculate the failure life (N_f) of each element ahead of the crack tip. The whole specimen is divided into the small elements of width ρ^* (see Fig.18) and each element is considered as a smooth uniaxial specimen for which the fatigue life can be estimated using the SWT parameter or Morrow equation. The crack advances by one element when the failure criterion for that element is met. The failure criterion is based on damage accumulation, and is explained in the sections ahead.

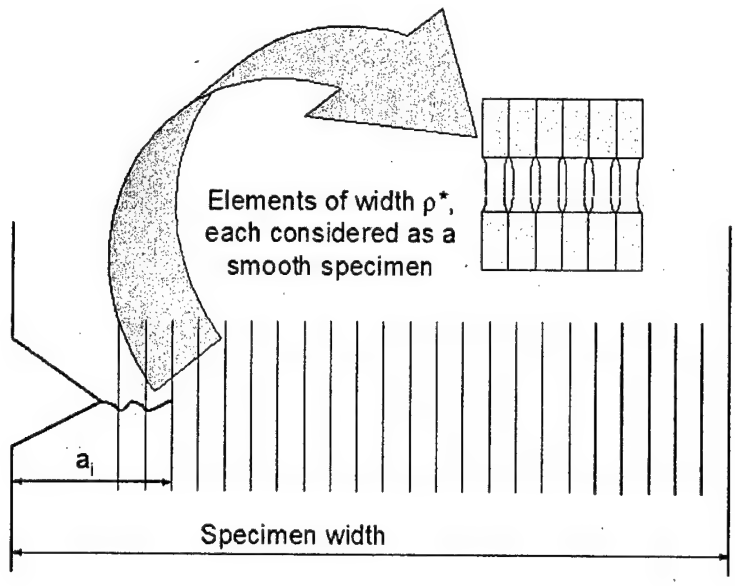

Figure 18. Representation showing the elements ahead of the crack tip considered as smooth specimens.

5.1 SMITH-WATSON-TOPPER (SWT) PARAMETER

The SWT equation for a smooth specimen can be written as

$$\sigma_{max}\varepsilon_a = \sigma_{max}\frac{\Delta\varepsilon}{2} = \frac{\sigma'^2_f}{E}(2N_f)^{2b} + \sigma'_f\,\varepsilon_f'(2N_f)^{b+c} \tag{32}$$

Since $\sigma_{max} = \dfrac{\Delta\sigma}{2(1-R)}$, by substituting this into Eq.(32)

In a modified form SWT can be written in terms of the stress and strain ranges as

$$\frac{\Delta\sigma\Delta\varepsilon}{2(1-R_{\rho*})} = \frac{\sigma'^2_f}{E}(2N_f)^{2b} + \sigma'_f\,\varepsilon_f'(2N_f)^{b+c} \tag{33}$$

Eq.(33) was obtained using $\sigma_{max} = \dfrac{\Delta\sigma}{1-R_\rho}$ where $R_\rho = (\sigma_{min}/\sigma_{max})_\rho$, is the stress ratio in the process zone, ρ*.

Eq.(33) results in a single curve, which can be drawn for various values of N_f vs. the SWT parameter, LHS of Eq.(33).

The failure life N_f can be evaluated faster by interpolating the values from the SWT curve rather than solving the equation numerically.

The RHS of Eq.(33) has two parts:

The elastic part, $\dfrac{\sigma_f'^2}{E}(2N_f)^{2b}$ and the plastic part, $\sigma_f'\,\varepsilon_f'\,(2N_f)^{b+c}$

Fig.19 shows the modified SWT curve for 4140 steel consisting of 250 values of N_f equally spaced on a log-log plot.

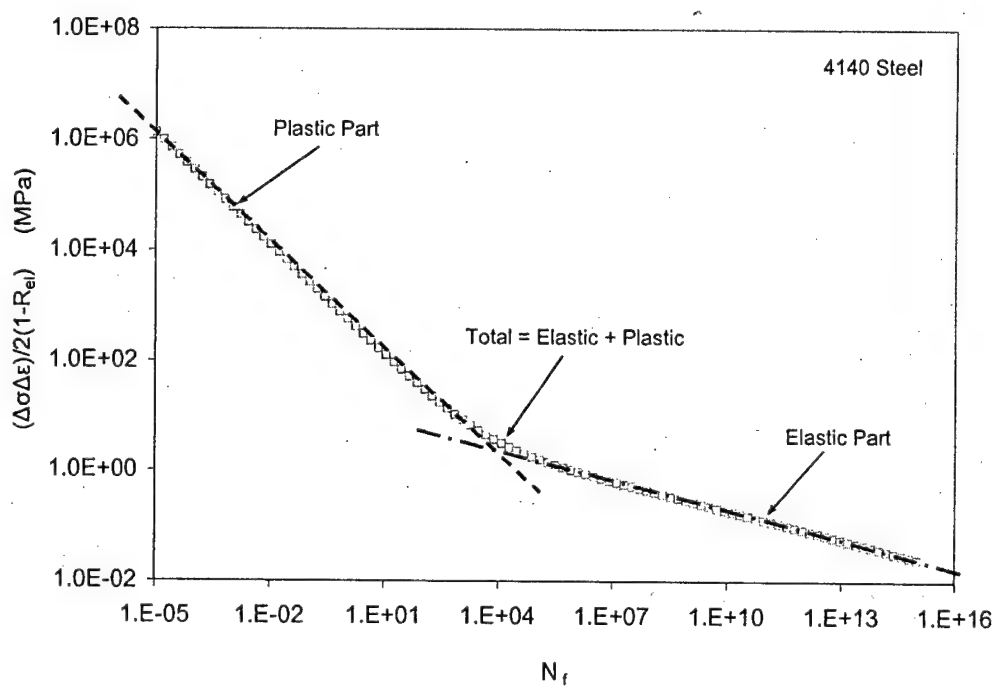

Figure 19. The plot of the modified SWT curve for 4140 steel.

Slope of the elastic part and plastic part is different for different materials, and depend on the exponents 'b' and 'c'. Also the transition point between the elastic part and plastic part is important in the crack growth prediction, which will be discussed in detail in the sections ahead.

Table 3. Mechanical properties of A533-B1 and C-Mn steel [15].

PROPERTY	SYMBOL	A533-B1 STEEL	C-Mn STEEL	UNITS
Young's Modulus	E	200	208	GPa
Yield Stress	σo	345	372	MPa
Cyclic hardening exponent	n'	0.165	0.141	
Fatigue strength coefficient	$\sigma f'$	869	868	MPa
Fatigue ductility coefficient	$\epsilon f'$	0.32	0.15	
Fatigue strength exponent	b	-0.52	-0.514	
Fatigue ductility exponent	c	-0.6	-0.101	

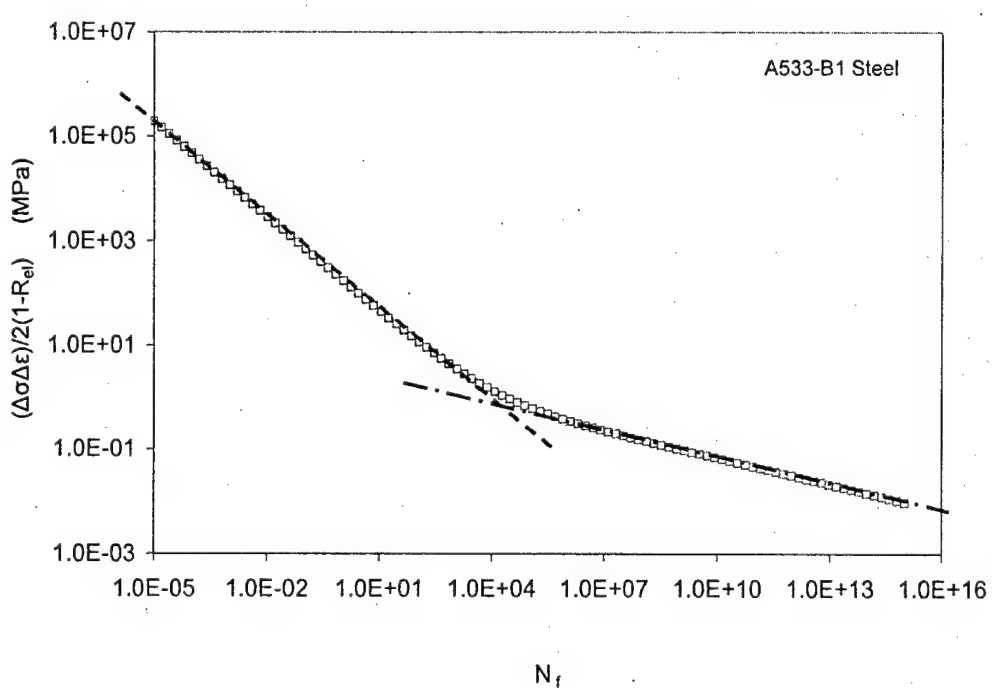

Figure 20. The plot of the modified SWT curve for A533-B1 steel.

5.2 MORROW EQUATION

The approach suggested by Morrow can be expressed as an equation giving the equivalent completely reversed stress amplitude, σ_{ar}, which is expected to produce the same life as given by combination of stress amplitude σ_a and mean stress σ_m.

$$\sigma_{ar} = \frac{\sigma_a}{1 - \frac{\sigma_m}{\sigma_f'}} \tag{34}$$

The stress life equation for completely reversed loading is

$$\sigma_{ar} = \sigma_f' (2N_f)^b \tag{35}$$

By combining Eq.(34) with Eq.(35), where σ_f' and b are evaluated for zero mean stress or R-ratio = -1.

$$\sigma_a = \sigma_f' \left[\left(1 - \frac{\sigma_m}{\sigma_f'} \right)^{\frac{1}{b}} (2N_f) \right]^b \tag{36}$$

Comparing it to Eq.(35) the effect of mean stress on N_f is such that

$$N^* = N_f \left(1 - \frac{\sigma_m}{\sigma_f'} \right)^{\frac{1}{b}} \tag{37}$$

Applying same modification to the strain-life equation

$$\varepsilon_a = \frac{\sigma_f'}{E} (2N^*)^b + \varepsilon_f' (2N^*)^c \tag{38}$$

By substituting N* value into Eq.(38) and neglecting the mean stress effect on the plastic strain part (second term) in Eq.(38) a single equation for family of strain-life curves can be obtained.

$$\varepsilon_a = \frac{\sigma_f'}{E}\left(1-\frac{\sigma_m}{\sigma_f'}\right)(2N_f)^b + \varepsilon_f'(2N_f)^c \tag{39}$$

The convenient graphical procedure for solving this equation can be, plotting the strain-life curve at zero mean stress. And for any mean stress, first the N* values can be read from the curve, which can be solved with Eq.(37) to get the N_f value for any mean stress.

This kind of approach with graphical procedure is shown in the Fig.21 below:

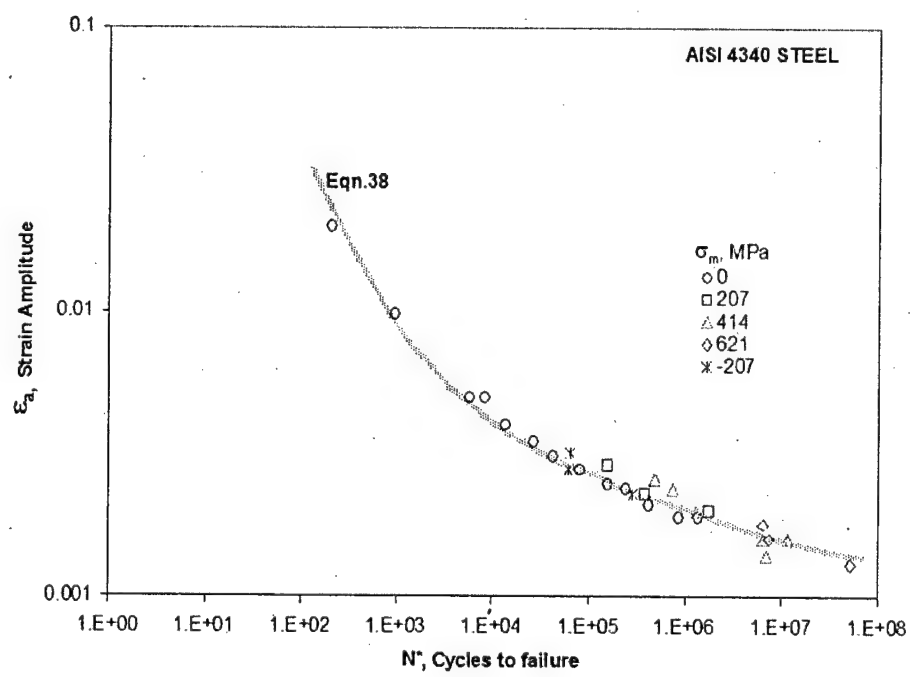

Figure 21. Mean stress data for AISI 4340 Steel, plotted vs. N* according to the Morrow equation.

If the family of strain-life curves is plotted it would look like shown in Fig.22, but it will be a long and time consuming method to interpolate the values between this family of the curves.

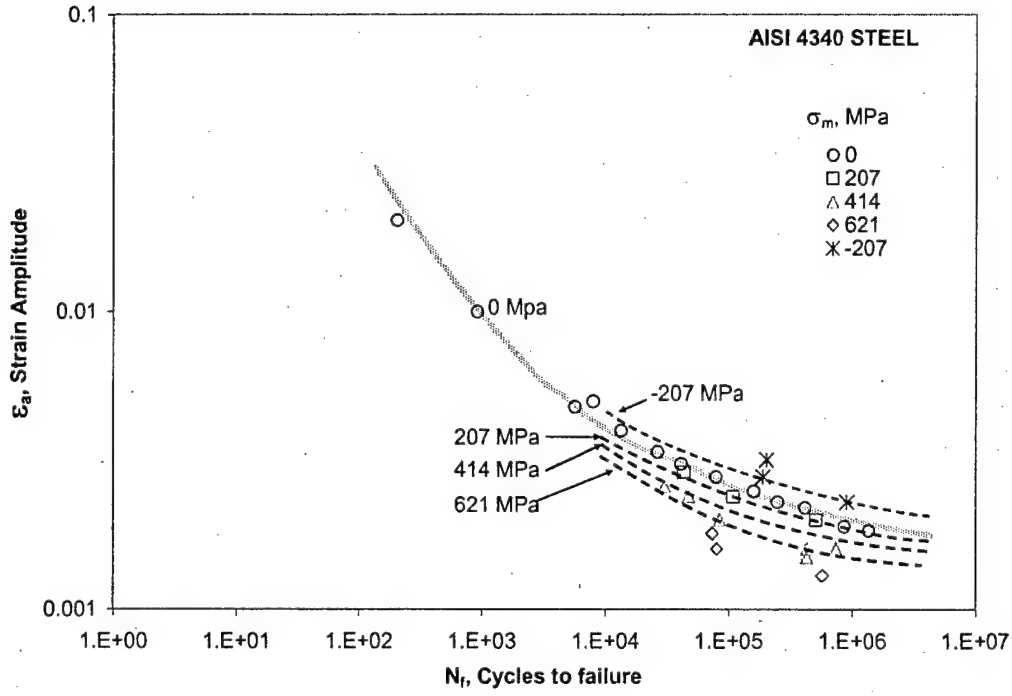

Figure 22. Family of strain life curves for 4340 Steel plotted vs. N_f according to the Morrow equation.

Both the approaches SWT and Morrow equation are in current use, and no consensus exists that any one of them is superior to the other. The data shown in Fig.21 is plotted in Fig.23 using the SWT equation.

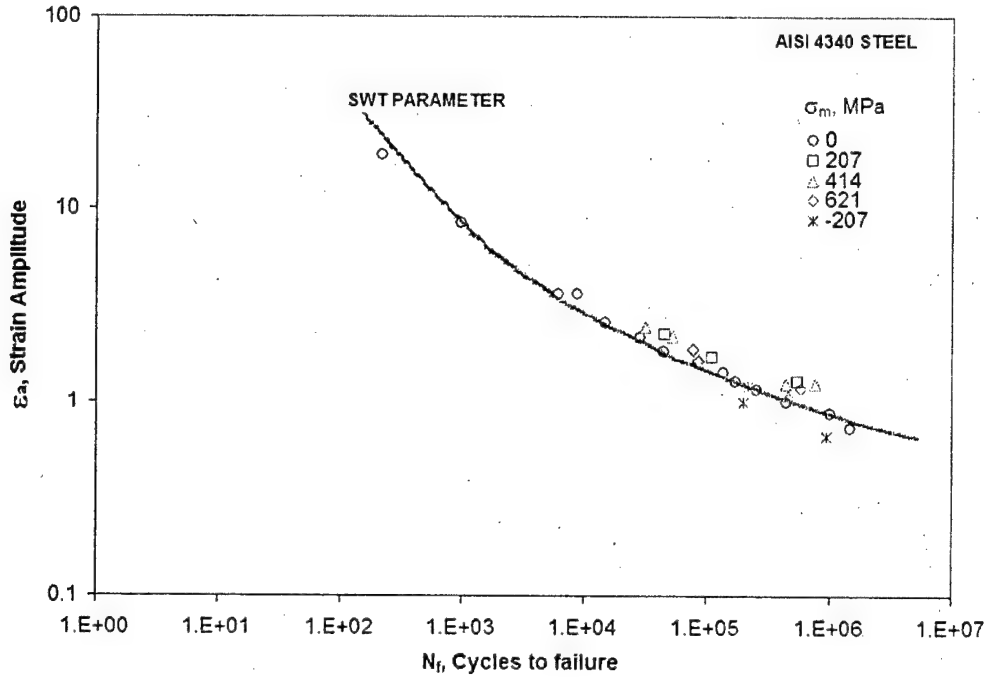

Figure 23. Mean stress data for AISI 4340 Steel, plotted vs. N_f according to the SWT parameter.

Morrow approach gives good results for steels, and in some cases it gives better results than the SWT parameter. However for some aluminum alloys SWT gives better results.

Dowling [3] concludes that SWT parameter appears to give good results for wide range of materials and is a good choice for general use. However, it may give non-conservative estimates for compressive mean stresses. Where refinement is desired, the choice among these parameters can only be based on fatigue test data involving mean stresses. In the present study SWT parameter will be used for all the calculations and driving force derivations.

6. RELATION BETWEEN SWT AND ΔK* PARAMETER

Recently, Glinka [40] derived the relation between the exponent α in the two parameter crack driving force equation $\Delta K^* = (K_{max})^{\alpha}(\Delta K^+)^{1-\alpha}$ proposed by Kujawski [41] and the cyclic strain hardening exponent n' utilizing the SWT parameter. He used the generalized Neuber law for the stress and strain calculation in the material elements at the crack tip region. A similar analysis is presented in this section where the stresses and strains in the crack tip region are calculated using modified Rice and elastic solutions discussed in the previous section.

The un-cracked region of the specimen is divided into small elements of width equal to ρ^* as shown in Fig.24. It is assumed that due to cyclic loading the significant fatigue damage is accumulated predominately in the first element of width ρ^* called the process zone. When the accumulated fatigue damage in the process zone reaches a critical value according to the SWT parameter, the crack tip will advance to the next element and the process is repeated. In other words, it is assumed that the material in the process zone can be considered as a hypothetical uniaxial specimen.

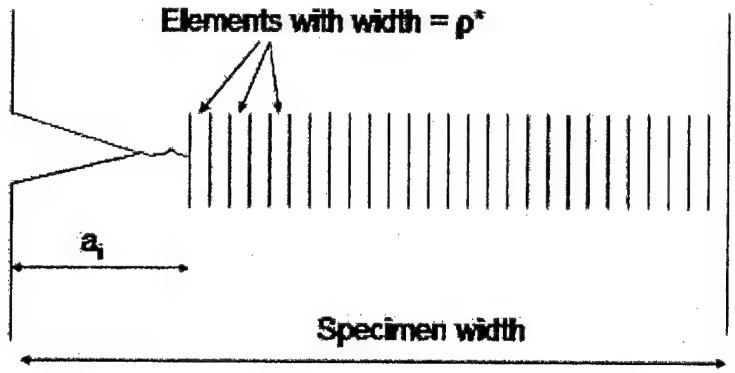

Figure 24. Schematic of the specimen divided into elements of width ρ^*.

It can be assumed that in the Paris region of crack growth the local deformation in the crack tip process zone is dominated by the plastic strain.

The corresponding plastic part of the SWT Eq.(32) is

$$\sigma_{max}\frac{\Delta\varepsilon}{2}=\sigma'_f\,\varepsilon_f'(2N_f)^{b+c} \tag{40}$$

From Rice solution Eq.(21) and Eq.(22) one obtains

$$\sigma_{max}\frac{\Delta\varepsilon}{2}=\sigma_0\left[\frac{K_{max}^2}{(1+n')\pi\sigma_0^2 x}\right]^{\frac{n'}{(1+n')}}\varepsilon_0\left[\frac{\Delta K^2}{4(1+n')\pi\sigma_0^2 x}\right]^{\frac{1}{(1+n')}} \tag{41}$$

Substituting RHS of Eq.(40) into Eq.(41) and after rearrangement the following relationship is obtained

$$\sigma'_f \varepsilon_f'(2N_f)^{b+c} = \left[\frac{4^{\frac{-1}{(1+n')}}}{(1+n')\pi E x}\right]\left[(K_{max})^{\frac{n'}{(1+n')}}(\Delta K)^{\frac{1}{(1+n')}}\right]^2 \tag{42}$$

Setting x = ρ* and solving for N_f

$$N_f = \frac{1}{2}\left[\frac{4^{\frac{-1}{(1+n')}}}{(1+n')\pi E \sigma'_f \varepsilon_f' \rho^*}\right]^{\frac{1}{b+c}}\left[(K_{max})^{\frac{n'}{(1+n')}}(\Delta K)^{\frac{1}{(1+n')}}\right]^{\frac{2}{b+c}} \tag{43}$$

Where N_f is a number of cycles required to break the process zone element and to advance the crack by the 'process zone' size ρ^*. Therefore, the corresponding average rate of crack growth, da/dN, can be calculated as

$$\frac{da}{dN} \cong \frac{\rho^*}{N_f} = (2\rho^*)\left[\frac{4^{\frac{-1}{(1+n')}}}{(1+n')\pi E \sigma'_f \varepsilon_f' \rho^*}\right]^{\frac{-1}{b+c}}\left[(K_{max})^{\frac{n'}{(1+n')}}(\Delta K)^{\frac{1}{(1+n')}}\right]^{\frac{-2}{b+c}} \tag{44}$$

The average crack growth rate in the Paris region can be expressed in the following form

$$\frac{da}{dN} = C_P[\Delta K^*]^{m_P} \tag{45}$$

Where $\Delta K^* = (\Delta K^+)^{1-\alpha}(K_{max})^{\alpha}$ is the two parameter driving force proposed by Kujawski [41] and C_P and m_P are fitting parameters.

Comparing Eq.(44) with Eq.(45) the corresponding exponents are related as

$$m_P = \frac{-2}{b+c} \quad , \quad \alpha = \frac{n'}{1+n'} \tag{46}$$

A similar analysis can be carried out for the near threshold region, where the crack growth is dominated by elastic stress and strain.

Thus, the elastic part of the SWT Eq.(32) will have the form of

$$\sigma_{max}\frac{\Delta\varepsilon}{2} = \frac{\sigma_f'^2}{E}(2N_f)^{2b} \tag{47}$$

The stress and strain at the process zone ρ* can be calculated using the elastic solution, Eq.(31) by setting x = ρ*

$$\sigma_{max}\frac{\Delta\varepsilon}{2} = \frac{K_{max}}{\sqrt{2\pi\rho^*}}\frac{\Delta K}{E\sqrt{2\pi\rho^*}} \tag{48}$$

Equating RHS of Eq.(47) and Eq.(48) and solving for N_f one gets

$$N_f = \frac{1}{2}\left(\frac{K_{max}\Delta K}{4\pi\rho^*\sigma_f'^2}\right)^{\frac{1}{2b}} \tag{49}$$

Considering that N_f cycles are required to propagate the crack by the process zone size ρ^*

$$\left(\frac{\rho^*}{N_f}\right) \cong \frac{da}{dN} = 2\rho^*\left[4\pi\sigma_f'^2\rho^*\right]^{\frac{1}{2b}}\left[K_{max}^{\frac{1}{2}}\Delta K^{\frac{1}{2}}\right]^{-\frac{1}{b}} \tag{50}$$

The average crack growth rate in the near threshold region can be expressed in the following form

$$\frac{da}{dN} = C_{th}\left[\Delta K^*\right]^{m_{th}} \tag{51}$$

Comparing Eq.(50) with Eq.(51) and Eq.(45), the following relations result

$$m_{th} = \frac{-1}{b}, \quad \text{and} \quad \alpha = \frac{1}{2} \tag{52}$$

The relations (46) and (52) demonstrate that the exponents of fatigue life and crack growth equations (or the slopes of the corresponding curves in log-log coordinates) are interrelated. They also show that the exponent α in the two parameter driving force, ΔK^*, is decreasing from ½ at the near threshold region to n'/ (1+n') at the Paris region. This indicates that sensitivity to K_{max} is decreasing with increasing crack growth rate.

In the following, a parametric study is presented that illustrates the sensitivity of the relationship between the slopes of the SWT curve, SWT vs. N_f, and the crack growth rate curve, da/dN vs. ΔK, in both elastic or the near threshold and plastic or the Paris regions. Fig.25 shows the relation between the slopes of the curves in the elastic region of the SWT plot versus the near threshold region of the crack growth. The relation corresponding to the plastic region of the SWT plot versus the Paris region of the crack growth is depicted in Fig.26. Both figures indicate the same trend. In particular, Fig.25 indicates that the variations in the slope of the elastic part of the SWT plot affect only the near threshold slope of the da/dN vs. ΔK predictions. Similarly, Fig.26 shows that for the slope variations of the plastic part of the SWT, the corresponding changes

occurred only in the Paris region slope of the da/dN vs. ΔK. It can be noted that somewhat higher sensitivity is observed in the elastic and the near threshold regions in comparison to the plastic and the Paris regions. This is consistent with the Eq.(46) and Eq.(52) for the Paris and the near threshold regions, respectively.

In Figs.25 and 26 some fluctuations in the predicted curves can be seen at the lower part of the Paris region. In the simulation, two straight lines with a sharp knee point were used instead of actual smooth SWT curve. This simplified representation of SWT curve resulted in fluctuations in the predicted curves when the corresponding lives of the crack tip elements were spread around the sharp knee point.

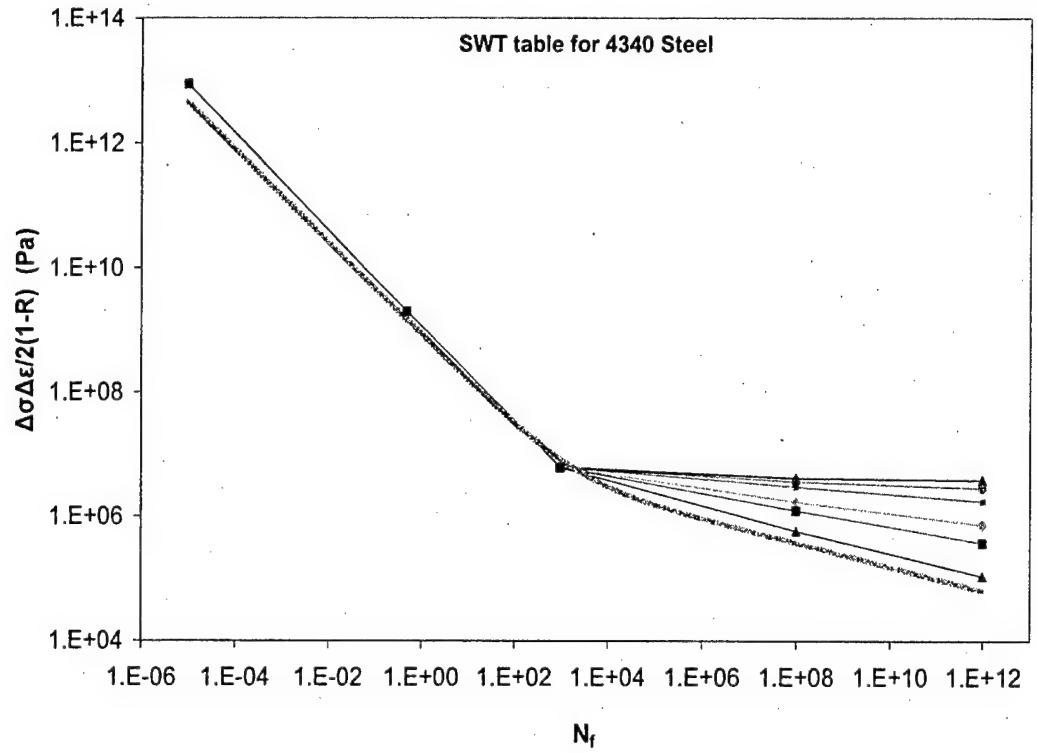

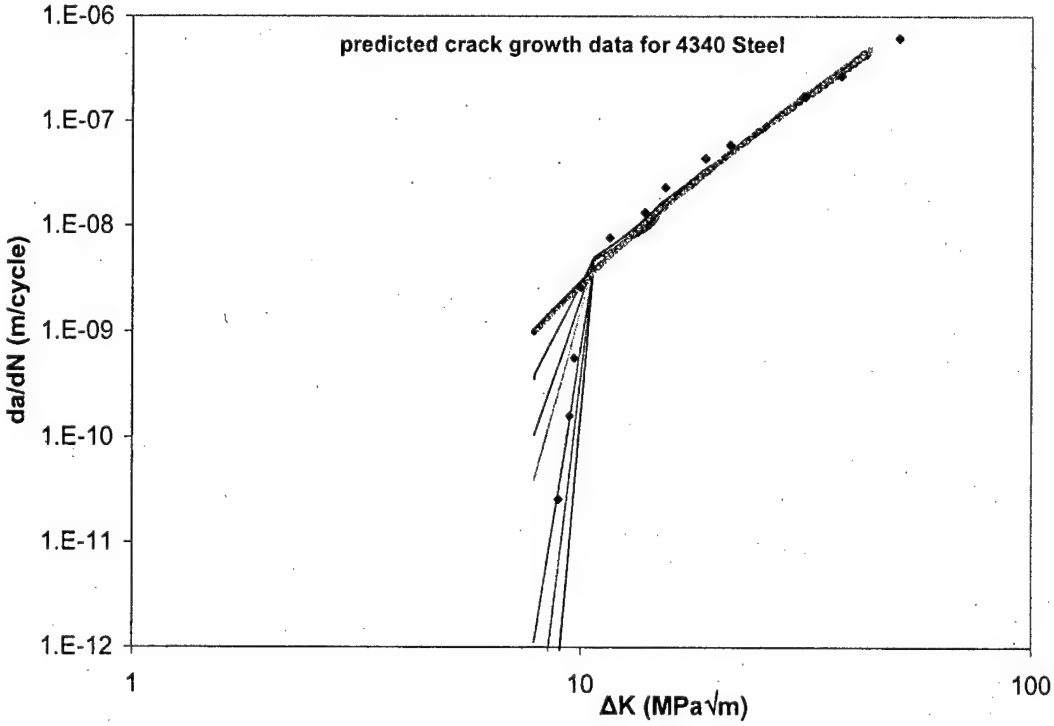

Figure 25. The relation between the elastic region of SWT and the near threshold region of the crack growth curve.

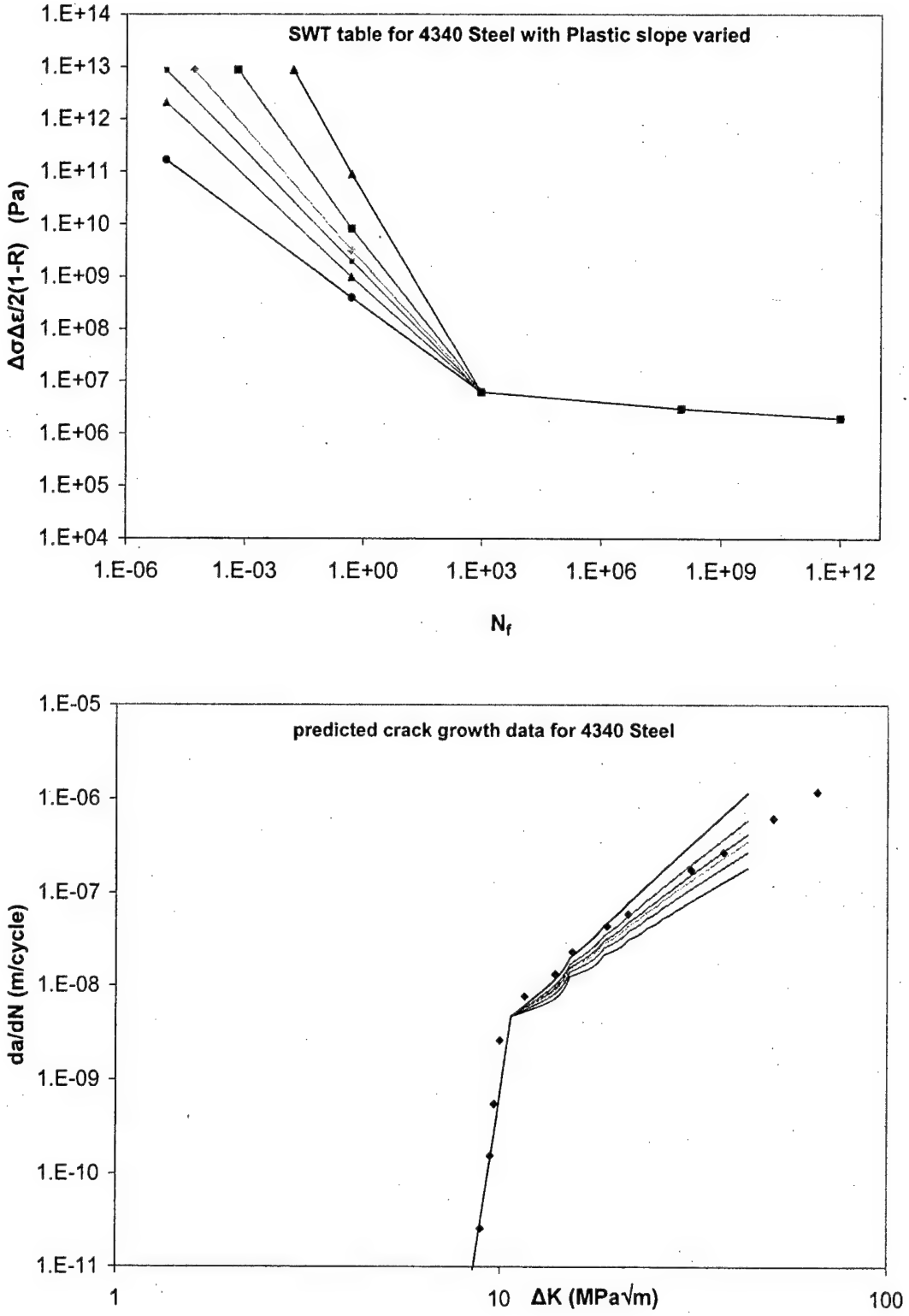

Figure 26. The relation between the plastic region of SWT and the Paris region of the crack growth curve.

7. DETERMINATION OF THE CRACK-TIP ELEMENT SIZE, ρ^*

The determination of the crack tip element size or the process zone size, ρ^*, is very important because it defines the distance ahead of the crack where the stress profile has a very low gradient due to yielding of the material and crack-tip blunting. The process zone size has been taken as constant by many researchers like Glinka [10-12], Ellyin and Kujawski [15-18, 42] and Antolovich [43]. Other researchers believe that the process zone size is variable and is dependant on ΔK [44] or it may be linked to the microstructure or the grain size of the material [45].

In this model, the process zone is considered to be constant for a given material. The process zone size, ρ^*, is calculated using one point of the crack growth rate data. This point corresponds to the transition between the Paris and near-threshold regions on the crack growth curve. It can be taken as the point of intersection of the best fit lines for the near-threshold region and the Paris region. Fig.27 shows a simplistic view, as to how this 'knee-point' is determined from the experimental data.

This knee-point should satisfy the driving force equations for both the Near-threshold region and the Paris region. By comparing these two driving forces at the knee-point, a relation for ρ^* can be obtained.

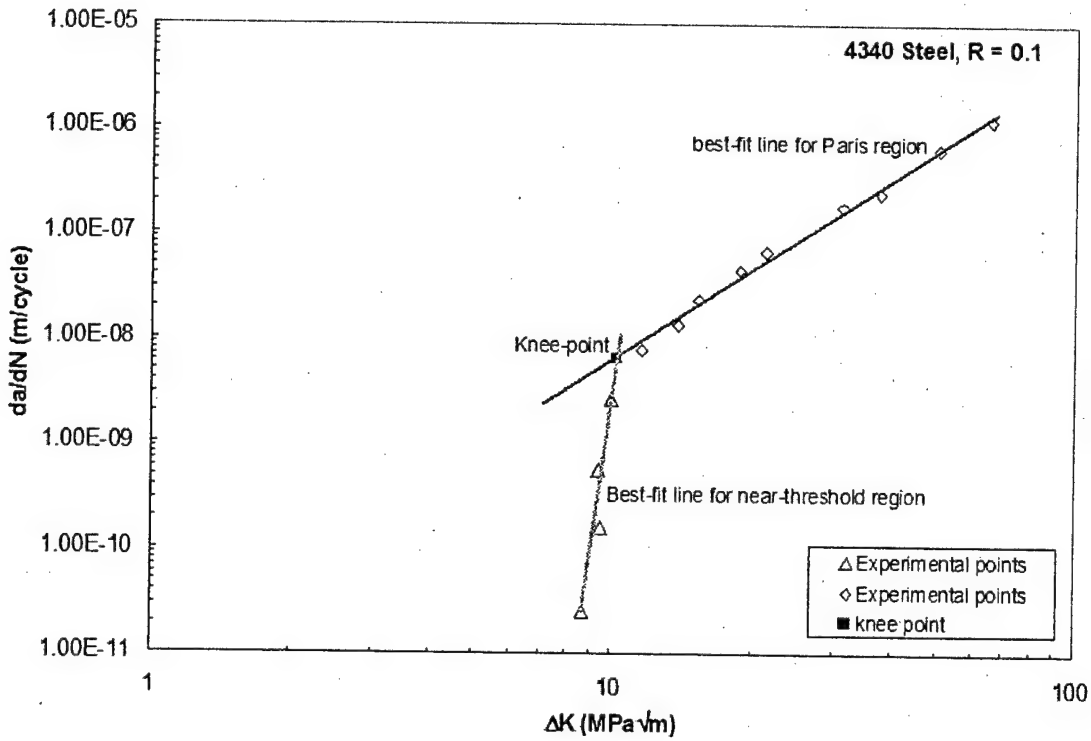

Figure 27. Best-fit line approach to determine the knee-point for the ρ* determination.

This point once determined, should provide the same da/dN for both the equations for crack growth rate in Paris region and the near-threshold region.

The expression for crack growth rate in Paris-region from Eq.(44)

$$\frac{da}{dN} \cong \frac{\rho^*}{N_f} = (2\rho^*)\left[\frac{4^{\frac{-1}{(1+n')}}}{(1+n')\pi E\sigma'_f\,\varepsilon_f'\,\rho^*}\right]^{\frac{-1}{b+c}}\left[(K_{max})^{\frac{n'}{(1+n')}}(\Delta K)^{\frac{1}{(1+n')}}\right]^{\frac{-2}{b+c}} \qquad (53)$$

And expression for da/dN in near-threshold region from Eq.(50)

$$\left(\frac{\rho^*}{N_f}\right) \cong \frac{da}{dN} = 2\rho^* \left[4\pi\sigma'^2_f \rho^*\right]^{\frac{1}{2b}} \left[K_{max}^{\frac{1}{2}} \Delta K^{\frac{1}{2}}\right]^{-\frac{1}{b}} \tag{54}$$

Comparing the Eq.(53) and Eq.(54) for same da/dN at the knee-point following equation is derived, which represents the final expression that is used to calculate ρ^*.

$$(\rho^*) = \left[\frac{\left[4^{\frac{1}{(1+n')}}(1+n')\pi E\sigma'_f \varepsilon_f'\right]^{\frac{1}{b+c}} \left[(K_{max})^{\frac{n'}{(1+n')}} (\Delta K)^{\frac{1}{(1+n')}}\right]^{\frac{-2}{b+c}}}{\left[4\pi\sigma'^2_f\right]^{\frac{1}{2b}} \left[K_{max}^{\frac{1}{2}} \Delta K^{\frac{1}{2}}\right]^{-\frac{1}{b}}}\right]^{\frac{1}{\frac{1}{2b} - \frac{1}{b+c}}} \tag{55}$$

8. ACCUMULATION OF DAMAGE AHEAD OF CRACK-TIP

Damage accumulation in the elements ahead of the crack tip is controlled by the Palmgren-Miner linear damage rule. Failure life for each element is calculated using the SWT failure criterion. Damage is stored in the elements within the plastic zone only, as it was seen that the damage past the plastic zone is negligible and can be considered as zero. The element is considered to fail when the damage in the element reaches unity. The detailed explanation of damage accumulation process and the element failure is presented ahead (see section 9).

The important thing to notice is the gradient of the damage ahead of the crack tip. Fig.28 and Fig.29 show the accumulated damage at steady state in the elements ahead of the crack tip for various K_{max} and R-ratio values. It can be seen in Fig.28 that the gradient of the accumulated damage is very high close to the crack tip, and the majority of the damage is in the elements within the cyclic plastic zone. After the cyclic plastic zone the gradient of the accumulated damage becomes nearly constant, at which point the damage is not very high.

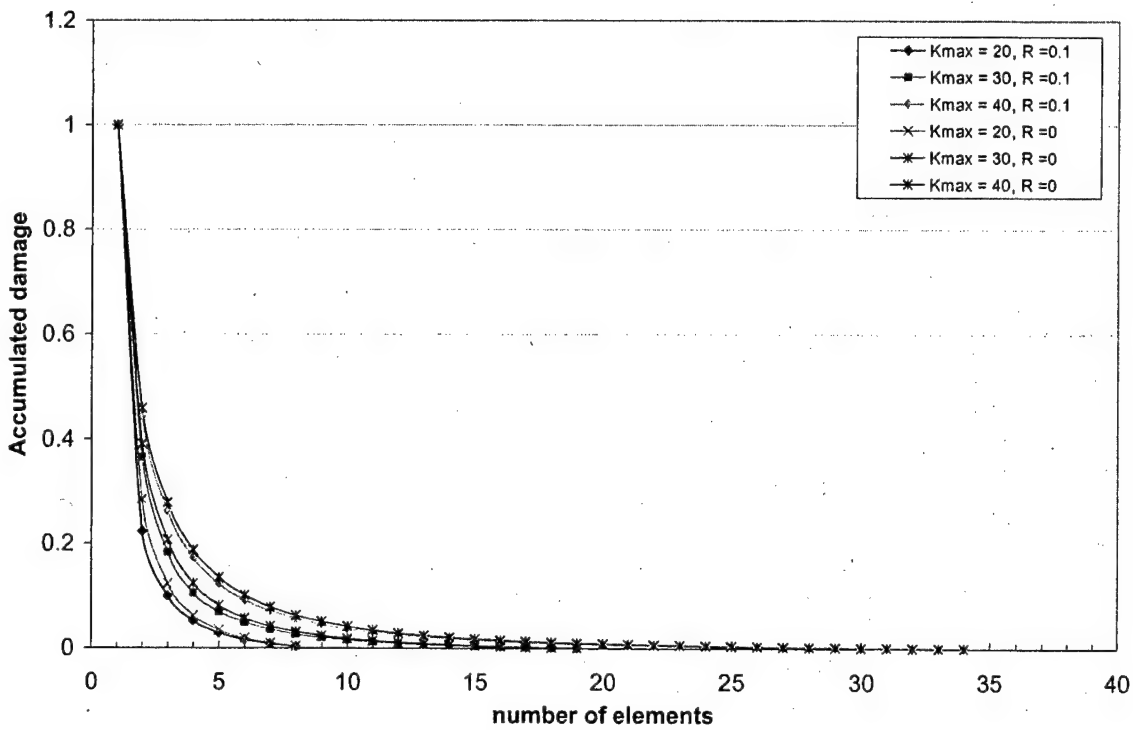

Figure 28. Accumulated damage distribution in elements for 4140 steel (linear scale).

Another important thing which can be noted from Fig.29 i.e. the log-log plot of damage accumulation is, that K_{max} controls the extent of the damage zone i.e. the monotonic plastic zone size, and ΔK values control the amount of damage in the elements. The data has been compared for R-ratio 0.1 and 0, It can be noted that for the same K_{max} value, accumulated damage is more for R = 0.

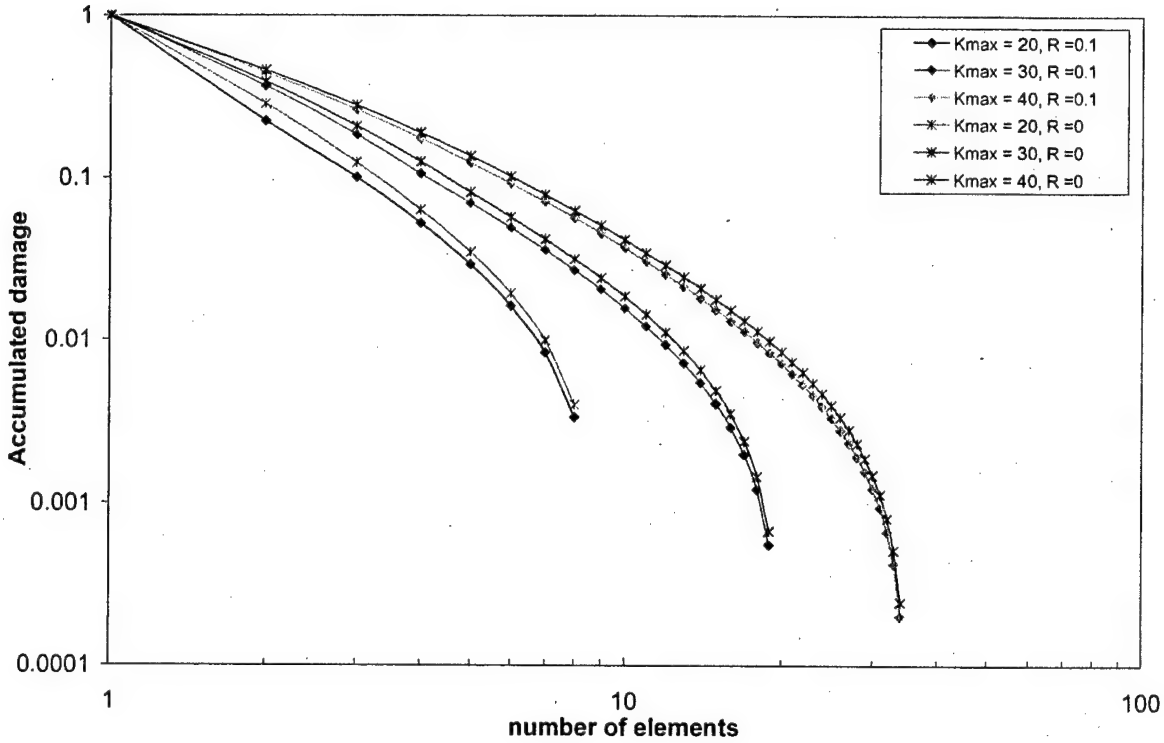

Figure 29. Accumulated damage distribution in elements for 4140 steel (log-log scale).

As explained above, Fig.28 and Fig.29 show the fact that the main damage accumulation ahead of the crack tip is in cyclic plastic zone, some damage of a very small magnitude is there up to the monotonic plastic zone, after that the damage is almost negligible. This is supported by the statements in references [7-12, 15-18], explained on the basis of the gradient of the stress-strain profiles.

9. CALCULATION OF THE CRACK GROWTH RATE

In the present approach, the un-cracked region of the specimen is modeled as a set of uniaxial specimens of width equal to ρ^*, see Fig.24. Then, for a given load cycle the maximum and minimum stress-strain distribution ahead of the crack tip is determined using the Rice and elastic solutions discussed earlier.

For every crack tip element, the SWT parameter term $\frac{\Delta\sigma\Delta\varepsilon}{2(1-R_{el})}$ is calculated

Where R_{el} is the local stress ratio of $\sigma_{min}/\sigma_{max}$ for that particular element. Based on the product for the SWT parameter, the fatigue life N_f for each element is determined.

Damage stored in i^{th} element is

$$d = \frac{N_f^i}{N_f^1} + (\text{previous damage } 'd^i') \tag{56}$$

Where N_f^1 = Fatigue life of 1st element, N_f^i = Fatigue life for the ith element.

For any previously damaged element, when crack tip arrives at that element the remaining fatigue life is calculated by using the Palmgren-Miner 'linear damage rule' [22], and by keeping track of how much previous damage 'd' is present in that element.

So the remaining failure life for an element is calculated as

$$N_r = (1-d)N_f \tag{57}$$

Basically, this gives the number of cycles required to make damage equal to one in that element at crack tip, which is considered broken when the damage 'd' reaches the value of 1.

Similarly, the damage for the elements from 2nd element onwards can be calculated by using this value of remaining life 'N_r' from Eq.(57) in the following way:

$$d_{new} = \frac{N_r}{N_f^1} + d_{stored} \tag{58}$$

The crack growth rate da/dN is found by dividing element width 'ρ^*' by the number of cycles, N_r, required to break this element at crack tip. Given by equation:

$$\frac{da}{dN} \cong \frac{\rho^*}{N_r} \tag{59}$$

This process is repeated for every element and the crack is propagated by one element each time, hence accumulating the damage in the elements ahead of the crack tip and breaking the elements for damage equal to unity.

Fig.30 and Fig.31 ahead, show the experimental and the predicted data using the above discussed damage accumulation approach, Eq.(59), for the 4140 steel and the 4340 steel respectively.

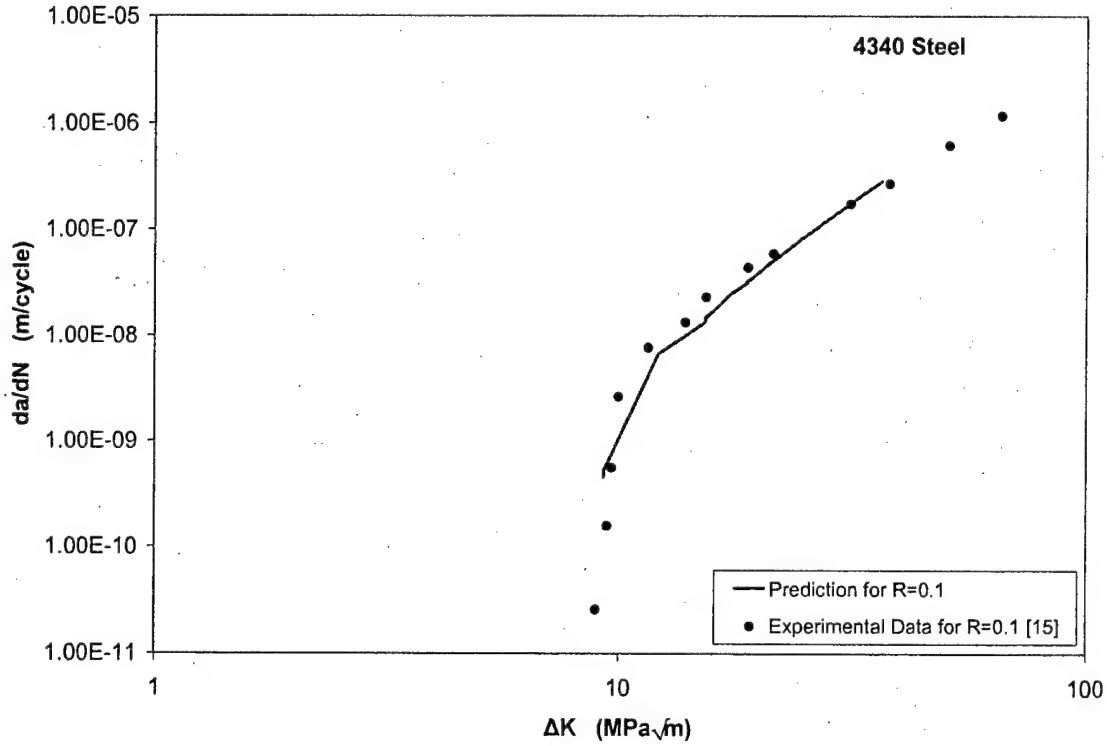

Figure 30. Predicted vs. Experimental crack growth data for 4340 steel, at R =0.1 and $\rho^* = 1.56e^{-5}$.

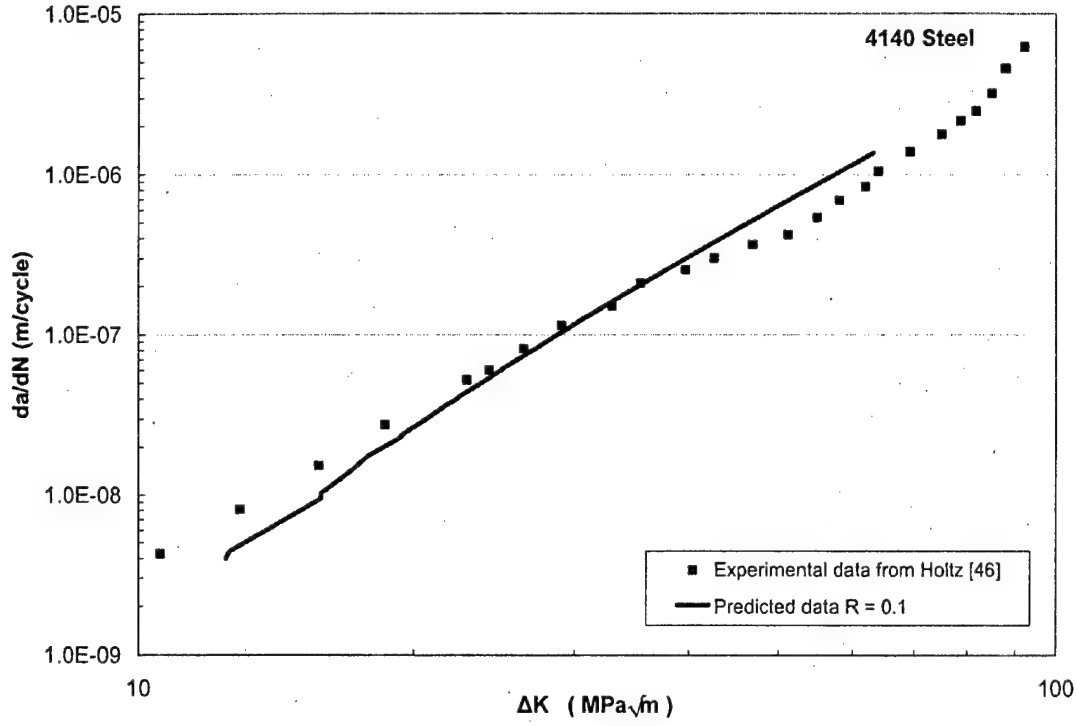

Figure 31. Predicted vs. Experimental crack growth data for 4140 steel, at R =0.1 and $\rho^* = 2.05e^{-6}$.

It can be noted from the predictions that the model works well for constant amplitude loading. The ρ^* parameter has been fitted to the experimental data for this prediction.

Any R-ratio can be predicted with this model, condition being that the experimental data should be known before hand, so that ρ^* can be determined.

More predictions have been shown for various materials at different R-ratios in Appendix-A.

10. OVERLOAD EFFECTS ON CRACK GROWTH RATE

The accurate prediction of fatigue crack growth behavior under variable amplitude loading depends on accurate modeling of load-interaction effects, one important load interaction effect being the retardation of fatigue crack growth due to application of an overload [48].

Extensive investigations have been conducted [1-5 in 49] in an attempt to explain the phenomenon of crack growth retardation resulting from tensile overloads. These investigations have resulted in proposal of several crack growth retardation theories. In general, these theories attribute delayed retardation behavior to crack closure [27], residual stresses [49, 50, 51], or a combination of these mechanisms [52].

The crack closure theory suggests that the delay in fatigue crack growth is caused by the formation of a zone of residual tensile deformation left in the wake of propagating crack. This deformation causes the crack to remain closed during a portion of applied tensile load cycle. Hence, the crack extends only due to the portion of the load cycle that is above the crack opening level.

The residual theory is somewhat similar to the crack closure theory except that it attempts to account for the crack growth based on actual forces acting at the crack tip. It focuses more on what is happening ahead of the crack tip and at the crack tip. This theory suggests that the application of high tensile load cycle forms residual compressive stresses in the vicinity of the crack tip, and these stresses reduce the rate of fatigue crack growth.

Lang [51] reports that the major restraint to crack extension is caused by residual compressive stresses ahead of the crack tip. Residual compressive stresses are the result of a reverse plastic zone created after a remote tensile stress has been removed.

In this study, an attempt has been made to model the residual/internal stress profiles ahead of the crack tip based on the data from the literature, to explain the crack growth retardation due to overload and effects on crack growth due to block loading.

10.1 MODELING RESIDUAL/INTERNAL STRESSES

The first objective for this kind of modeling should be to investigate the distribution of residual stresses and to determine the correlation of these measurements with the residual stress theories.

Experimental test results for the measurements of the residual stresses at the crack tip, before and after application of the overload have been analyzed; from the studies that measured the stress distributions in the vicinity of the crack tip by x-ray diffraction techniques [49, 50 and 52]. Holloway [49] in his study measured the residual stress profiles before and after the overload, and after some crack extension from the point of application of the overload for 1020 Steel.

The residual stress profiles before and after the overload are shown in Fig.32, The overload is twice of the base maximum load.

It can be noted from the Fig.32 that the residual stress at the crack tip is quite bigger than the base load. The point of minimum stress is the point of application of overload.

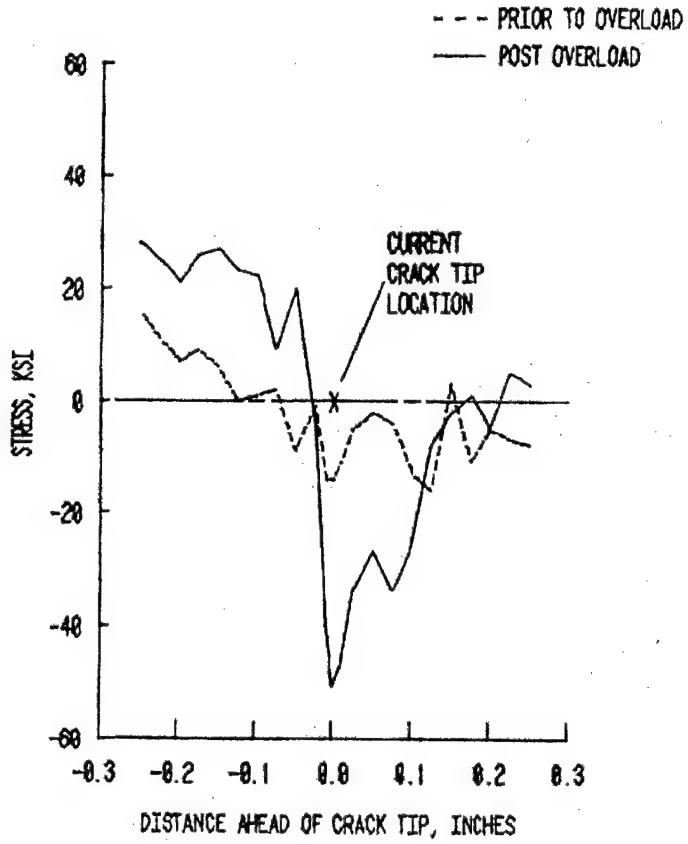

Figure 32. Residual stress profiles measured by x-ray diffraction in 1020 Steel before and after the overload [49].

Residual stress profile after overload and residual stress profile after a crack extension of 0.054 inches past the overload are shown in Fig.33. The distribution shows that the residual stress profile remains essentially undisturbed by crack extension.

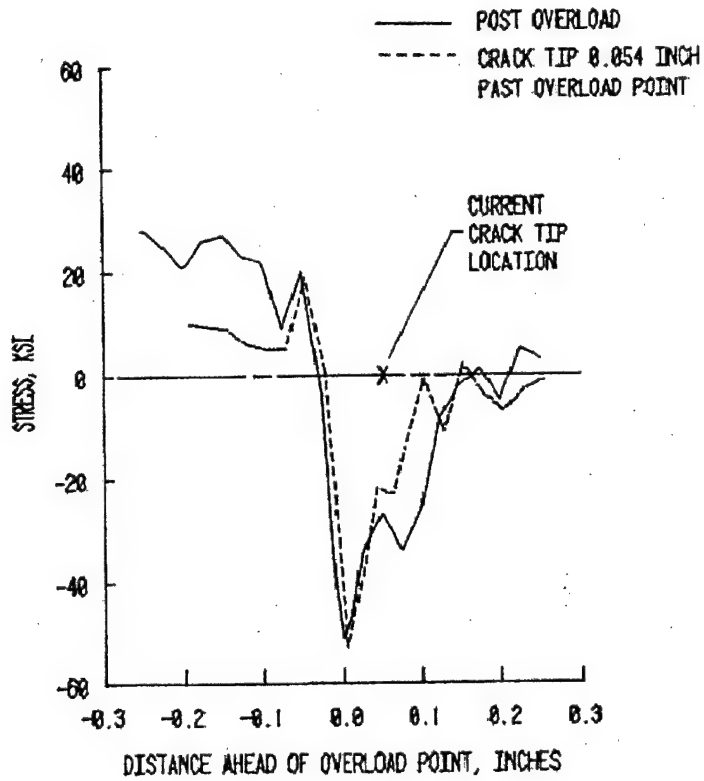

Figure 33. Residual stress profiles after overload and after crack extension of 0.054 inches past point of overload [49].

Upon some more crack extension to 0.111 inches past the overload point, the maximum residual compressive stress was found to be reduced, while the stresses behind and ahead of the crack tip remained essentially the same, Fig.34 shows the measured stress profiles.

Similar trend was noted when the crack was extended further to 0.265 inches past the overload point. The point of overload application remained under maximum compressive residual stress, while there were some positive stresses seen immediately behind the crack tip.

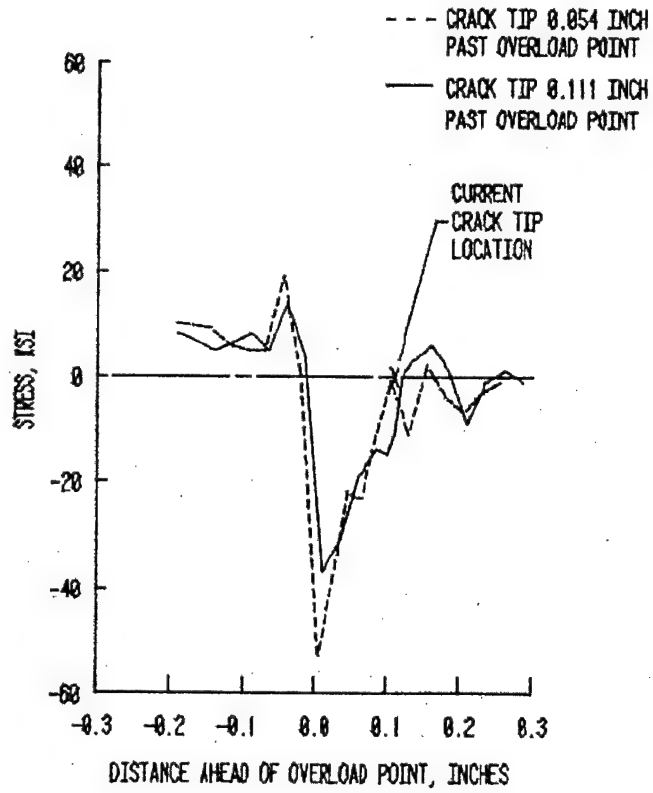

Figure 34. Residual stress profiles after crack extensions of 0.054 and 0.111 inches past the point of overload [49].

Results from this suggest, that a region of residual compressive stresses from the overload exists, and is evident. This region of residual compressive stresses remained undisturbed when the crack advanced through it.

When the crack tip was grown past the influence of the overload induced plastic zone, tensile stresses were found in the wake of the crack between the point of overload application and crack tip. This finding is in direct contrast with the crack closure concept which suggests that stresses behind a crack tip are compressive in nature. Holloway [49] concluded

that overload retardation is due to residual compressive stresses generated due to the overload application, and that the compressive stress due to this overload essentially stays undisturbed by the crack growth.

Allison [52] conducted a similar study on 1045 steel to determine the residual stresses before and after the application of overload.

Fig.35 shows the residual stress profiles before and after the overload application and the maximum stress profile at the base load.

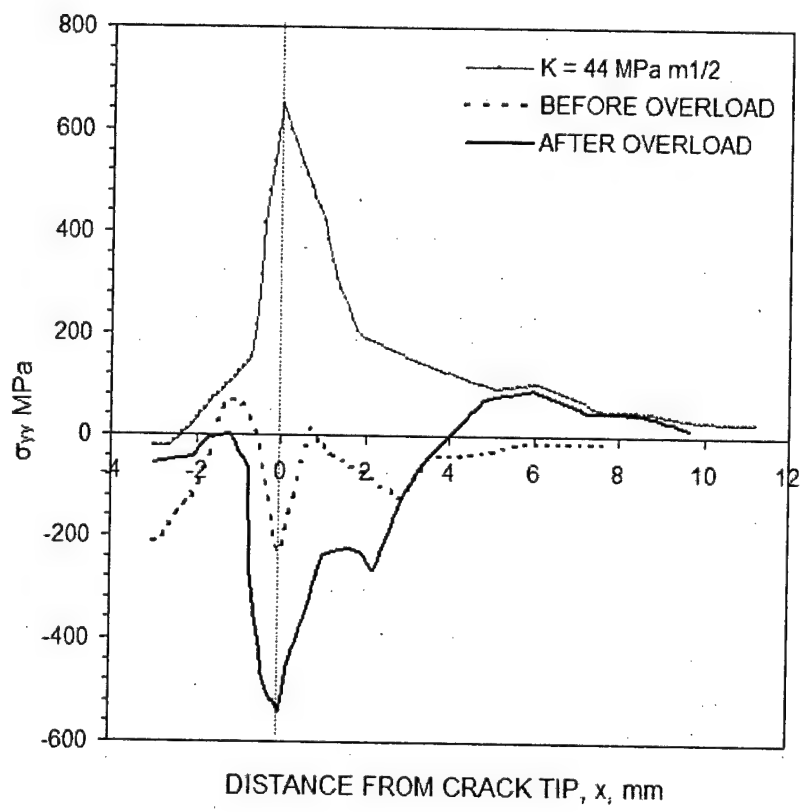

Figure 35. Residual stress profiles measured by Allison [52], before and after the application of overload.

He measured the residual stress profiles after a crack extension of 1.04 mm beyond the point of application of overload and is shown in Fig.36.

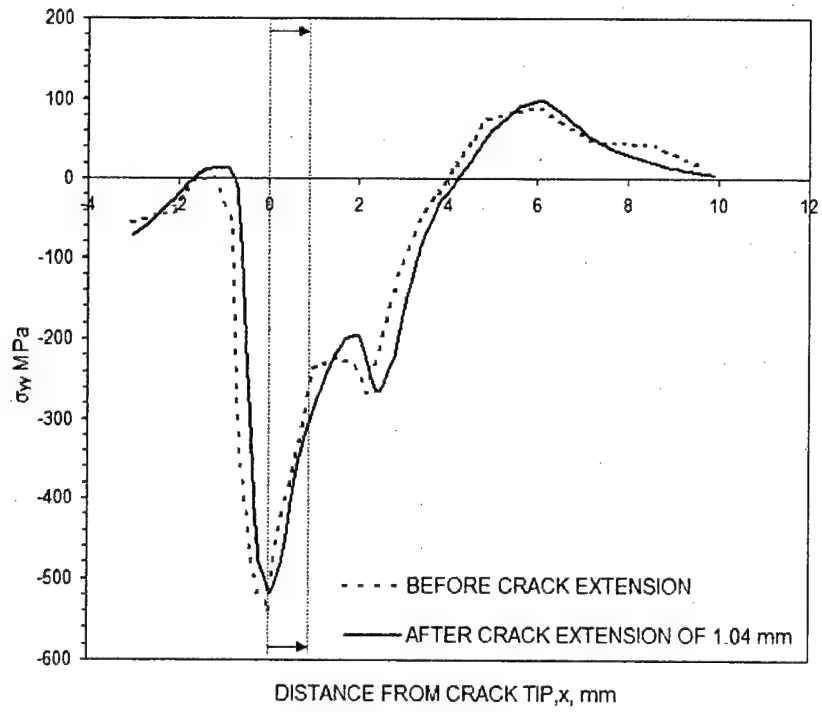

Figure 36. Residual stress profiles after the overload and after a crack extension of 1.04 mm [52].

This study indicates that the residual stress profile behavior before and after the overload and after the crack extension is very similar to what was shown by Holloway.

Allison also reached similar conclusions as Holloway, but the difference being that he referred to closure being a surface phenomenon, because of the stress imbalance that exists inside and outside of the specimen.

The analytical modeling of the residual stress can be done with the Rice and elastic solution at the unloaded state as was shown earlier, which is consistent with the model.

Once this residual stresses have been modeled, it is needed to apply the effect of these residual stresses on the driving force. For this Residual stress intensity factor K_{res}, or Internal stress intensity factor K_{int}, in case of block loading is needed to be calculated.

To calculate the K_{res} or K_{int} from the stress profiles, weight function method has been used, and a subroutine has been developed. The detailed explanation of the weight function procedure and its adaptation to the current model is given in the next section.

10.2 WEIGHT FUNCTION PROCEDURE

The Stress Intensity Factor solutions for several simple cases have been published in the handbooks, but for several non-uniform stress fields and practical cases, the handbook solutions are inadequate.

The Weight Function method proposed by Bueckner [53] and Rice have proved to be very useful for calculation of Stress Intensity Factors, especially for cracks subjected to non-uniform stress fields. Later Glinka [54, 55] and Niu [56, 57] have derived weight functions for various geometries which are easy to be incorporated into a computer algorithm for quick calculations.

The unique feature of weight function approach is that once the weight function for a particular cracked body is determined, the stress intensity factor, K, for any loading system applied to the body can be calculated by a simple integration of the expression of following form:

$$K = \int_0^a \sigma(x) m(x,a) dx \tag{60}$$

where $\sigma(x)$ is the stress field, $m(x,a)$ is the weight function for the particular geometry, 'x' is the distance from the crack tip and 'a' is the crack length.

The technique for deriving the weight function was proposed by Petroski and Achenbach [58], and later by Glinka [54-57].

It was shown by several authors that the Petroski-Achenbach method can sometimes lead to inaccurate weight functions. The crack opening displacement function proposed by Petroski and Achenbach for

determination of the weight functions was not accurate for the discontinuous and high gradient reference stress fields.

10.2.1 Glinka's weight function approach

Glinka and Niu [54-57] had an important finding that the weight functions for a variety of crack configurations had the same general mathematical form. They derived a universal weight function expression which could be applied to a wide variety of Mode I cracks regardless of geometry. The associated parameters of the weight function corresponding to the particular cracked body geometric configuration may be different. Glinka et al. used the Petroski-Achenbach approach to derive a general weight function of the form

$$m(x,a) = \frac{2}{\sqrt{2\pi(a-x)}}\left[1 + M_1\left(1-\frac{x}{a}\right) + M_2\left(1-\frac{x}{a}\right)^2\right] \qquad (61)$$

Where m(x,a) is the weight function, 'a' is the crack length, 'x' is the distance from the crack tip, and M_1, M_2 are the weight function parameters. Details about the determination of the weight function parameters are presented in the discussion ahead

Accuracy of weight function approximated by Eq.(61) depends on the type of the reference stress intensity factor 'K_r' and the associated reference stress field '$\sigma_r(x)$'and it is inaccurate for very non-uniform or discontinuous local reference stress field $\sigma_r(x)$. It was later pointed out by

Glinka and Niu that in some cases the three-term expression of Eq.(61) was not sufficient, requiring sometimes more than three terms.

For this reason a general weight function in the form of Eq.(62) is used

$$m(x,a)=\frac{2}{\sqrt{2\pi(a-x)}}\left[1+M_1\left(1-\frac{x}{a}\right)+M_2\left(1-\frac{x}{a}\right)^2+....+M_n\left(1-\frac{x}{a}\right)^n\right] \quad (62a)$$

$$m(x,a)=\frac{2}{\sqrt{2\pi(a-x)}}\left[1+M_1\left(1-\frac{x}{a}\right)^{1/2}+M_2\left(1-\frac{x}{a}\right)^1+....+M_n\left(1-\frac{x}{a}\right)^{n/2}\right] \quad (62b)$$

However, it is not known how many terms in Eq.(62) should be used for a particular geometry since there are some weight functions which can not be approximated by using even seven terms in the expression.

Although other forms of weight functions are admissible for crack problems, expressions (61) and (62) are the most frequently used.

To determine the stress intensity factor, weight function method requires an integration of the stress field and the weight function, where the weight function can be evaluated from the expression for Universal weight function of the form of Eq.(61) and Eq.(62).

10.2.2 Determination of the weight function for a geometry

The technique that has to be followed to evaluate the constants M_1, M_2, M_3 ....M_n is explained below which has been proposed by Glinka.

It was shown by Glinka [54, 55] that the three term expression of Eq.(61) can approximate weight functions for shallow edge and central through cracks of relative depth $a/t < 0.5$, while the four-term form of Eq.(62) can

be sufficiently accurate for a variety of cracks without any limitations regarding their depth.

10.2.2.1 General approach for 1D cracks

If the four term expression of Eq.(62) is used, the derivation of a weight function for any particular geometry can be reduced the determination of three parameters M_1, M_2, and M_3. Thus, the weight function m(x,a) can be determined without crack opening displacement function. Only two reference stress intensity factors have to be known. Once these are known, a set of three equations can be defined for the three reference stress intensity factors K_{r1}, K_{r2} and K_{r3}.These three equations involve the three constants M_1, M_2, and M_3. So the equations can be derived by integration of Eq.(60)

If the four term expression of Eq.(62b) is used,

$$K_{r1} = \int_0^a \frac{2\sigma_{r1}(x)}{\sqrt{2\pi(a-x)}}\left[1+M_1\left(1-\frac{x}{a}\right)^{\frac{1}{2}}+M_2\left(1-\frac{x}{a}\right)+M_3\left(1-\frac{x}{a}\right)^{\frac{3}{2}}\right]dx \qquad (63a)$$

$$K_{r2} = \int_0^a \frac{2\sigma_{r2}(x)}{\sqrt{2\pi(a-x)}}\left[1+M_1\left(1-\frac{x}{a}\right)^{\frac{1}{2}}+M_2\left(1-\frac{x}{a}\right)+M_3\left(1-\frac{x}{a}\right)^{\frac{3}{2}}\right]dx \qquad (63b)$$

$$K_{r3} = \int_0^a \frac{2\sigma_{r3}(x)}{\sqrt{2\pi(a-x)}}\left[1+M_1\left(1-\frac{x}{a}\right)^{\frac{1}{2}}+M_2\left(1-\frac{x}{a}\right)+M_3\left(1-\frac{x}{a}\right)^{\frac{3}{2}}\right]dx \qquad (63c)$$

Eq.(63a) - Eq.(63c) can be used as a set of three simultaneous algebraic equations which can be solved for M1, M2 and M3 and these values can be used to calculate SIF associated with any stress field.

10.2.2.2 General approach for 2D cracks

For two-dimensional cracks it is necessary to calculate the SIF for at least two points

The deepest point, A

$$K_A = \int_0^a \sigma_A(x) m_A(x,a) dx \tag{64}$$

The surface point, B

$$K_B = \int_0^a \sigma_B(x) m_B(x,a) dx \tag{65}$$

The weight functions, $m_A(x,a)$ and $m_B(x,a)$ are calculated as follows:

$$m_A(x,a) = \frac{2}{\sqrt{2\pi(a-x)}}\left[1 + M_{1A}\left(1-\frac{x}{a}\right)^{\frac{1}{2}} + M_{2A}\left(1-\frac{x}{a}\right) + M_{3A}\left(1-\frac{x}{a}\right)^{\frac{3}{2}}\right] \tag{66}$$

$$m_B(x,a) = \frac{2}{\sqrt{2\pi(a-x)}}\left[1 + M_{1B}\left(1-\frac{x}{a}\right)^{\frac{1}{2}} + M_{2B}\left(1-\frac{x}{a}\right) + M_{3B}\left(1-\frac{x}{a}\right)^{\frac{3}{2}}\right] \tag{67}$$

The parameters $M1_A$, $M2_A$, $M3_A$ for the deepest point, and $M1_B$, $M2_B$, $M3_B$ for the surface point are calculated depending on the crack geometry.

10.2.3 Numerical algorithm for weight function procedure

The SIF solutions by weight function method require huge functions to be integrated, so analytical integration requires too much calculation time and can be very rarely solved due to its complexity. So an algorithm based on Glinka's weight function has been followed to solve the integration numerically.

The general weight function expression in the form of Eq.(60) can be written as

$$K = \int_0^1 \frac{\sigma(u)2a}{\sqrt{2\pi a(1-u)}}\left[1 + M_1(1-u)^{\frac{1}{2}} + M_2(1-u) + M_3(1-u)^{\frac{3}{2}}\right]du \qquad (68)$$

Where u = x/a

Then the integration domain $0 \le u \le 1$, may be divided into "n" sub-intervals, in each of which the stress function σ (u) is approximated by a straight line similar to treatment shown in Fig.37.

$$\sigma_i(u) = A_i u + B_i \ , \qquad u_{i-1} \le u \le u_i \qquad (69)$$

where

$$A_i = \frac{\sigma(u_i) - \sigma(u_{i-1})}{u_i - u_{i-1}} \ , \qquad B_i = \sigma(u_i) - A_i u_i \qquad (70)$$

The number of sub intervals must be chosen with such a way as to approximate the stress function by straight lines with reasonable accuracy. So now the Eq.(68) can be written in the form of Eq.(71) below

$$K = a\int_{u_i}^{u_{i-1}} m(u,a)(A_i u + B_i u)du \qquad (71)$$

where

$$m(u,a) = \frac{2a}{\sqrt{2\pi a(1-u)}}\left[1 + M_1(1-u)^{\frac{1}{2}} + M_2(1-u) + M_3(1-u)^{\frac{3}{2}}\right] \tag{72}$$

So finally the stress intensity factor can be calculated from

$$K = a\sum_{i=1}^{n} S_i^* m\left(a, U_i^*\right) \tag{73}$$

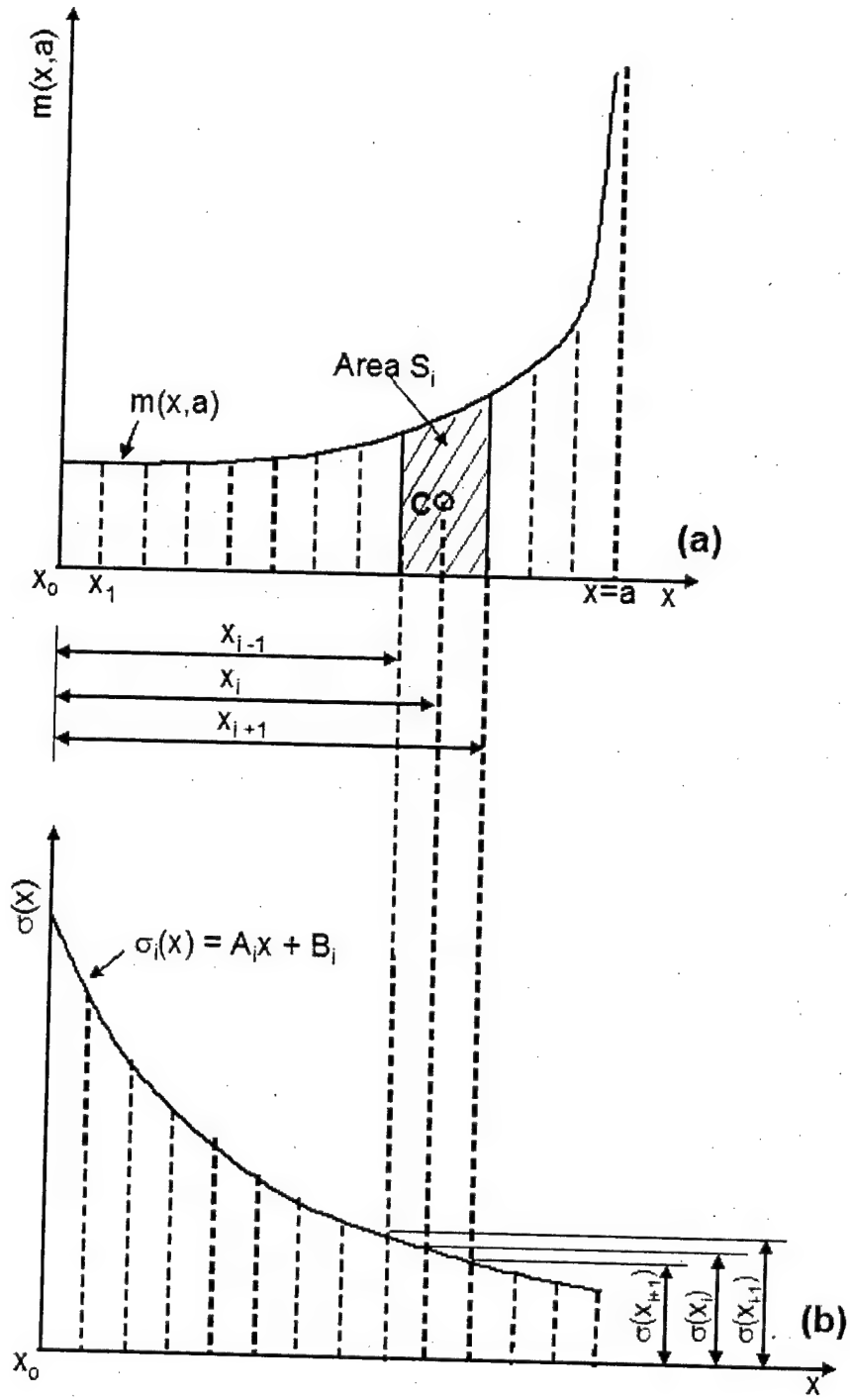

Figure 37. Illustration of integration method based on piecewise linearization of the stress function a) Weight function m(x, a). b) Piecewise stress function.

The term $m(a,U^*_i)$ represents the value of the weight function for $u = U^*_i$. The parameter S^*_i and U^*_i are the area under the normalized stress curve σ (u) and the coordinate 'u' of its centroid, respectively, corresponding to the sub interval "i" similar to that shown in Fig.37.

$$S_i^* = \frac{1}{2}(\sigma(u_i) - \sigma(u_{i-1}))(u_i - u_{i-1}) \tag{74}$$

$$U_i^* = u_i - (u_i - u_{i-1})\frac{[2\sigma(u_{i-1}) + \sigma(u_i)]}{3[\sigma(u_i) + \sigma(u_{i-1})]} \tag{75}$$

The singularity of the weight function near the end of the integration interval "i" where ($u \rightarrow 1$) makes it inappropriate to use Eq.(73) in this region, for $0.95 \leq u \leq 1$. Therefore for this particular interval or for some very other small interval depending upon the stress profile analytical expression can be derived for the integration. The analytical expression can be used for the singularity condition in the algorithm that has been used for the software, summation of the analytical expression is used throughout the whole crack length.

10.2.3 <u>Comparison of S.I.F results with results by Glinka's subroutine</u>

The results for different geometries were matched, for the SIF calculation by Glinka's FALPR05 application and the developed MATLAB procedure. The results matched very accurately with differences of less than about 0.1%. The calculation time required has been reduced using analytical piecewise integration expression.

The comparison graphs of some results have been shown Fig.38 - Fig.41:

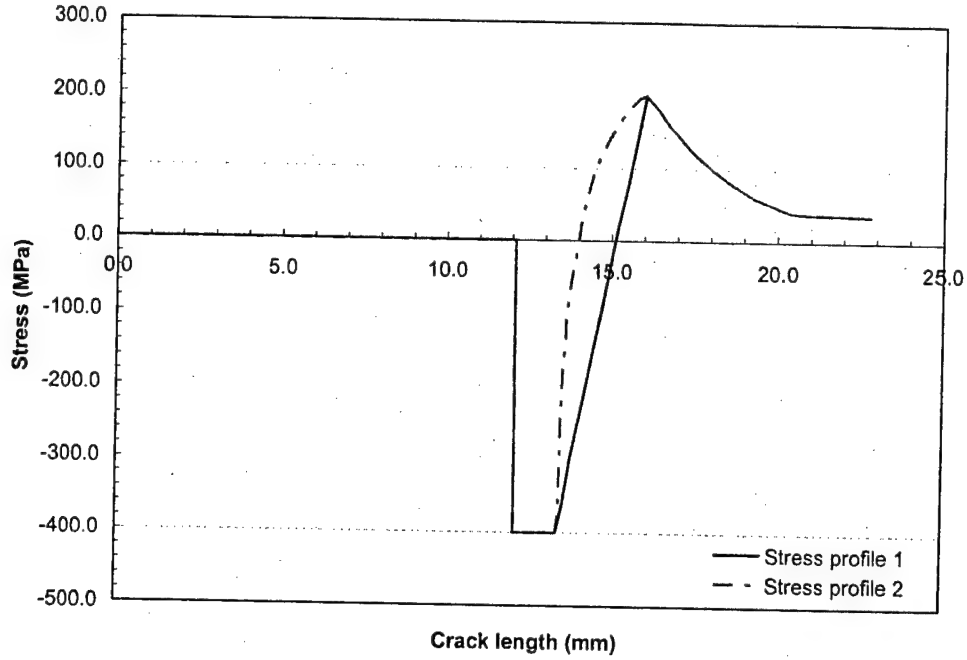

Figure 38. Typical residual stress profiles ahead of the crack tip.

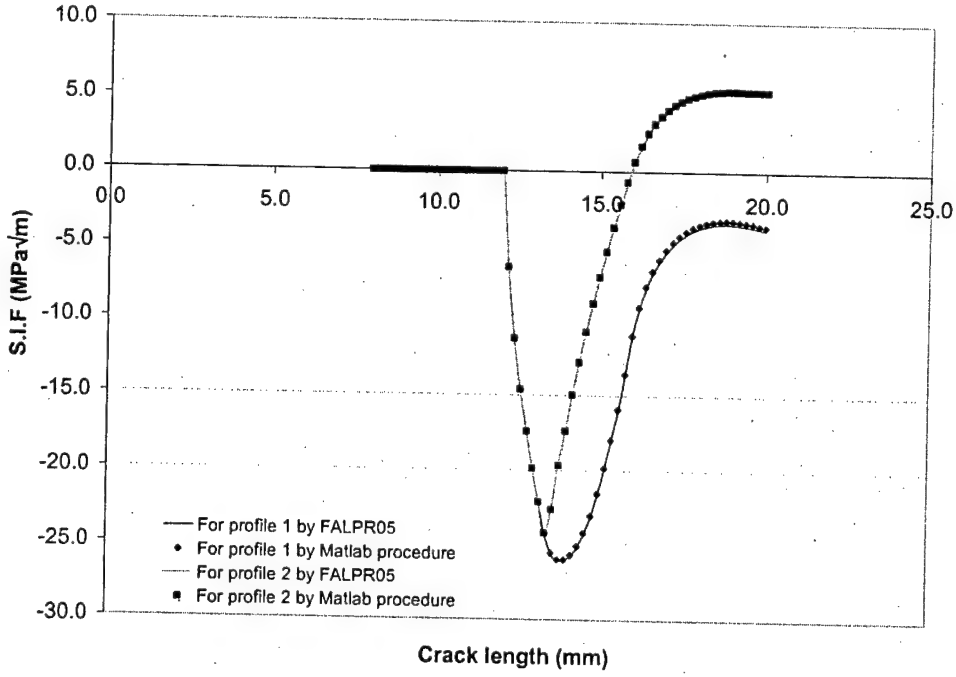

Figure 39. Comparison of S.I.F calculation for the stress profiles by Matlab procedure and Glinka's FALPR05.

There is around 0.1% difference in the results calculated, which arises due to the analytical piecewise integration used throughout in the Matlab procedure to boost the calculation speed.

To see how the good the procedure works for very sharp gradient profiles, Residual stress profiles in Fig.40 are the data digitized for situation after a spike overload at the interior and at the surface of the specimen.

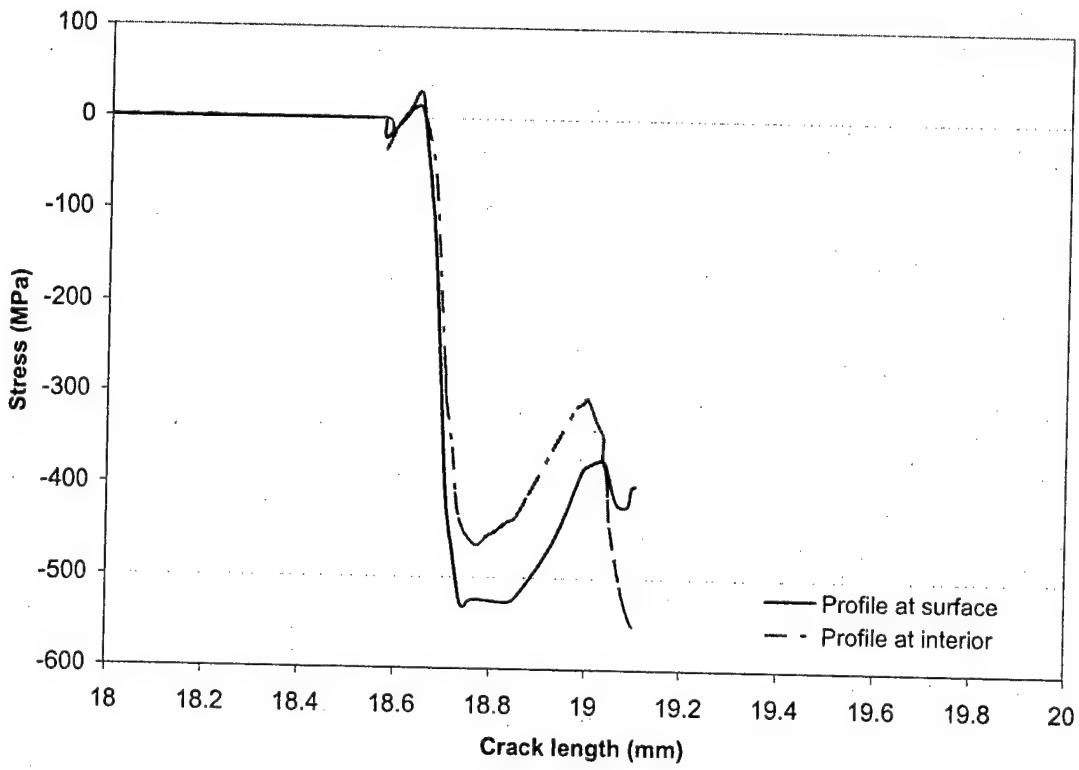

Figure 40. Residual stresses ahead of the crack tip after application of a spike overload at interior and surface of the centre crack specimen.

Fig.41 below shows the calculated S.I.F for the stress profiles after the spike overload using FALPR05 and Matlab procedure.

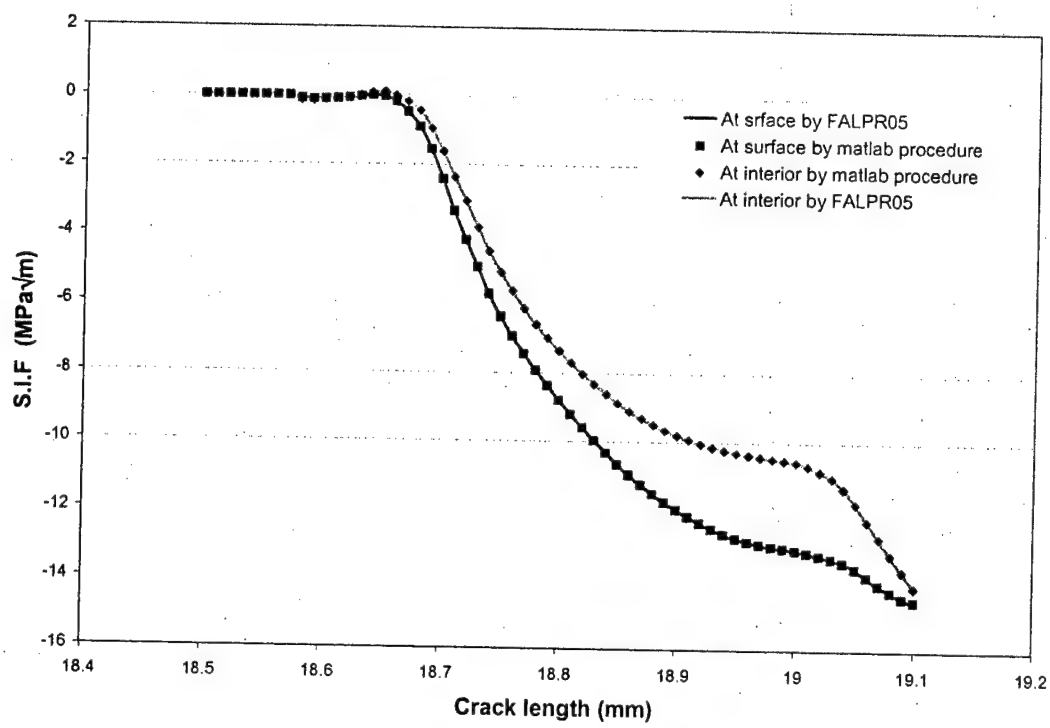

Figure 41. S.I.F calculation by FALPR05 and Matlab procedure for the residual stress profiles in a centre crack specimen after a spike overload.

The difference in the calculation between Glinka's FALPR05 and the Matlab procedure is very small, as it can be seen from the comparison study performed above. For even very sharp gradient profiles, the accuracy of the procedure does not vary. So this procedure can be utilized effectively to evaluate the S.I.F by weight function procedure.

10.3 RESIDUAL STRESS PROFILE MODELING

For the residual stress prediction ahead of the crack tip, rice and elastic solution in unloading have been used. The minimum stress profile at the zero-load is considered as the residual stress in the material.

The results from Holloway's [49] x-ray diffraction measurement study were modeled after unloading to zero from base load and overload. Fig.42 shows the prediction and the experimental data. The material used is 1020 steel, the base load maximum stress intensity factor is 25.38 MPa√m and the overload maximum stress intensity factor is 50.774 MPa√m.

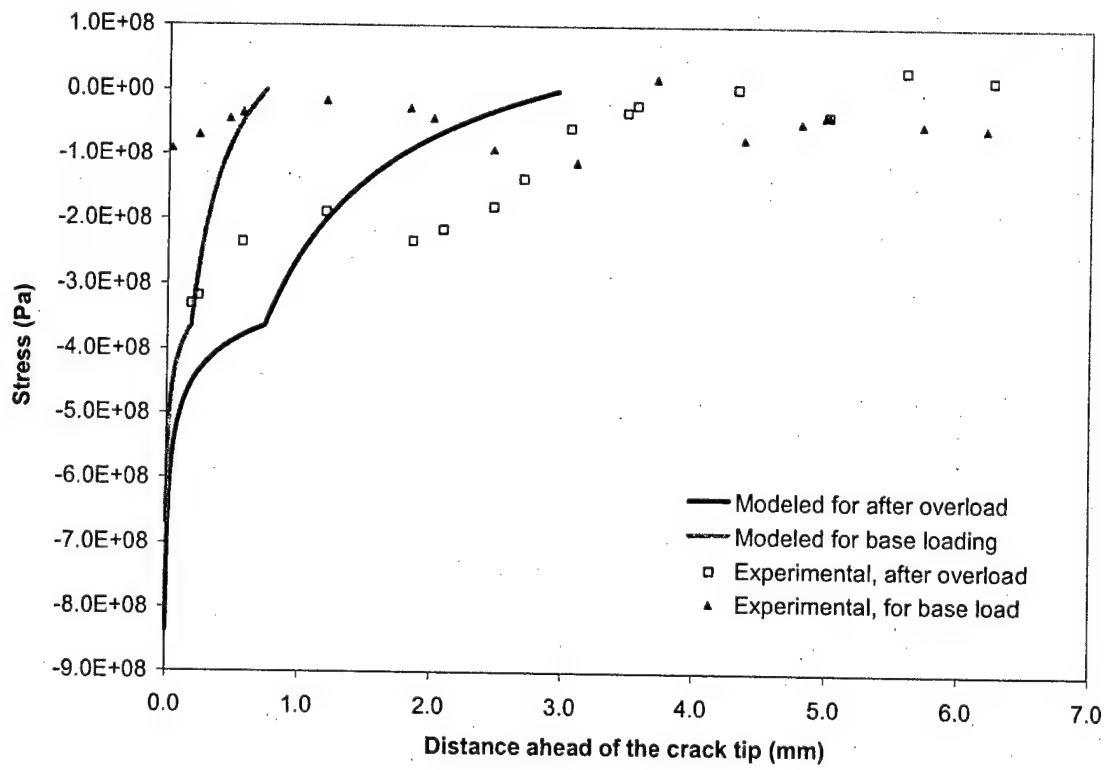

Figure 42. Residual stresses, experimental vs. modeled, before and after the overload application.

There is some similarity in the trends in Fig.42, but close to the crack tip the stresses observed by the experimental procedure are very less, compared to those predicted using Rice and elastic solution. This can be attributed to the fact that the x-ray diffraction method uses the average value of the stress within the region at which the beam is focused. The size of the x-ray beam spot used in experimental study by Holloway was 0.635 mm in diameter on the specimen surface.

There are various approaches that have been tried to model the residual stress intensity factor, K_{res}, profile that will be affecting the applied stress intensity factor in the overload affected region. The logical ones are (a) to use the residual stress profile after the overload to calculate the residual-K profile or (b) to use the difference between the minimum stress at the base load and the residual stress after the overload to calculate the residual-K profile.

10.4 PREDICTIONS WITH THE MODEL

The retardation of the overload is predicted for the experimental data from Holtz [46], and the analysis is presented ahead.

The data has been obtained for 4140 Steel at ΔK = 19.3 MPa$\sqrt{m}$ at R =0.1, and the K_{max} overload is twice that at the base load. Fig.43 shows the stress distribution before and after the overload.

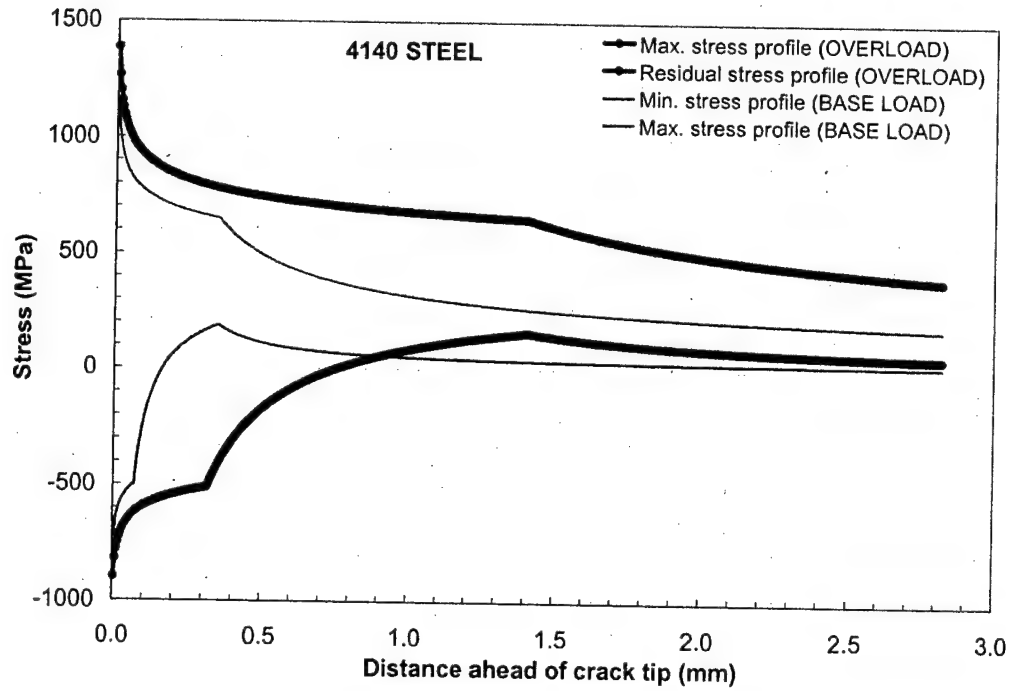

Figure 43. Stress profiles ahead of the crack tip at base load and after overload for 4140 steel.

Residual stress after the overload is considered to stay in the material ahead of the crack. Based on this residual stress profile, K_{res} is calculated,

which will affect the applied K_{max} and the applied ΔK. Fig.44 shows the K_{res} profile for the modeling.

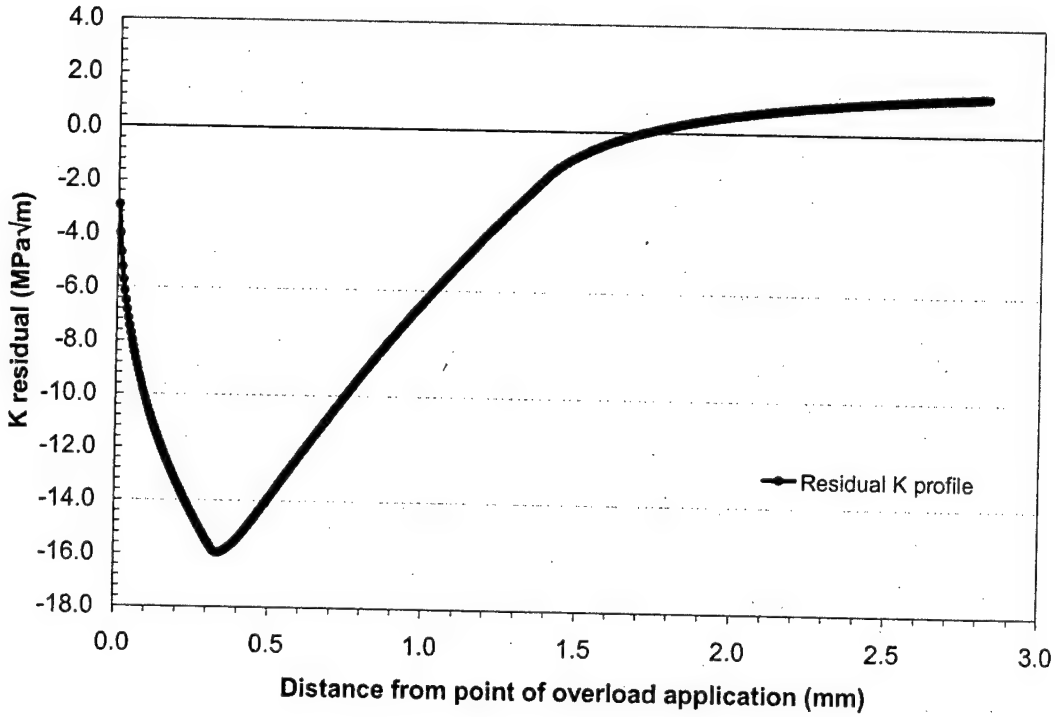

Figure 44. K residual profile calculated from the modeled residual stress in the material, after the overload application by using weight function approach.

The residual K affects the applied K_{max} and ΔK in the following way:

$$K_{max} = K_{max}^{appl.} + K_{res} \tag{76}$$

$$K_{min} = K_{min}^{appl} + K_{res}, \qquad \text{for } K_{min} > 0 \tag{77}$$

$$K_{min} = 0, \qquad \text{for } K_{min} < 0 \tag{78}$$

Fig.45 shows the predicted crack growth rate obtained by this approach

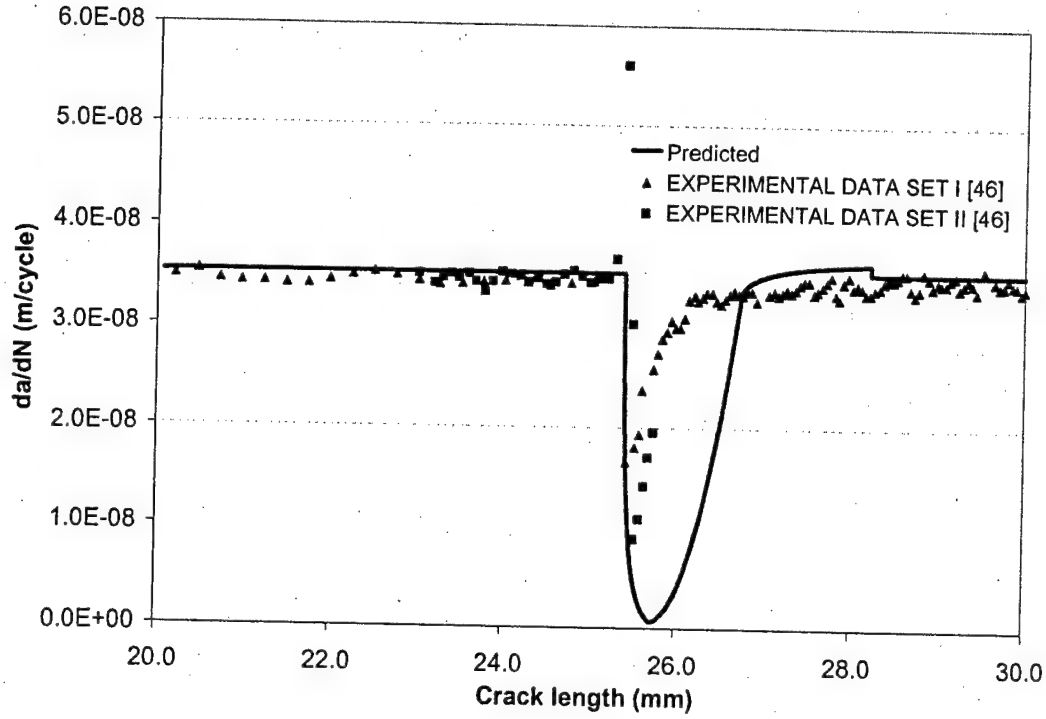

Figure 45. Effect of overload modeled for 4140 steel data from Holtz [46], using the K_{res} calculated by weight function method.

From Fig.45 it can be seen that the retardation obtained by the model is more than the retardation obtained by experiments. The maximum retardation point, in terms of crack length, obtained by the model is very close to the one obtained by experiments. The residual K profile calculation needs some refinement to predict the real behavior.

In the second approach, residual K is calculated from the stress profile obtained from the difference between the residual stress at overload and

the minimum stress at base load, assuming that the overload 'over-writes' the base load minimum profile. Fig.46 shows the stress profile.

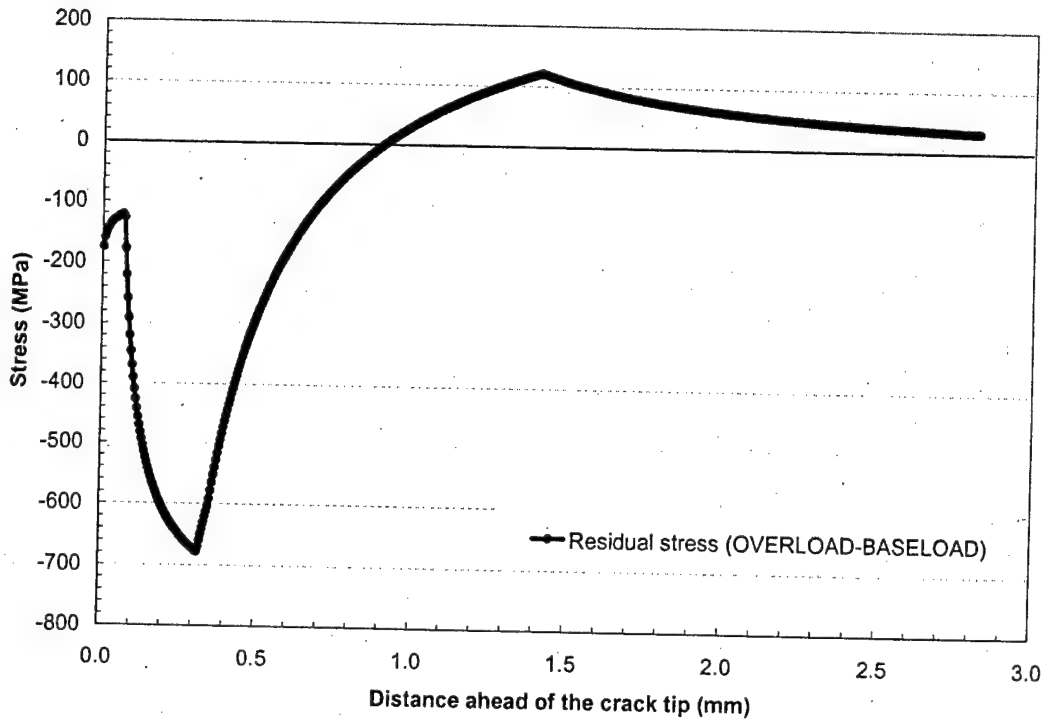

Figure 46. Residual stress profile obtained from difference between the residual stress at overload and minimum stress at base load.

The K residual profile has been calculated from the stress profile in Fig.46 using the weight function. The predicted crack growth data for the overload affected region is shown in Fig.47. It can be seen from this prediction that there is a longer retardation in the predicted crack growth rate. This approach of using the difference between the residual stress at overload and minimum stress at base load, based on the assumption that the minimum stress profile at base load stays in the material as a steady

state affecting the driving force. Fig.47 shows that the method explained above does not give good results in comparison to the approach used for obtaining results in Fig.45.

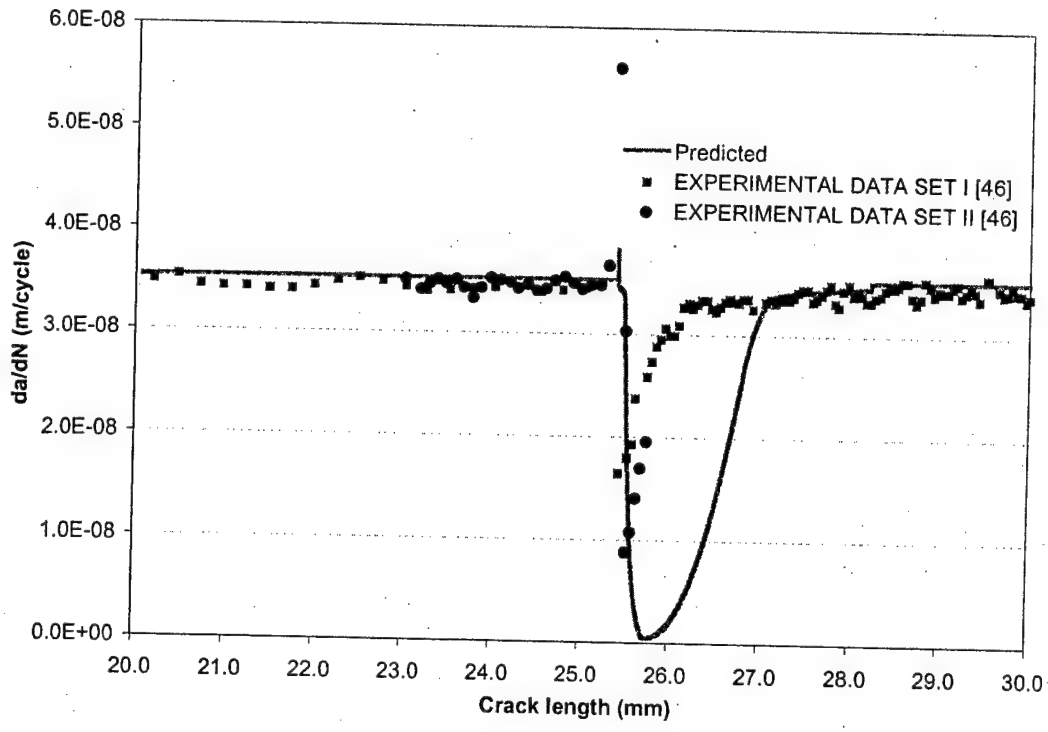

Figure 47. Crack growth retardation due to overload predicted using the residual K approach for 4140 Steel.

Another set of overload data from Stoychev [59] is modeled using the K_{res} approach. For this data the base load was applied at R=0.1 and a single overload, twice the base load was applied and the crack growth rate was acquired using the optical measurements. Fig.48 shows the 3 sets of experimental data and the predicted data using K_{res} for 2324 Aluminum alloy.

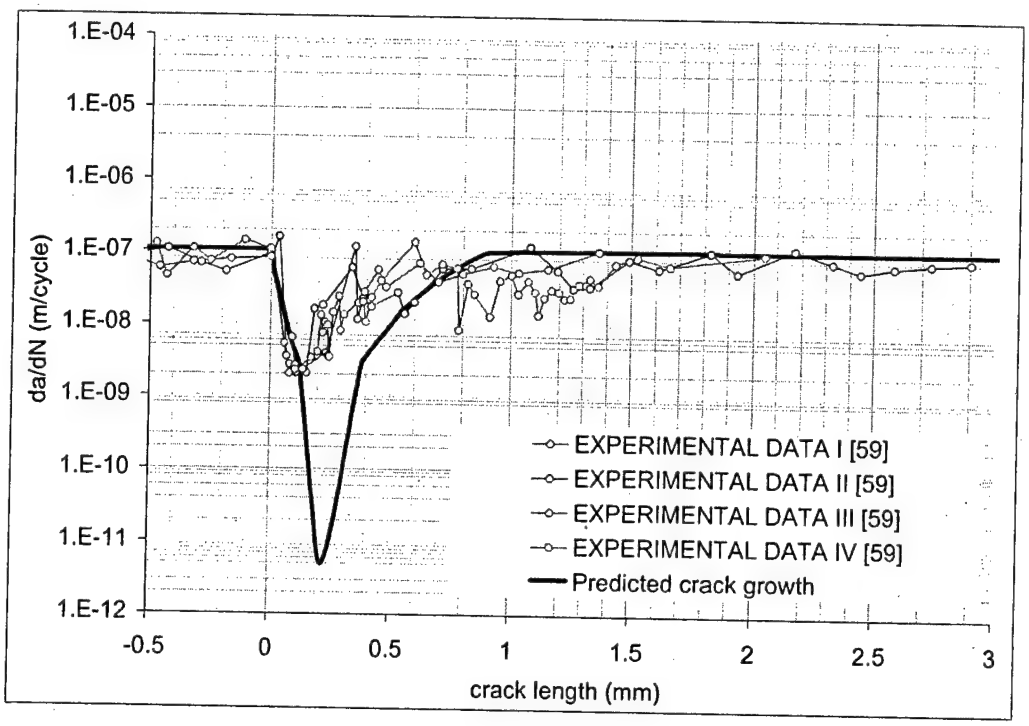

Figure 48. Overload data for 2324 Al. alloy from [59], predicted using K_{res} approach.

The crack growth retardation predicted by the model is more than the experimental data. The above prediction is based on the constants found by fitting of the experimental data for the constant R=0.1 for 2324-T39 alloy. Fig.49 shows the fitted constant R-ratio data. The slope used in the near threshold region was m_{th}=15.6. Since there is not much experimental data in the near threshold region the best fit slope was estimated.

In the overload affected region the ΔK is close to the values in the near threshold region. So the prediction for the crack growth retardation

overload should be very sensitive to the slope of crack growth curve in the near threshold region.

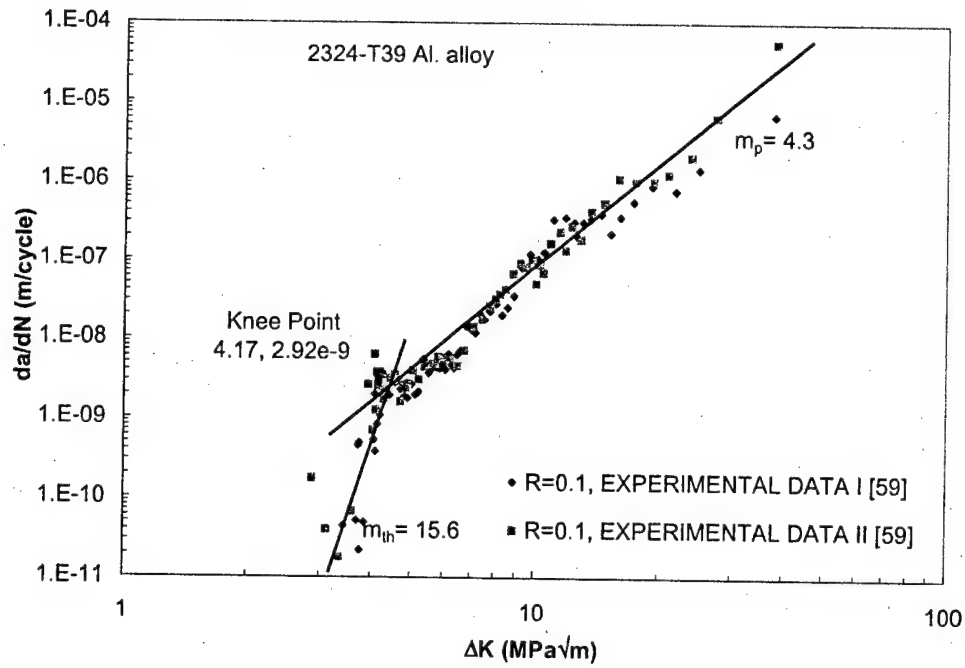

Figure 49. Constant R-ratio data fitted to find the knee point and the constants 'b' and 'c' for 2324-T39 Al. alloy at R=0.1.

To verify the observation, that the more retardation predicted by the model may be due to the high slope used in the near threshold region the experimental data was again fitted with a lesser slope in the threshold region with the knee point being the same. New values for constants 'b' and 'c' were determined and the simulation was run again for the crack growth retardation due to single overload application.

Fig.50 shows the fitted constant load ratio data with a slope m_{th}=11.4 in the near threshold region. Based on the constants determined from this fitting the results for the prediction are shown in the Fig.51.

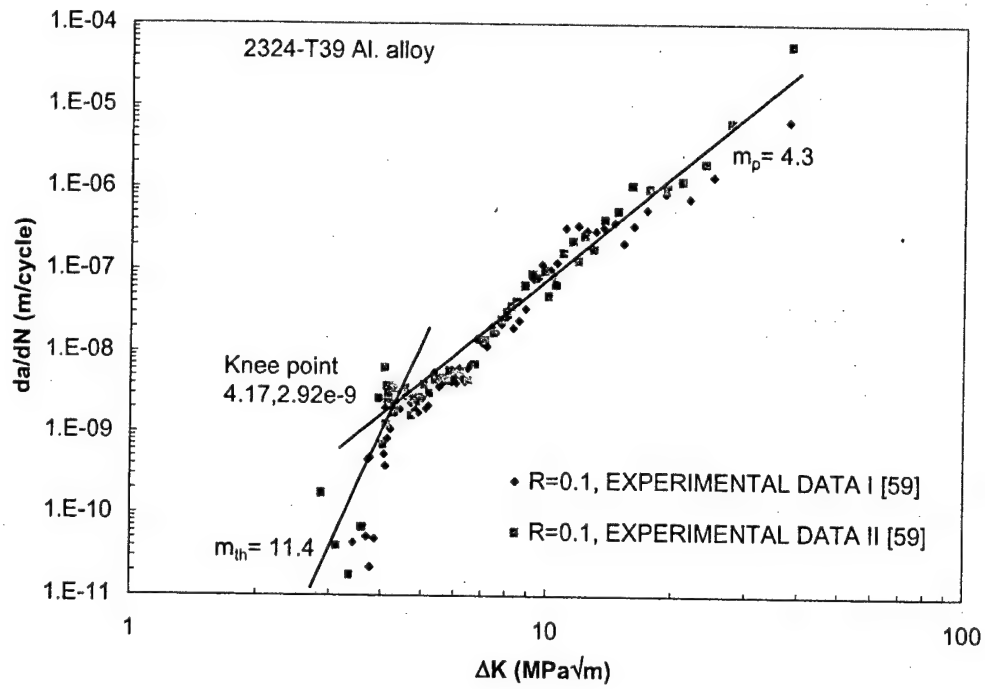

Figure 50. Constant R-ratio data fitted with a slope of 11.4 in the near threshold region to see the sensitivity on the prediction.

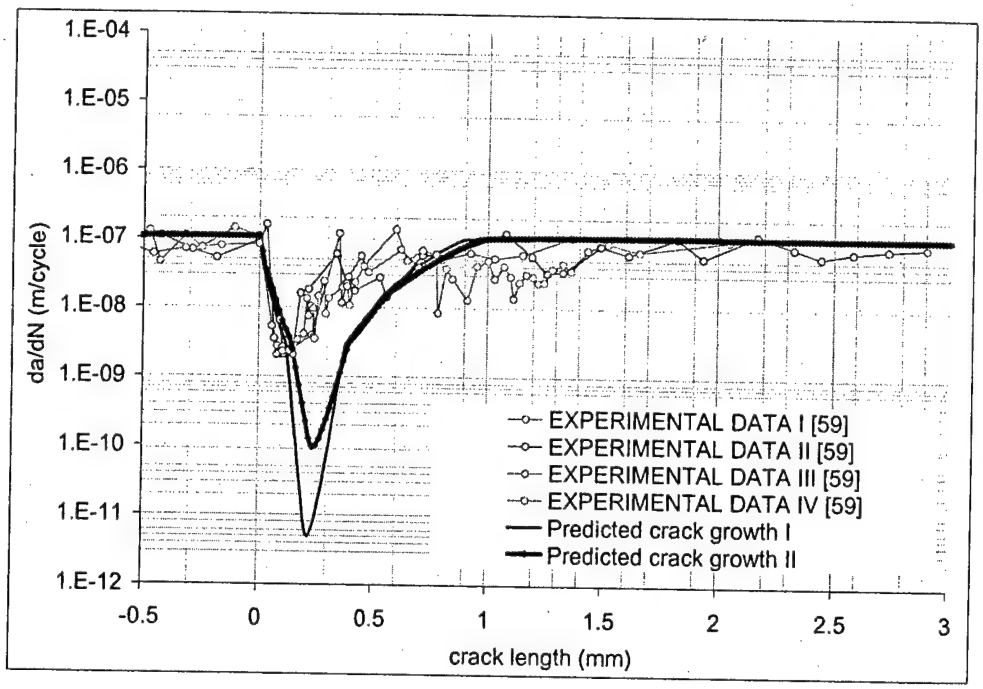

Figure 51. Sensitivity of the model to the slope in the threshold region to predict the crack growth rate in overload affected region.

It can be noted that for a change in the slope m_{th} from 15.6 to 11.4, the minimum crack growth rate for the overload data shifted by order of more than 1 decade on the crack growth rate axis. The model is very sensitive to the slope in the near threshold region. So for better prediction results with the model, there should be sufficient experimental data in the near threshold region.

11. PREDICTION OF THE R-RATIO EFFECT WITH THE MODEL

Load ratio effect was predicted using the current model. A constant value of ρ^* was used to predict the R=0.1 and R=0.5 for 4340 steel. The experimental data is taken from [15]. Results for the prediction are shown in the Fig.52.

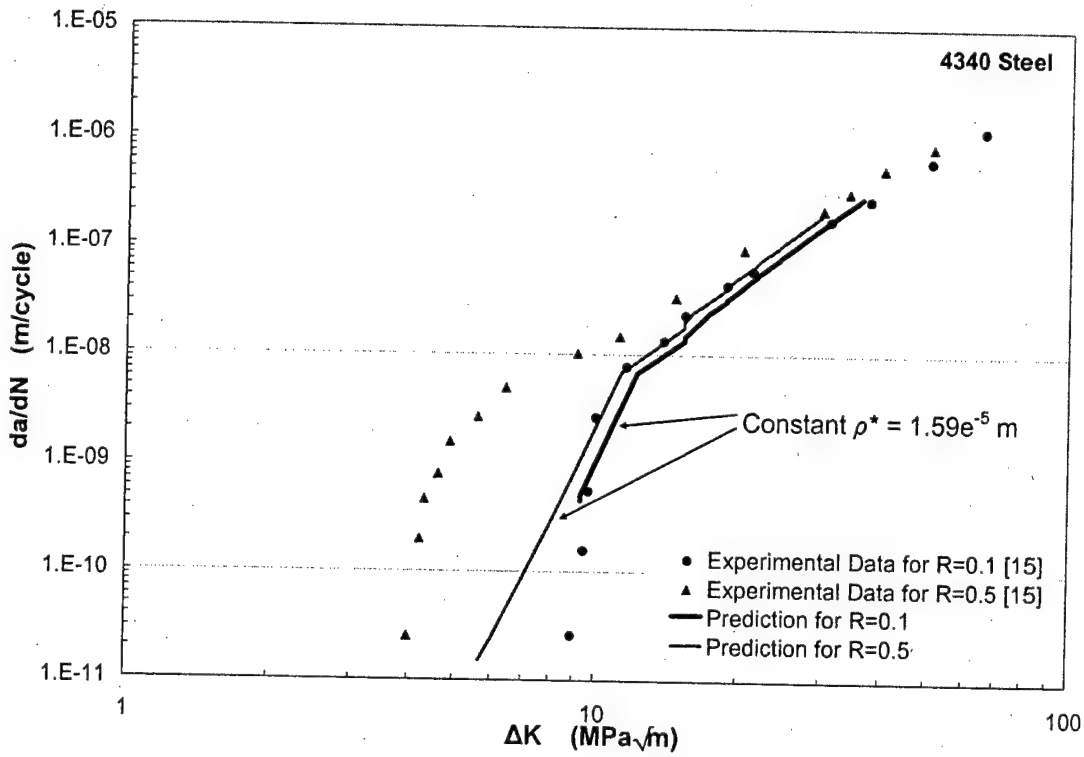

Figure 52. Experimental and predicted crack growth rate data for 4340 steel, R =0.1 and 0.5.

The developed model does not predict the R-ratio effect very well. There is a very small shift in the crack growth rate for different R-ratios. This can be related to the fact that this model uses the local load-ratio in the

elements to predict for the failure life from the SWT equation. Since very close to the crack-tip the local R $\approx$-1 or has a very low gradient and is nearly constant. The local R-ratio in the elements ahead of the crack tip modeled by rice and elastic solution is shown in Fig.53.

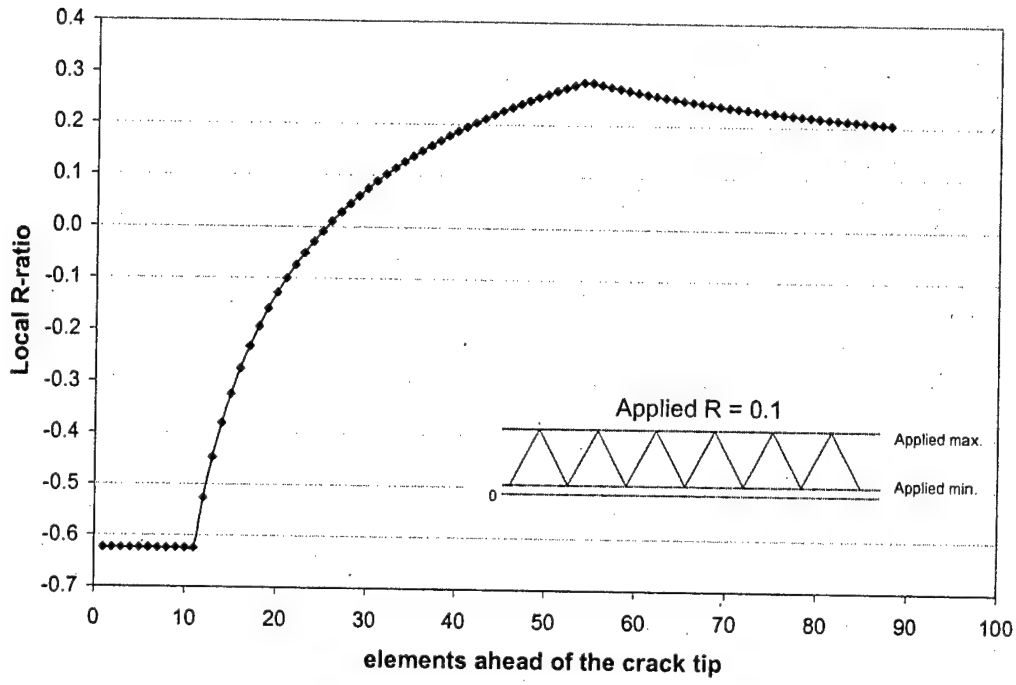

Figure 53. Local R-ratio in the elements ahead of the crack tip.

Since the maximum damage is present in the elements within the cyclic plastic zone. The local R-ratio of these elements controls the predicted R-ratio shift by the SWT failure criterion.

To predict the R-ratio effects with the current model, ρ^* can be used as a fitting parameter to fit the crack growth rate to the R-ratio to be predicted.

The data for Fig.52 is fitted with a different ρ^* for each R-ratio, the predicted results are shown in Fig.54.

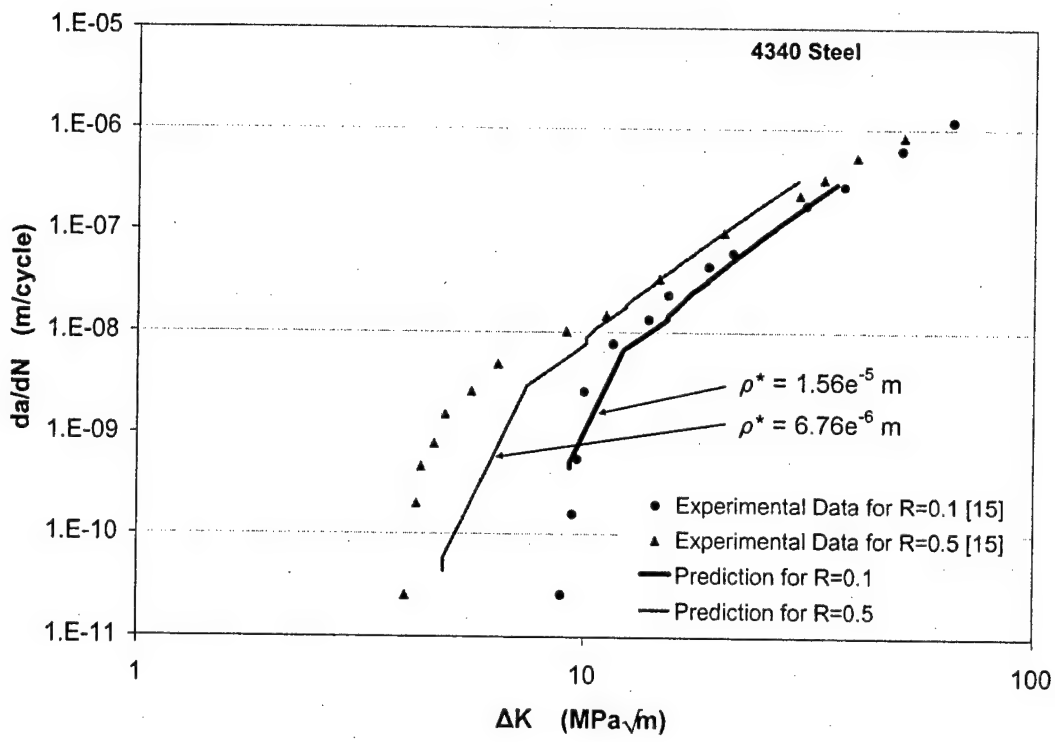

Figure 54. Crack growth rate predicted for R=0.1 and 0.5 for 4340 steel using different ρ* value for each R-ratio.

The different ρ^* to fit the data for each R-ratio works well, but the experimental data should be known before hand. So the proper modeling of the local R-ratio in the first few elements is very important.

12. CONCLUSIONS

As mentioned earlier, the main objective of this study was to develop a mathematical model for the fatigue crack propagation utilizing the stress and strain state near the crack tip region and the damage accumulation process. The model has been developed and a Matlab based application is made to run all the simulations and obtain the results. The study leads to the following conclusions:

(a) The Rice solution for the local stresses and strains ahead of the crack tip within the plastic zone and elastic solution for region outside the plastic zone works good with the model, and to make the distribution continuous, Irwin correction for the crack tip needs to be applied to the elastic solution.

(b) The fatigue exponents in the SWT equation have been related to the slope of the crack growth curve in the Paris and near threshold region.

(c) The approximate value of the fatigue exponents 'b' and 'c' for a material can be determined from the average of the slopes of the crack growth rate curves for different R-ratios.

(d) Both K_{max} and ΔK are the contributing parameters to the driving force for the model which is consistent with the recently proposed two parameter approach.

(e) Constant R-ratio data for various materials has been predicted with the current model, with process zone, ρ^*, being a calibrating

parameter. The predictions are in good agreement with the experimental data.

(f) The damage accumulation with local R-ratio underestimates the load interaction effects on the crack growth rate, Variation in the damage and the local R-ratio does not predict enough retardation or acceleration as predicted by the experimental data.

(g) Residual stresses are assumed to stay in the material due to the overload application; these residual stresses ahead of the crack have been used in addition to the variation in the local R-ratio and accumulated damage to model the overload effects. Weight function methodology has been used to calculate K_{res}.

(h) The results of the K_{res} calculation from the four term weight function expression have been compared to the results from the FALPR05 application by Glinka and the results match very well.

(i) It has also been shown in the study that the amount of retardation is very sensitive to the slope of the elastic part of the SWT curve or the slope of the crack growth curve in the near threshold region.

(j) The predicted results for the crack growth retardation are in reasonable agreement to the experimental data and are considered qualitatively valid for overload effect in different materials.

13. RECOMMENDATIONS FOR FUTURE WORK

Working on this model based on damage accumulation, some limitations in its application were found and explored while many other questions were developed as a result.

(a) It is believed that through some future exploration ρ^* parameter can be made independent of the load ratio to be a material parameter rather than being a calibrating parameter for each load ratio.

(b) Study should be done to improve the local R-ratio prediction within the cyclic plastic zone with the model. It is believed that local R-ratio within cyclic plastic zone is not very realistic which might be a reason for the inability of the model to predict the R-ratio effect.

(c) There is room for improvement in the prediction of the load interaction effects; future work should be focused on the numerical determination of the stress-strain distribution and better estimation of the parameters influencing the crack tip driving force.

14. REFERENCES

[1] A.V de Forest, The rate of growth of fatigue cracks, Journal of applied mechanics Vol.3, 1936, pp. 9-23.

[2] J. Schijve, Four Lectures on fatigue crack growth, Engineering mechanics Vol.11, 1978, pp. 161 – 221.

[3] N.E Dowling, Mechanical Behavior of Materials, second edition, Prentice Hall. 1998

[4] A.F Grandt, Fatigue for Engineers, In: ASME career development series, 2001.

[5] R.L Brockenbrough and B.G Johnson, 1981, USS Steel Design Manual, ADUSS 27-3400-04, United States Steel Corp, Monroville, PA.

[6] P.C Paris, F Erdogan, A critical analysis of crack propagation. American Society of Mechanical Engineers, Series D, Journal of Basic Engineering, Vol.85, 1963, pp. 528-534.

[7] J.R Rice, Mechanics of crack tip deformation and extension by fatigue, In: Fatigue crack propagation, ASTM STP 415, American Society for Testing and Materials, 1967, pp. 247-311.

[8] S.X Wu, B Cotterell, A model of fatigue crack growth based on Dugdale model and damage accumulation, International Journal of Fracture, Vol.57, 1992, pp. 253-267.

[9] T.V Duggan, A theory of fatigue crack propagation, Engineering Fracture Mechanics, Vol.9, 1977, pp. 735-747.

[10] G Glinka, A Cumulative model of fatigue crack growth, International Journal of Fatigue, Vol.4, 1982, pp. 59-67.

[11] G Glinka, C Robin, A Cumulative model of fatigue crack growth and the closure effect, International Journal of Fatigue, Vol.6, 1984, pp. 37-47.

[12] G Glinka, A notch stress-strain analysis approach to fatigue crack growth, Engineering Fracture Mechanics, Vol.21, 1985, pp. 245-261.

[13] K.R Lehr, H W Liu, Fatigue crack propagation and strain cycling properties, International Journal of Fracture, Vol.5, 1969, pp. 45-55.

[14] K.H Schwalbe, Comparison of several fatigue crack propagation laws with experimental results, Engineering Fracture Mechanics, Vol.6, 1974, pp. 325-341.

[15] D Kujawski, F Ellyin, A fatigue crack growth model with load ratio effects, Engineering Fracture Mechanics, Vol.28, 1987, pp. 367-378.

[16] D Kujawski, F Ellyin, A fatigue crack propagation model, Engineering Fracture Mechanics, Vol.20, 1984, pp. 695-704.

[17] D Kujawski, F Ellyin, On the size of plastic zone ahead of the crack tip, Engineering Fracture Mechanics, Vol.25, 1986, pp. 229-236.

[18] F Ellyin, D Kujawski, Crack growth rate under cyclic loading effect of different singularity fields, Engineering Fracture Mechanics, Vol.25, 1986, pp. 463-473.

[19] K.N Pandey, S Chand, Fatigue crack growth model for constant amplitude loading, Fatigue Fracture of Engng Material Structure, Vol.27, 2003, pp. 459-472.

[20] J.C Radon, A model of fatigue crack growth in threshold region, International Journal of Fatigue, 1982, pp. 161-166.

[21] S.S Manson, Interpretive report on cumulative fatigue damage in low cycle range, Welding Journal Research, Vol.43, 1964, pp. 344s-352s.

[22] M.A Miner, Cumulative damage in fatigue, Journal of Applied Mechanics, Vol.67, 1945, pp. 159-164.

[23] F.A McClintock, Discussion of Fracture Testing of High Strength Sheet Metals, Materials Res. Standards, Vol.1, 1975, pp. 277-279.

[24] R.W Lardner. A dislocation model for fatigue crack growth in metals, Vol.17, 1968, pp. 71-80.

[25] A Fatemi, L Yang, Cumulative fatigue damage and life prediction theories: a survey of state of the art for homogeneous materials, International Journal of Fatigue, Vol.20, 1998, pp. 9-34.

[26] K Walker, The effect of stress ratio during crack propagation and fatigue for 2024-T3 and 7075-T6 aluminum. In: ASTM STP 462, Philadelphia, PA, 1970, pp. 1-14.

[27] W Elber, The significance of fatigue crack closure, In: ASTM STP 486, 1971, pp.230-242.

[28] S Dinda, D Kujawski, Correlation and prediction of fatigue crack growth for different R-ratios using K_{max} and ΔK^{+} parameters, Engineering Fracture Mechanics, Vol.71, 2004, pp. 1779-1790

[29] J Harter, Comparison of contemporary FCG life prediction tools, Vol.21, 1999, pp. 181-185.

[30] A.K Vasudevan, K Sadananda, G Glinka, Critical parameters for fatigue damage, International Journal of Fatigue, Vol.23, 2001, pp. S39-S53.

[31] A.K Vasudevan, K Sadananda, Analysis of fatigue crack closure and threshold, ASTM STP, Vol.25, 1993, pp. 484-501.

[32] F.S Silva, crack closure inadequacy at negative stress ratios, International Journal of Fatigue, Vol.26, 2004, pp. 241-252.

[33] K Donald, P.C Paris, An evaluation of ΔK_{eff} estimation procedure on 6061-T6 and 2024-T3 aluminum alloys, International Journal of Fatigue, Vol.21, 1999, pp. S47-S57.

[34] K Donald, H Tada, P.C Paris, Service load fatigue damage-a historical perspective, International Journal of Fatigue, Vol.21, 1999, S35-S46.

[35] R.C McClung, The influence of applied stress, crack length and stress intensity factor on crack closure, Metallurgical Transactions, Vol. 22A, 1991, pp. 1559-1571.

[36] K Donald, G.H Bray, Introducing the K_{max} sensitivity concept for correlating fatigue crack growth data, The Minerals, Metals and Materials Society, 1997.

[37] K Sadananda, A.K Vasudevan, Crack tip driving forces and crack growth representation under fatigue, International Journal of fatigue, Vol.26, 2003, pp. 39-47.

[38] K Sadananda, A.K Vasudevan, Extension of unified approach to fatigue crack growth to environmental interactions, International Journal of fatigue, Vol.23, 2001, pp. S277-S286.

[39] K Sadananda, A.K Vasudevan, N Louat, A review of crack closure, fatigue crack threshold and related phenomenon, Material Science Engineering, Vol.188, 1994, pp. 1-22.

[40] Development of a two parameter model (K_{max}, ΔK) for Fatigue crack growth analyses (Constant amplitude cyclic loading), Progress Report No.2, March 2004.

[41] D Kujawski, A new driving force parameter for crack growth in aluminum alloys, International Journal of Fatigue, Vol.23, 2001, pp. 733-740.

[42] D Kujawski, F Ellyin, A unified approach to mean stress effect on fatigue threshold conditions, International Journal of Fatigue, Vol.17, 1995, pp. 101-106.

[43] Antolovich, S D Saxena, A model for fatigue crack propagation, Engineering Fracture Mechanics, Vol.7, 1975, pp. 649-652.

[44] D M Li, C S Lee, An Improvement on prediction of fatigue crack growth from low cycle fatigue properties, Engineering Fracture Mechanics, Vol.60, 1998, pp. 397-406.

[45] S Sahn, M Schaper, Damage evolution ahead of a sharp notches under cyclic loading, Nuclear Engineering Design, 1994, pp.1-14.

[46] R Holtz, Private communication, June 2004.

[47] G Glinka, Private communication, June 2004.

[48] J Schijve, Advances in aeronautical sciences, 2nd International Conference on Aeronautical Sciences, Zurich, Pergammon Press, 1960, pp. 387–398.

[49] D.R Holloway, X-ray diffraction measurements of crack tip stresses as a crack advances through a single overload affected zone, Technical report AFFDL-TR-79-3006, 1979, pp. 1-25.

[50] G.A Webster, Residual stress distributions and their influence on fatigue lifetimes, International Journal of Fatigue, Vol.23, 2001, pp. S375-S383.

[51] M Lang, A model for fatigue crack growth, part1: phenomenology, Fatigue and Fracture of Engineering Material Structure, Vol.23, 2000, pp. 587-601.

[52] J.E Allison, Measurement of crack tip stress distribution by X-ray diffraction, Fracture Mechanics, ASTM STP 677, 1979, pp. 550-562.

[53] H.F Bueckner, A novel principle for the computation of stress intensity factors. Math. Mech., Vol.50, 1970, pp. 529-535.

[54] G Glinka and G Shen, Universal features of weight functions for cracks in mode I. Engineering Fracture Mechanics, Vol.40, 1991, pp.1135-1146.

[55] A.A Moftakhar and G Glinka, Calculation of stress intensity factors by efficient integration of weight functions. Engineering Fracture Mechanics, Vol.43, 1992, pp. 749-756.

[56] X Niu and G Glinka, On the limitations of Petroski-Achenbach crack opening displacement approximation for the calculation of weight function- do they really exist? Engineering Fracture Mechanics, Vol.26, 1990, pp.701-706.

[57] X Niu and G Glinka, Weight functions for edge and surface semi-elliptical cracks in flat plates and plates with corners, Engineering Fracture Mechanics, Vol.36, 1990, pp.459-476.

[58] H.Y Petroski, F.D Achenbach, Computation of weight functions from a stress intensity factor. Engineering Fracture Mechanics, Vol.10, 1978, pp.257-266

[59] S Stoychev, D Kujawski, In: International Conference on Fatigue Damage of Structural Materials V, 2004, MA, USA.

APPENDIX A

KNEE-POINT DETERMINATION TO FIND ρ^* AND CONSTANT R-RATIO PREDICTIONS FOR DIFFERENT MATERIALS

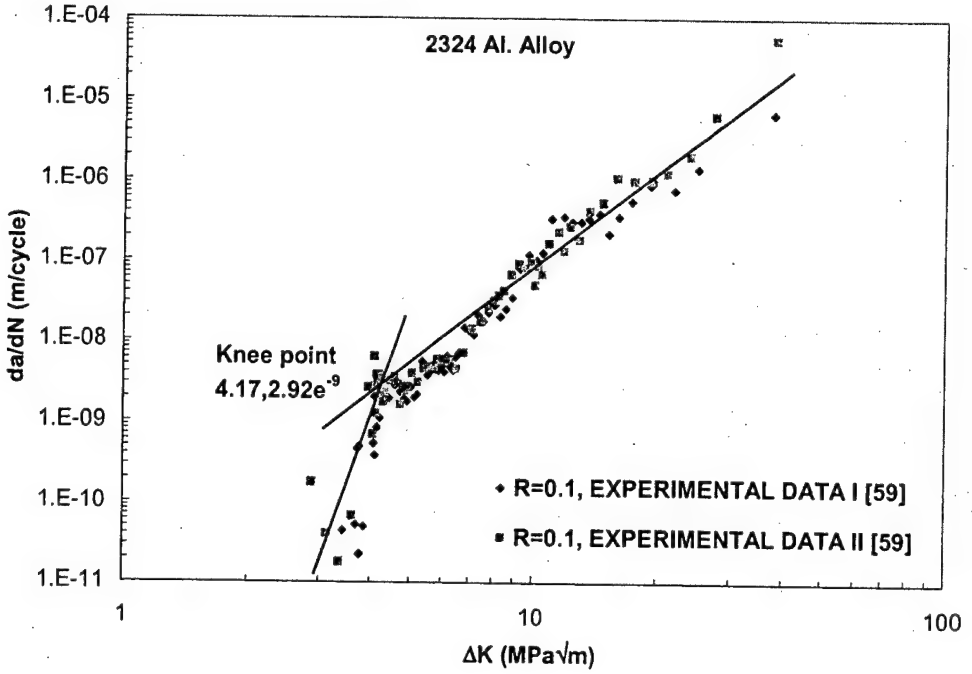

Figure A1. Knee point used to find ρ* for R =0.1, 2324-T39 Al. alloy [59].

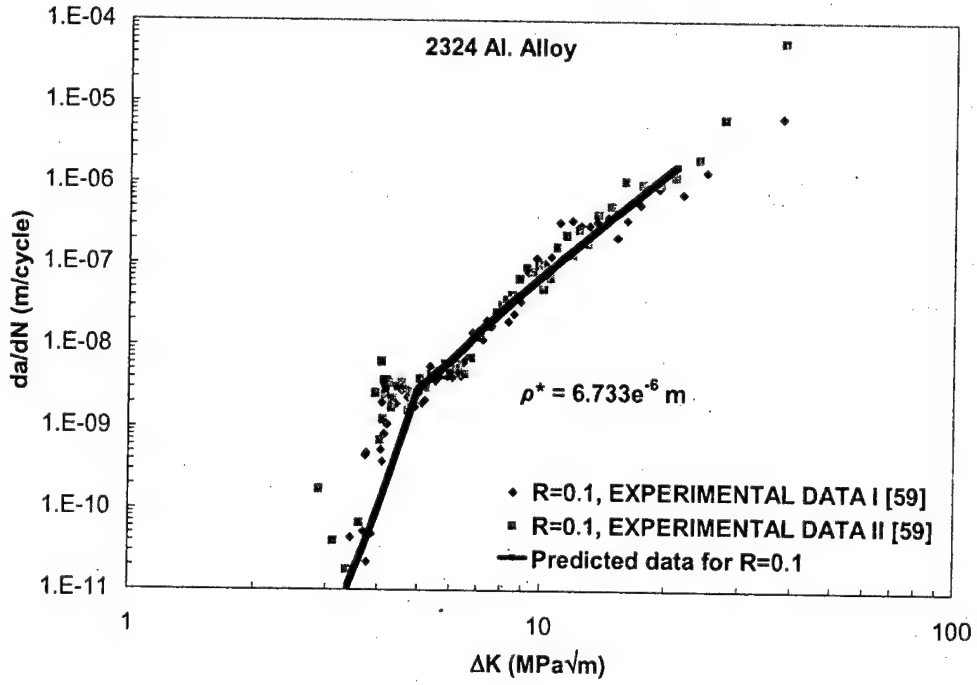

Figure A2. Predicted vs. experimental data for R=0.1, 2324-T39 Al. alloy [59].

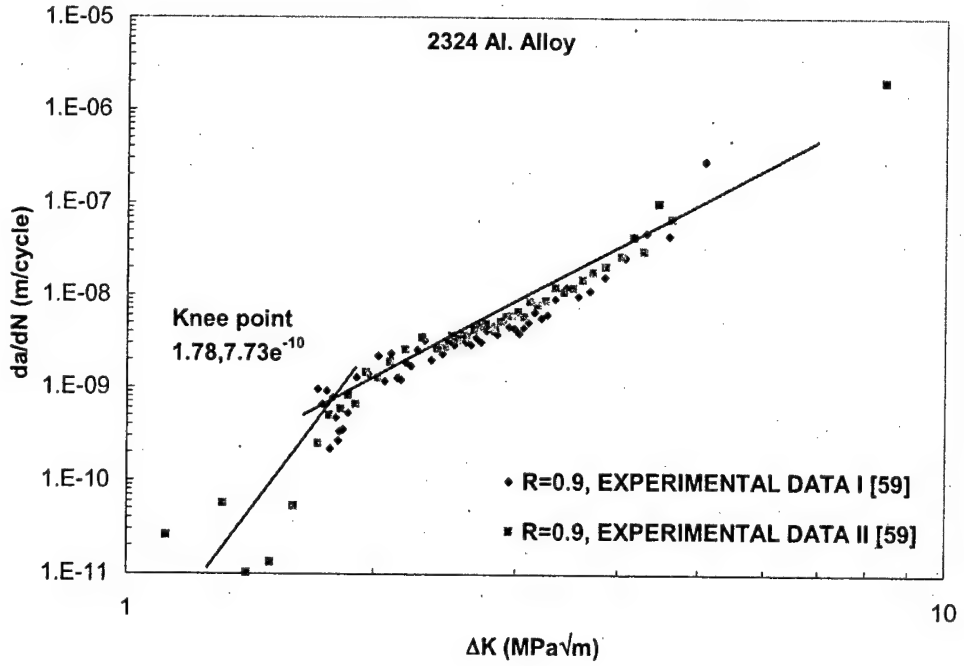

Figure A3. Knee point used to find ρ* for R =0.9, 2324-T39 Al. alloy [59].

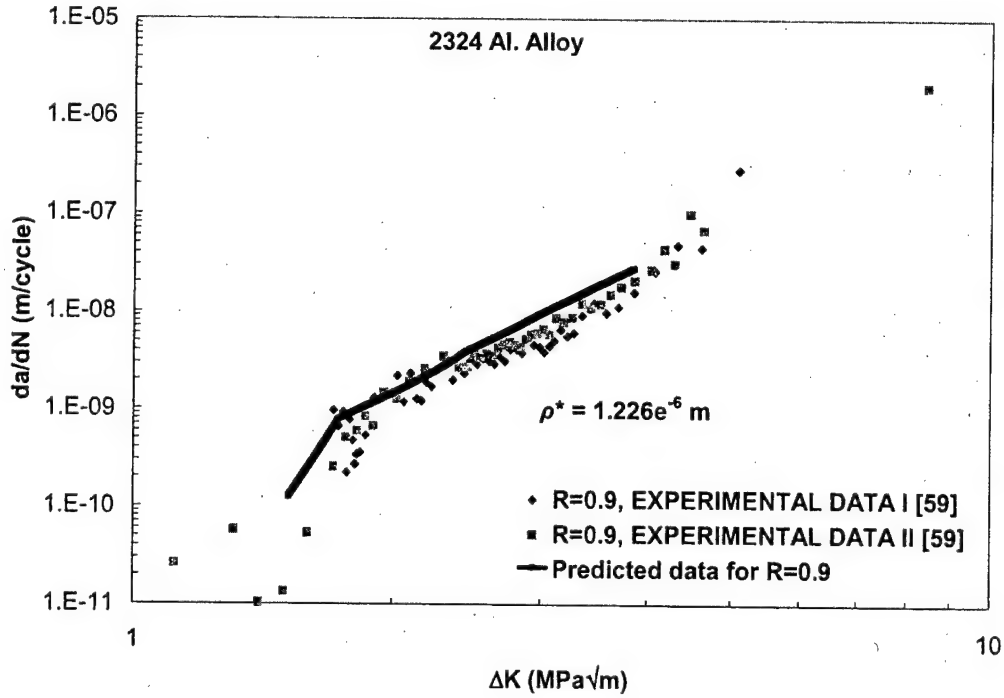

Figure A4. Predicted vs. experimental data for R=0.9, 2324-T39 Al. alloy [59].

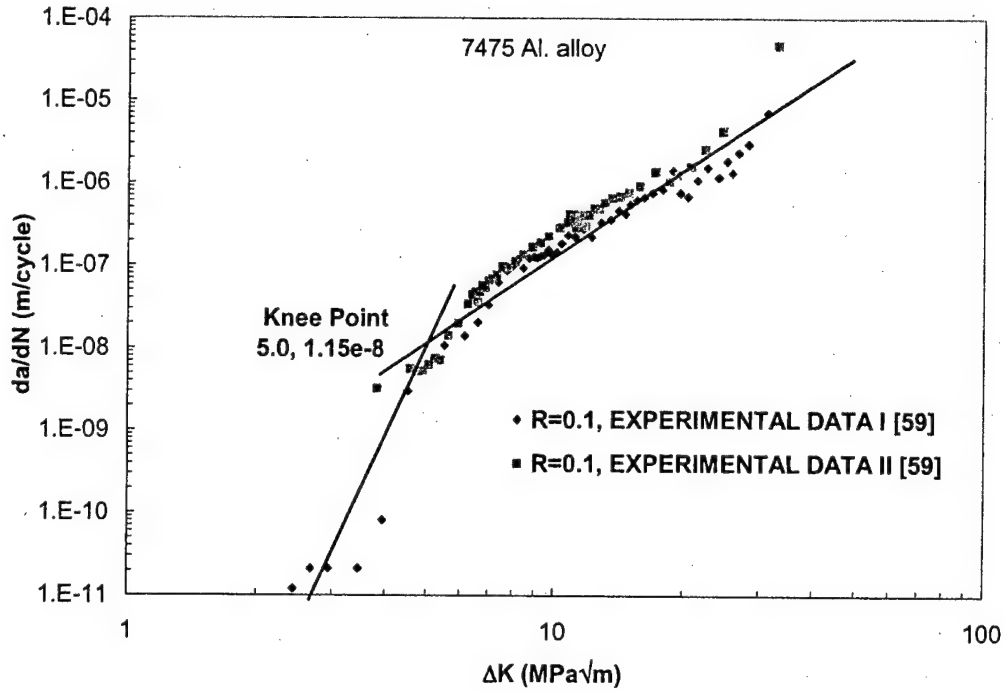

Figure A5. Knee point used to find ρ* for R =0.1, 7475 Al. alloy [59].

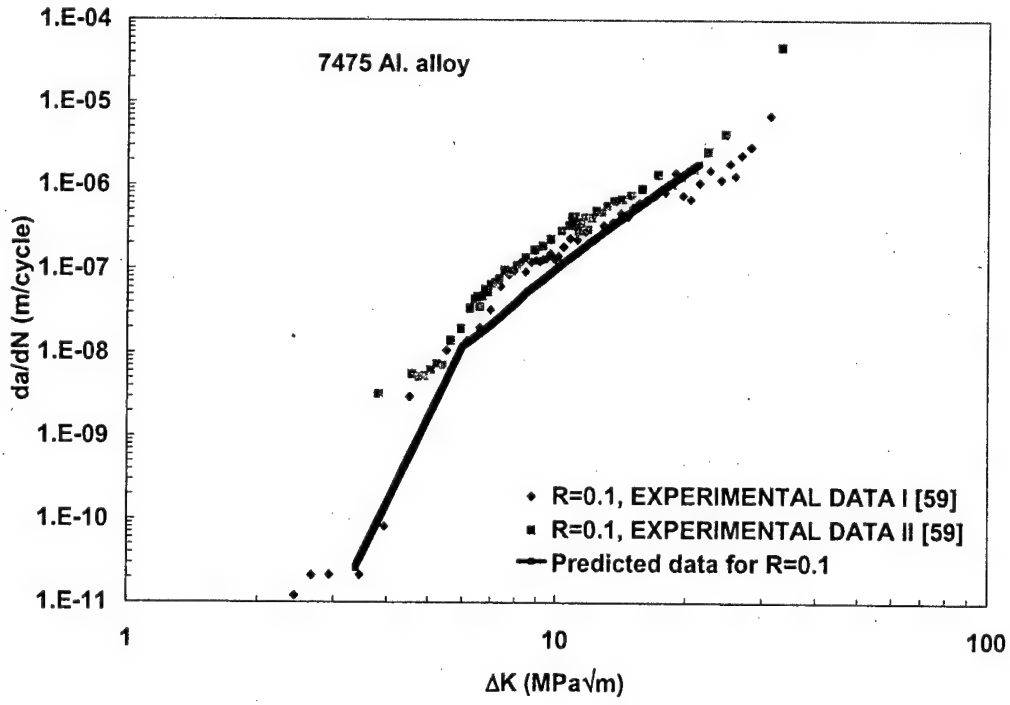

Figure A6. Predicted vs. experimental data for R=0.1, 7475 Al. alloy [59].

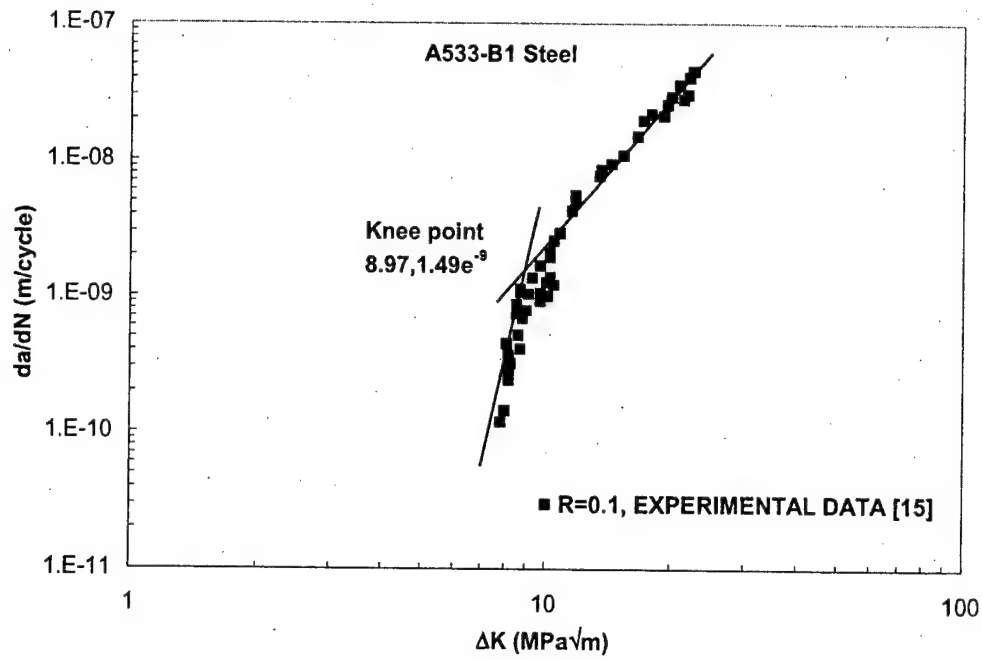

Figure A7. Knee point used to find ρ* for R =0.1, A533-B1 steel [15].

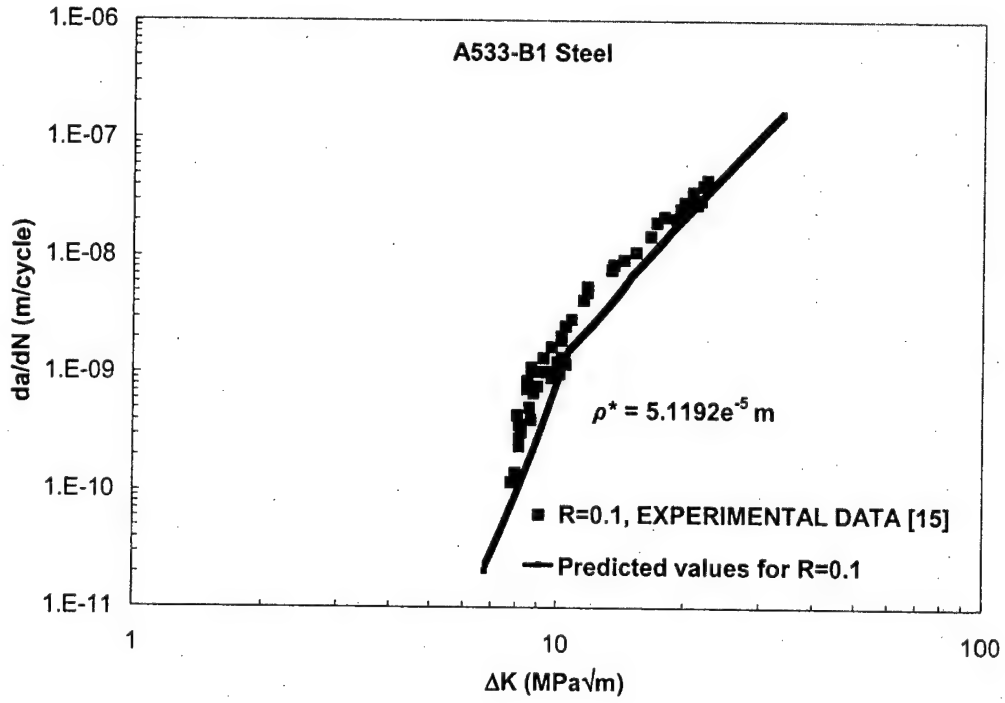

Figure A8. Predicted vs. experimental data for R=0.1, A533-B1 steel [15].

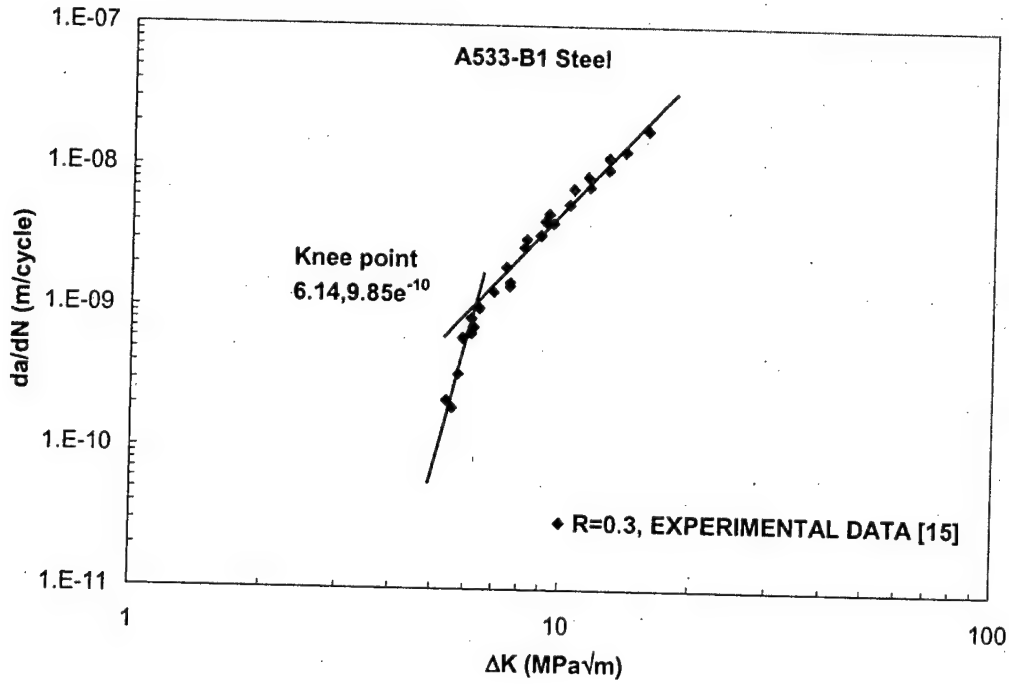

Figure A9. Knee point used to find ρ* for R =0.3, A533-B1 steel [15].

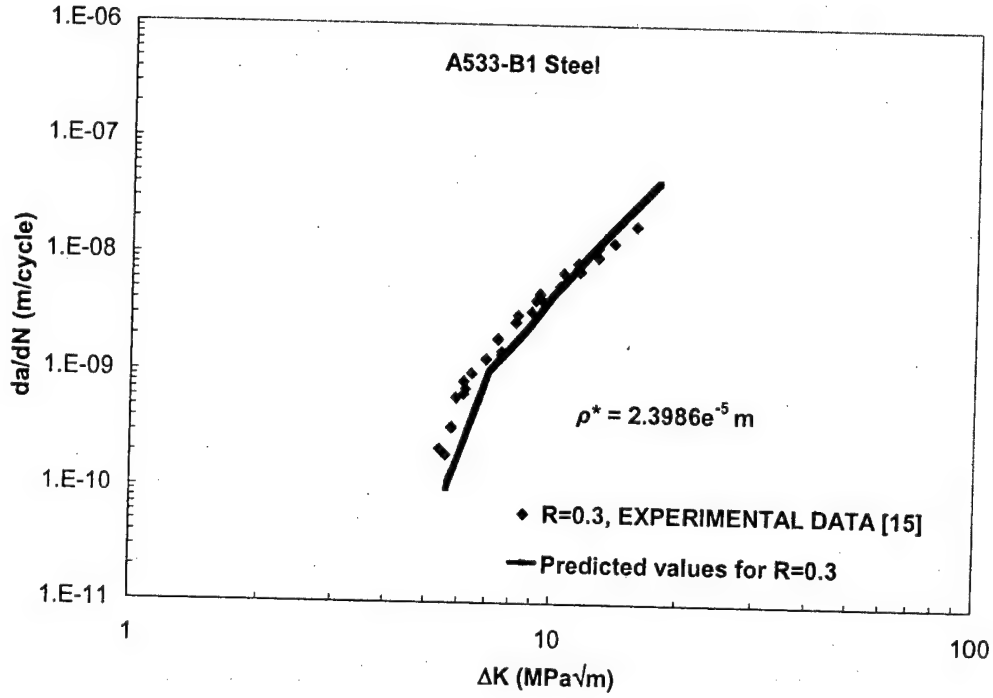

Figure A10. Predicted vs. experimental data for R=0.3, A533-B1 steel [15].

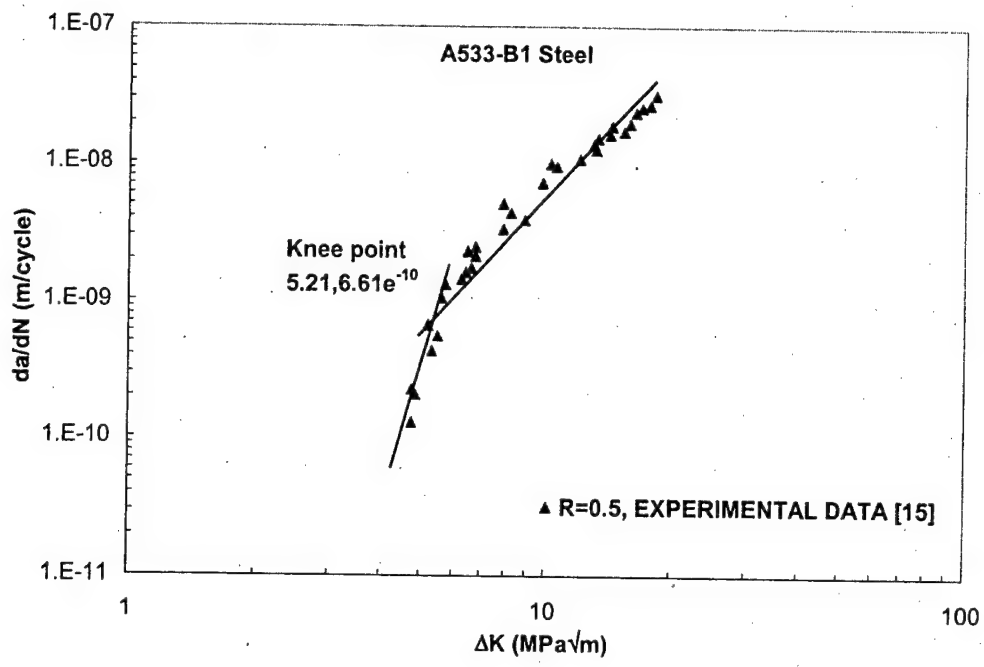

Figure A11. Knee point used to find ρ* for R =0.5, A533-B1 steel [15].

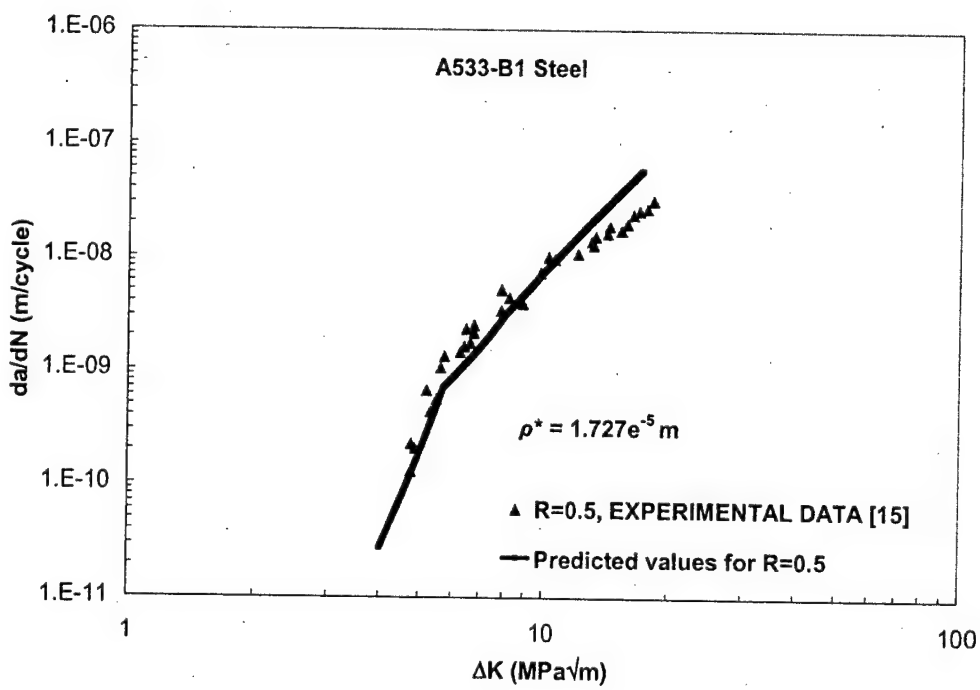

Figure A12. Predicted vs. experimental data for R=0.5, A533-B1 steel [15].

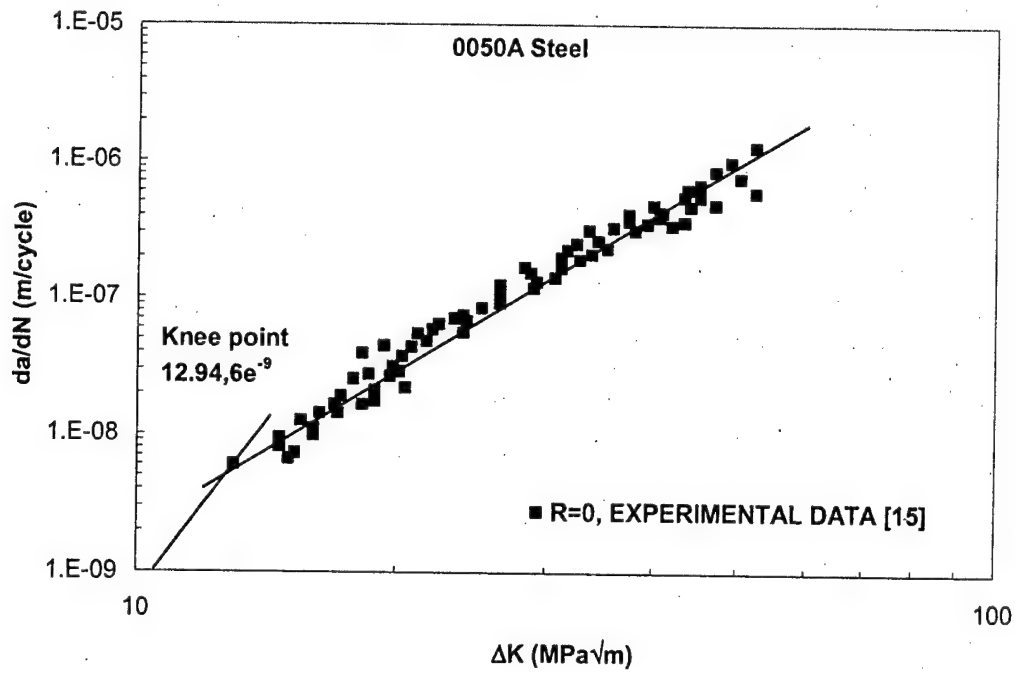

Figure A13. Knee point used to find ρ* for R =0, 0050A cast steel [15].

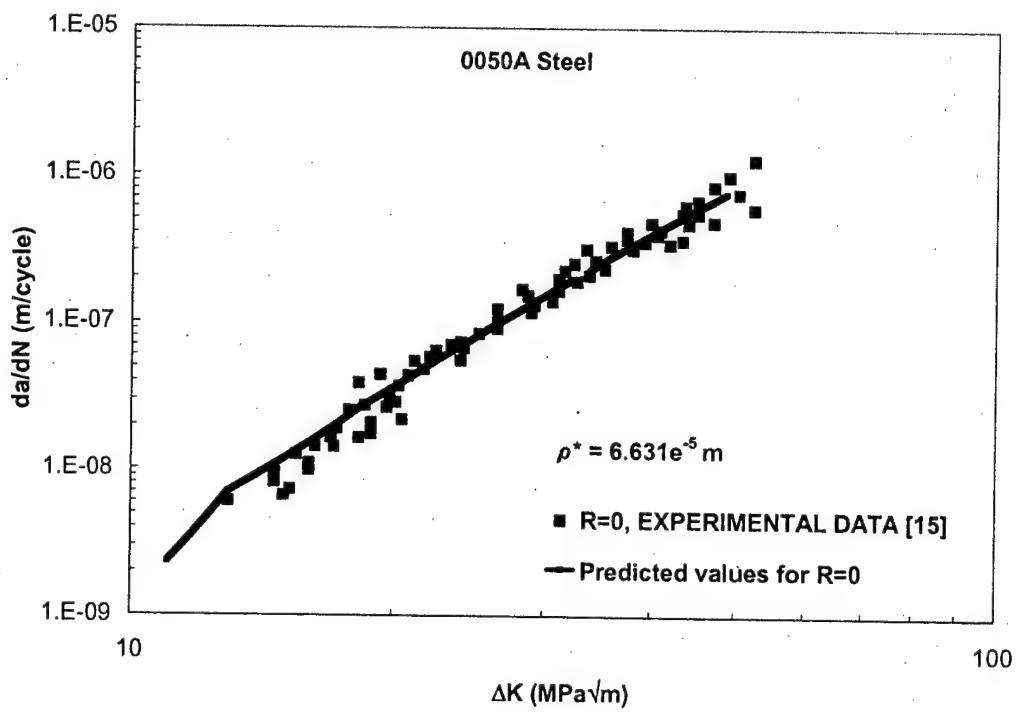

Figure A14. Predicted vs. experimental data for R=0, 0050A cast steel [15].

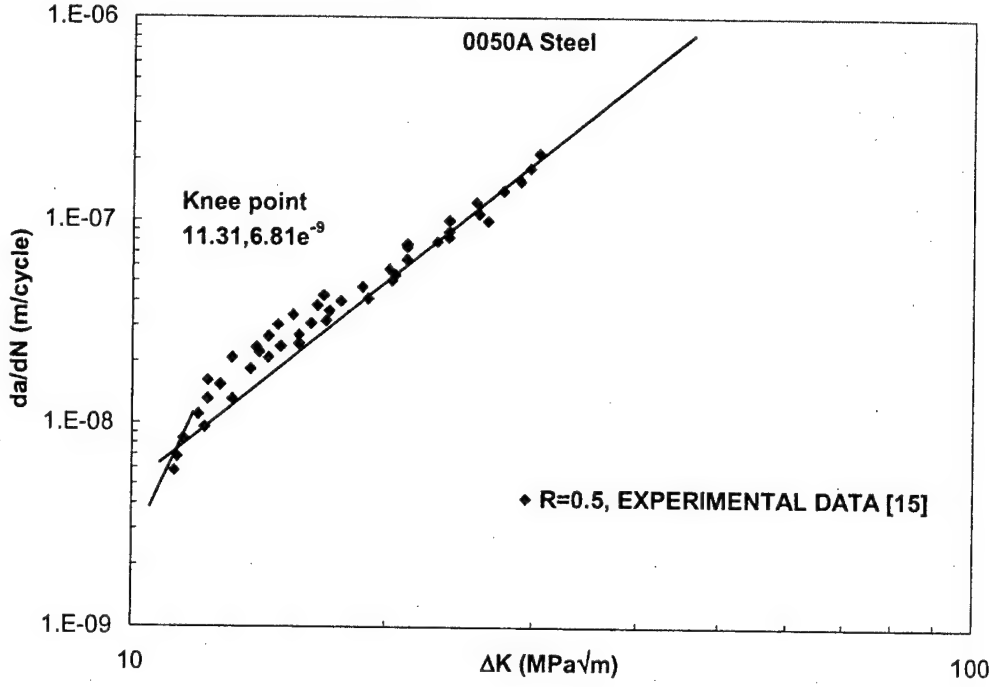

Figure A15. Knee point used to find ρ* for R =0.5, 0050A cast steel [15].

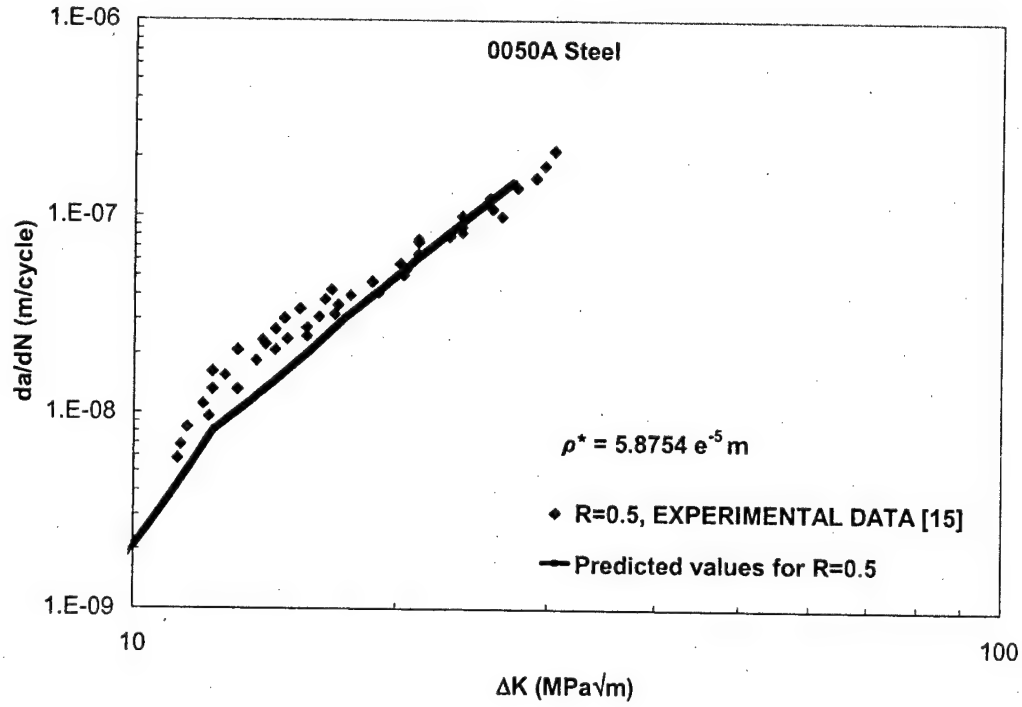

Figure A16. Predicted vs. experimental data for R=0.5, 0050A cast steel [15].

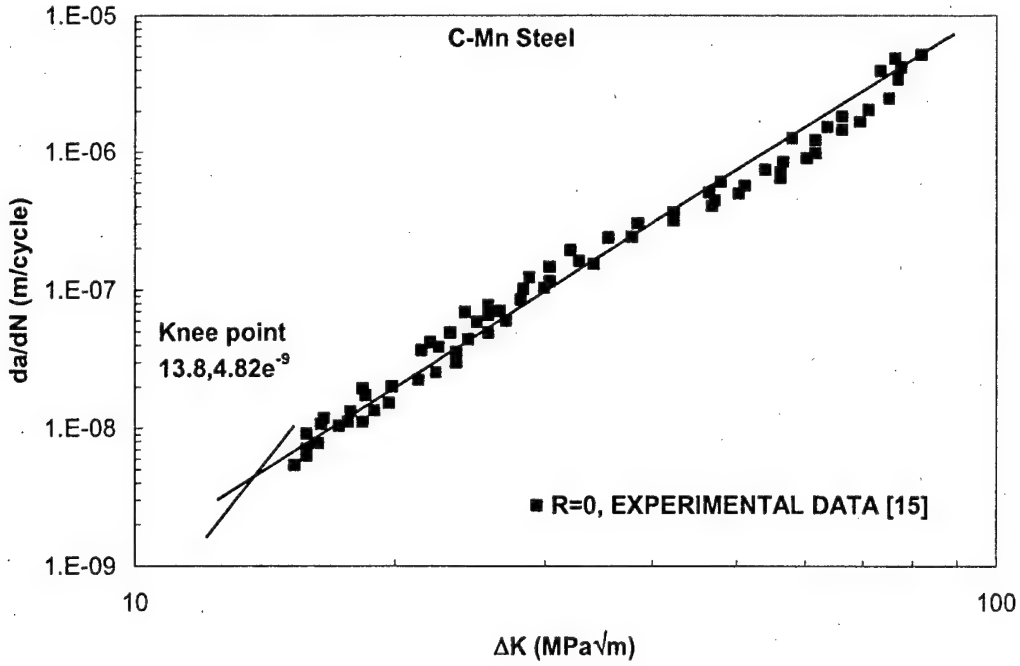

Figure A17. Knee point used to find ρ* for R =0, C-Mn cast steel [15].

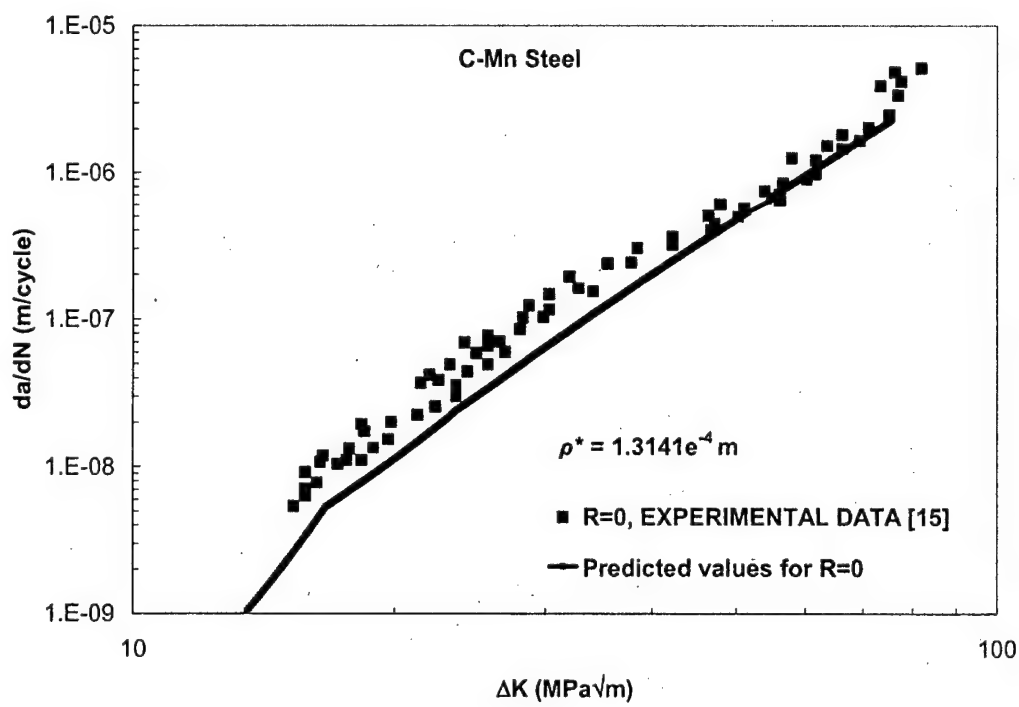

Figure A18. Predicted vs. experimental data for R=0, C-Mn cast steel [15].

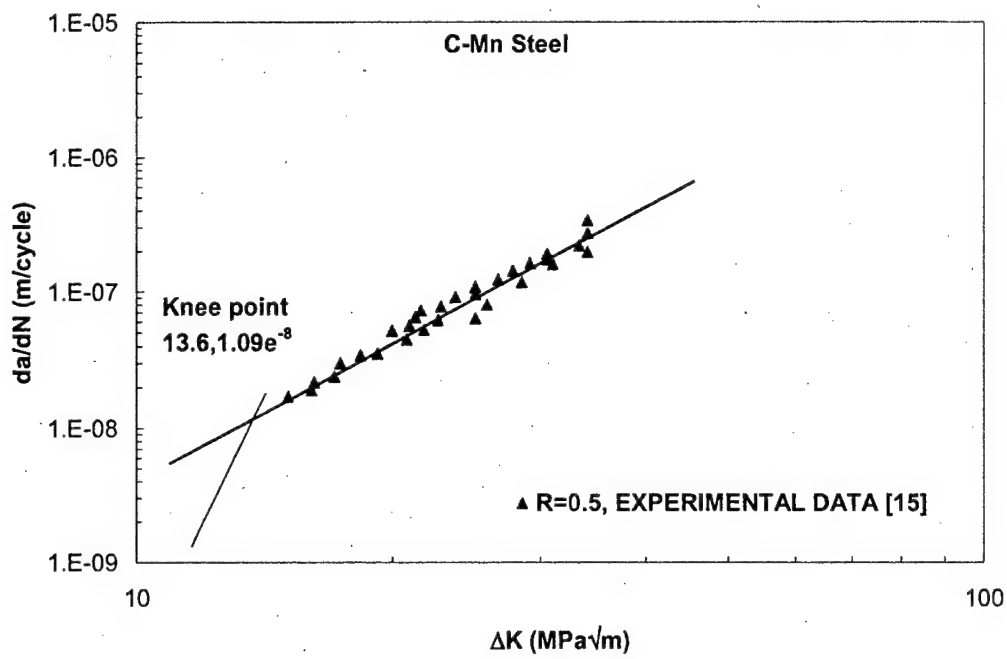

Figure A19. Knee point used to find ρ* for R =0.5, C-Mn cast steel [15].

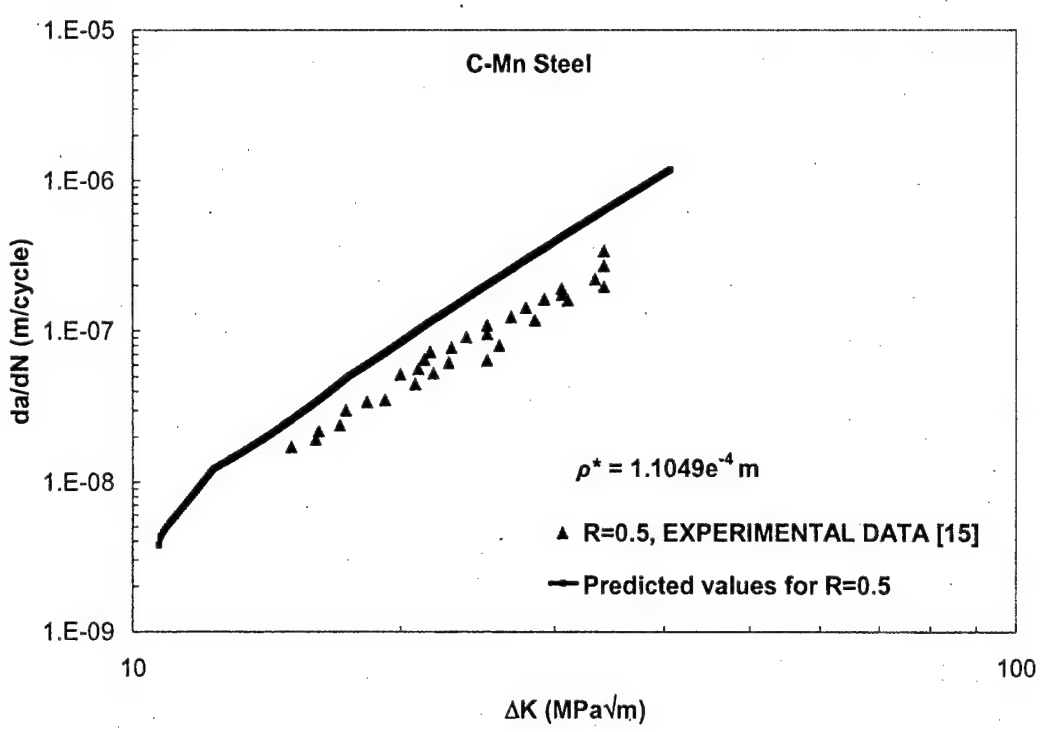

Figure A20. Predicted vs. experimental data for R=0.5, C-Mn cast steel [15].

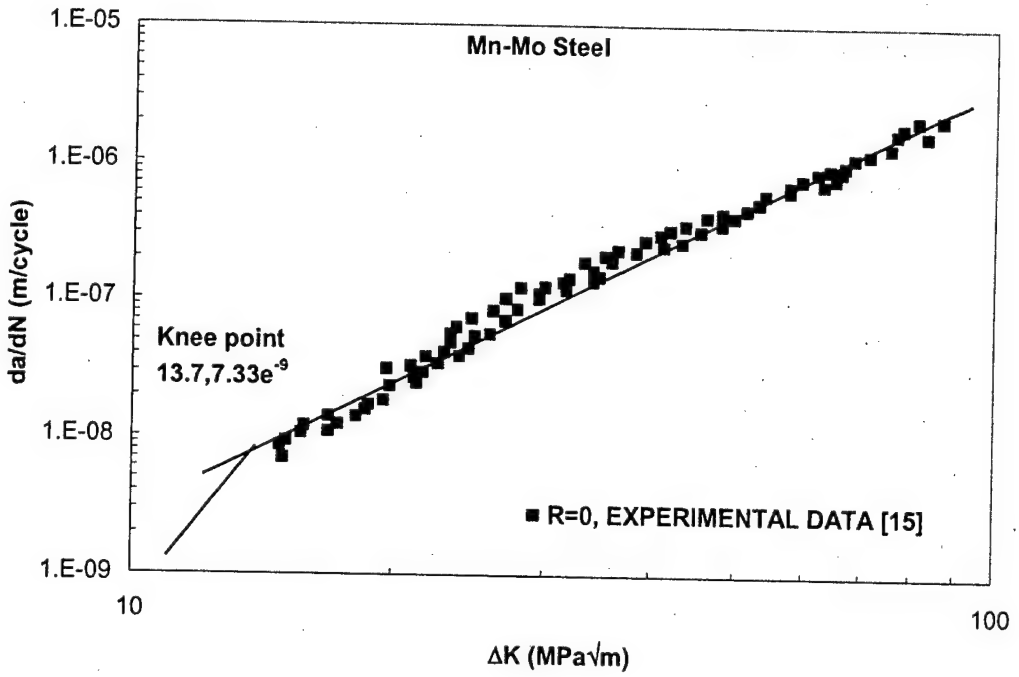

Figure A21. Knee point used to find ρ* for R =0, Mn-Mo cast steel [15].

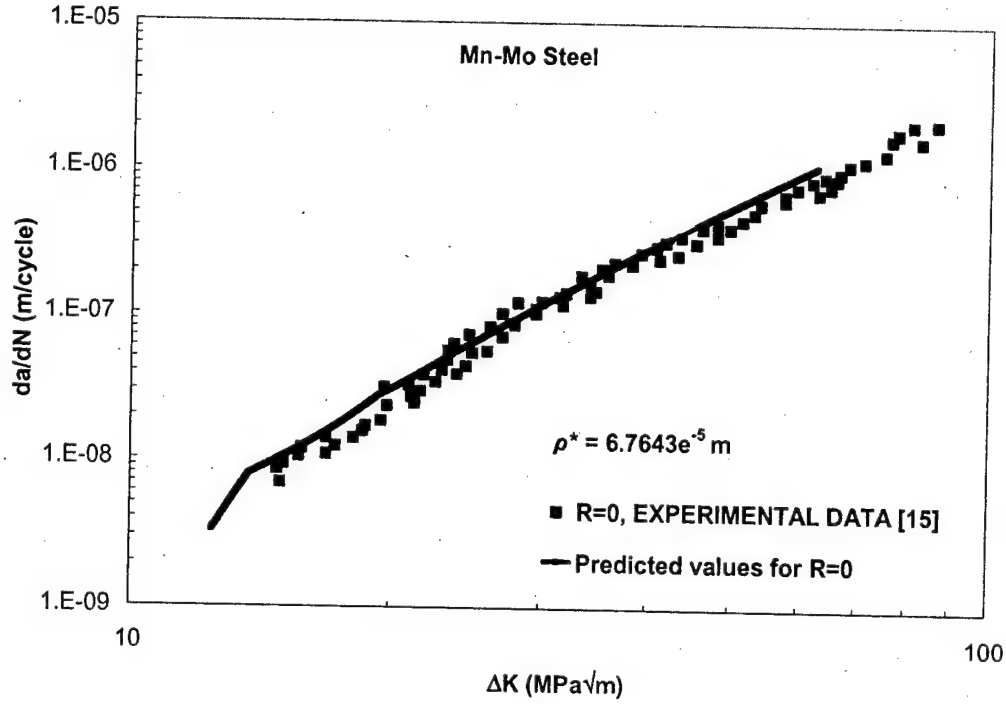

Figure A22. Predicted vs. experimental data for R=0, Mn-Mo cast steel [15].

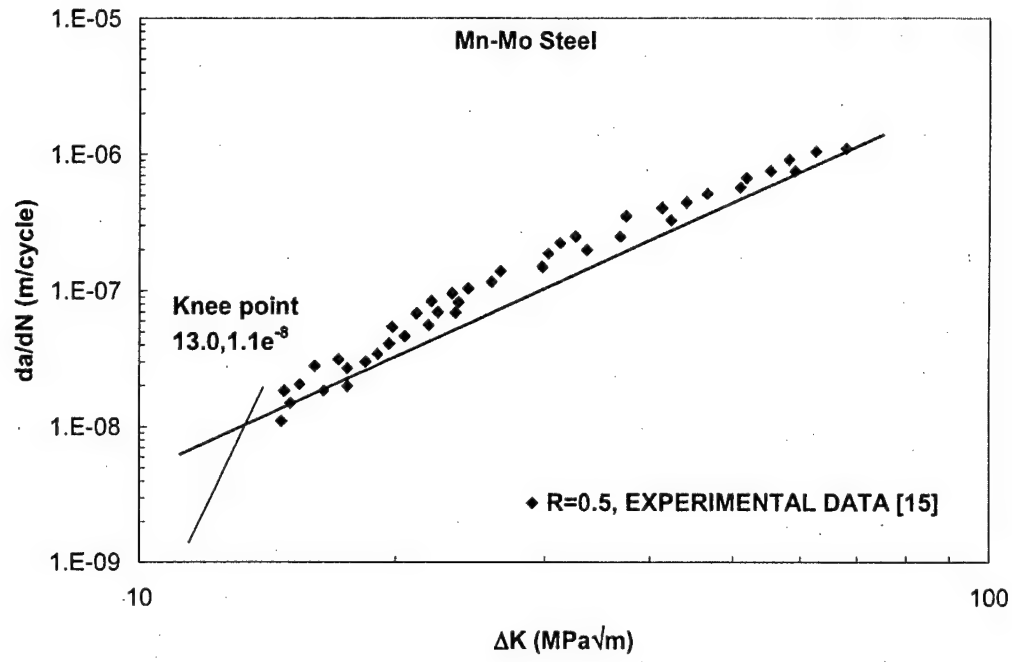

Figure A23. Knee point used to find ρ* for R =0.5, Mn-Mo cast steel [15].

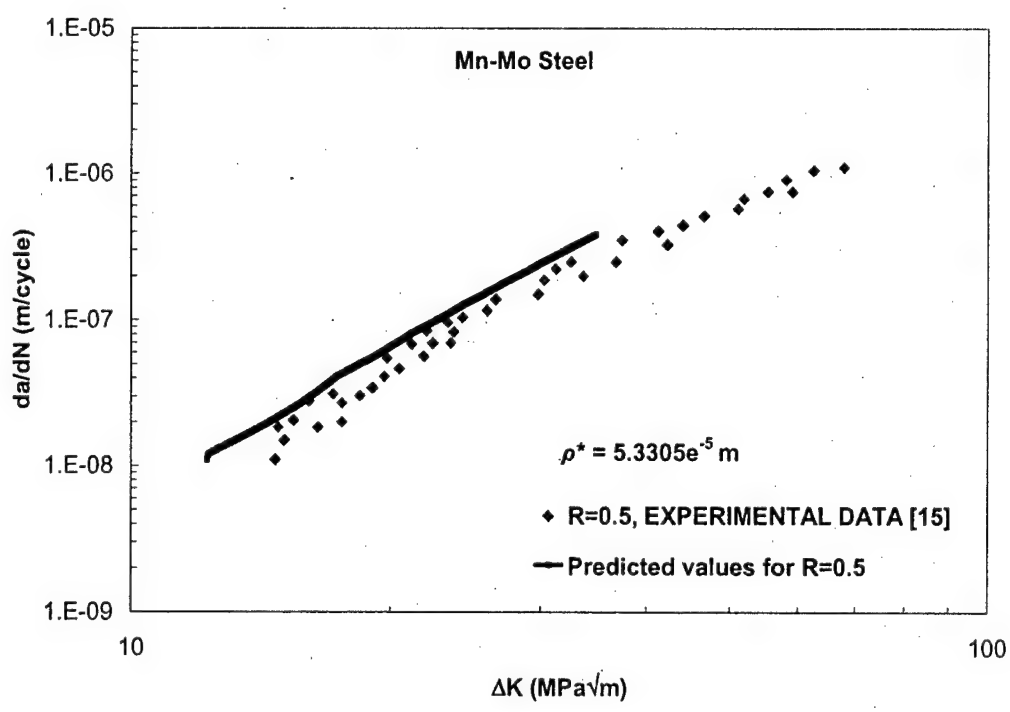

Figure A24. Predicted vs. experimental data for R=0.5, Mn-Mo cast steel [15].

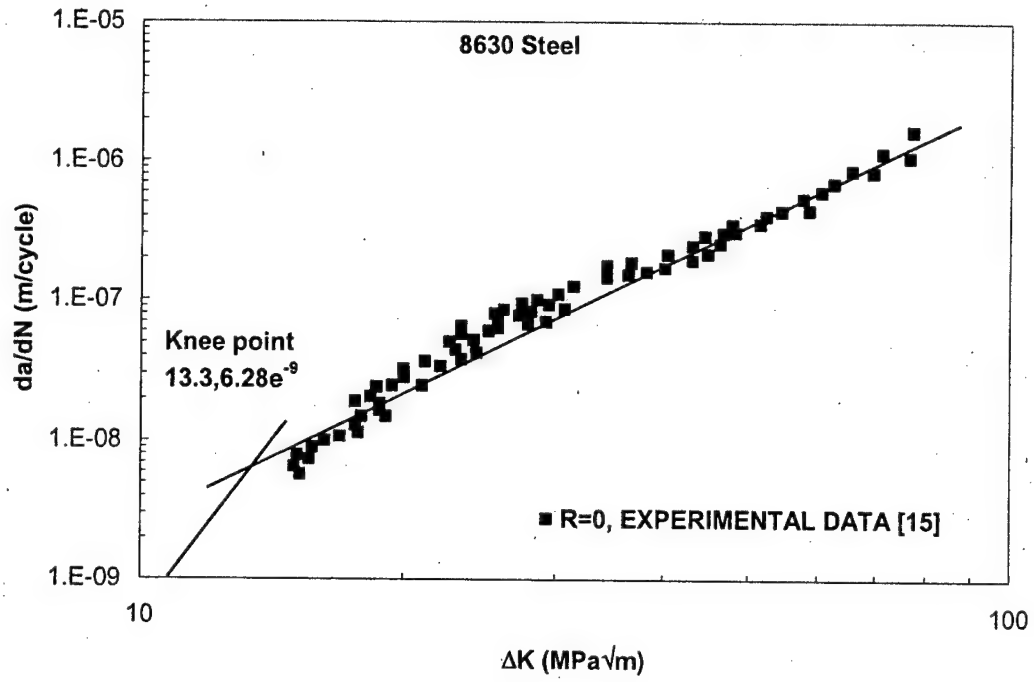

Figure A25. Knee point used to find ρ* for R=0, 8630 cast steel [15].

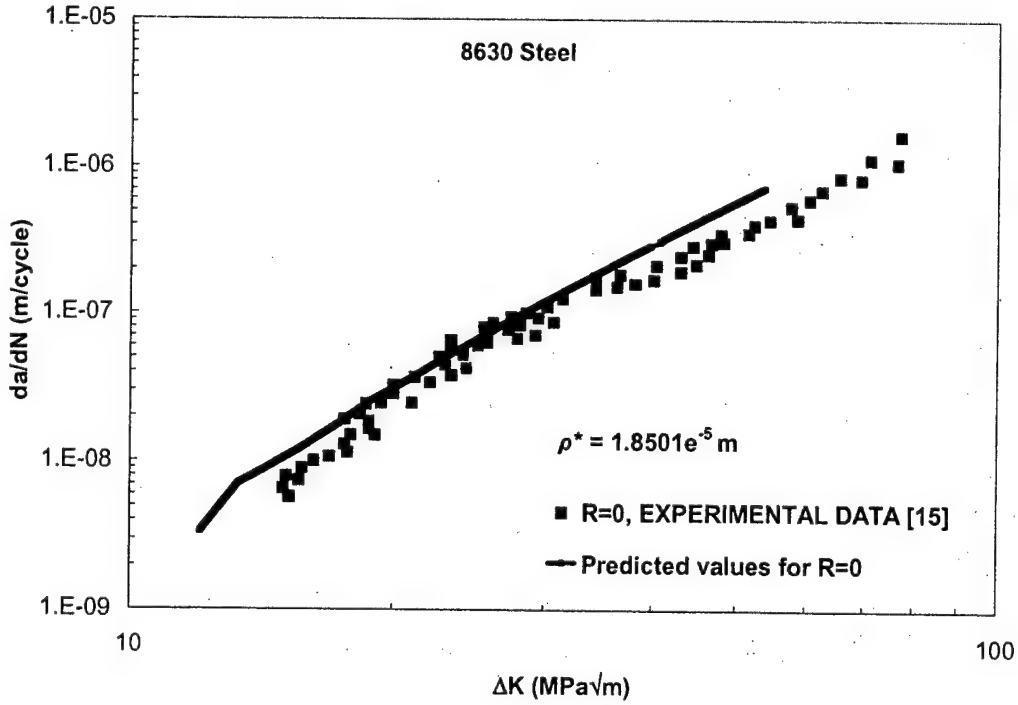

Figure A26. Predicted vs. experimental data for R=0, 8630 cast steel [15].

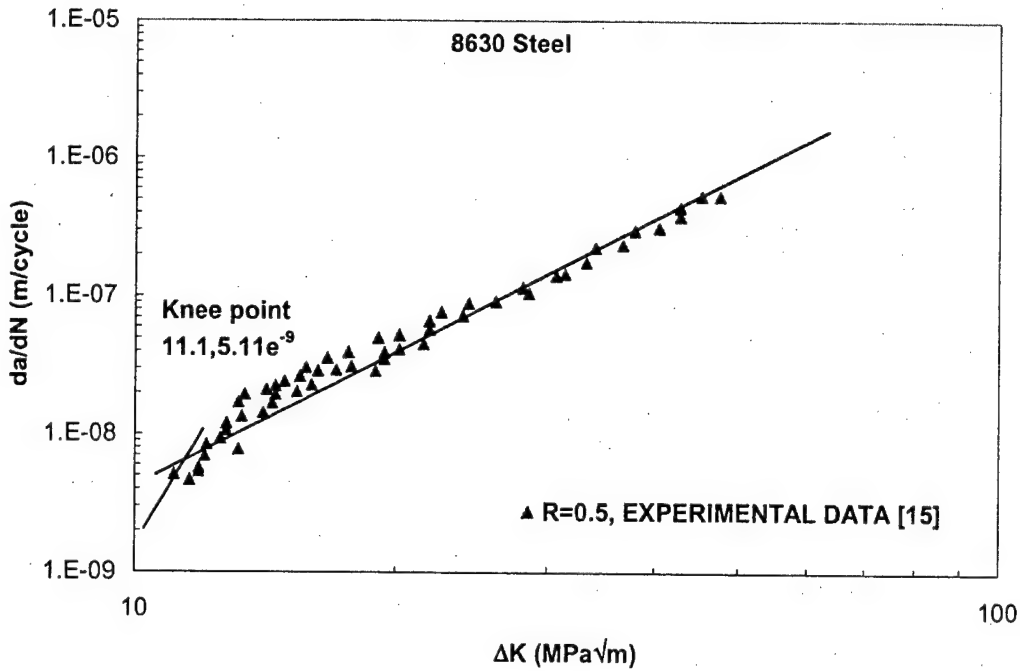

Figure A27. Knee point used to find ρ* for R =0.5, 8630 cast steel [15].

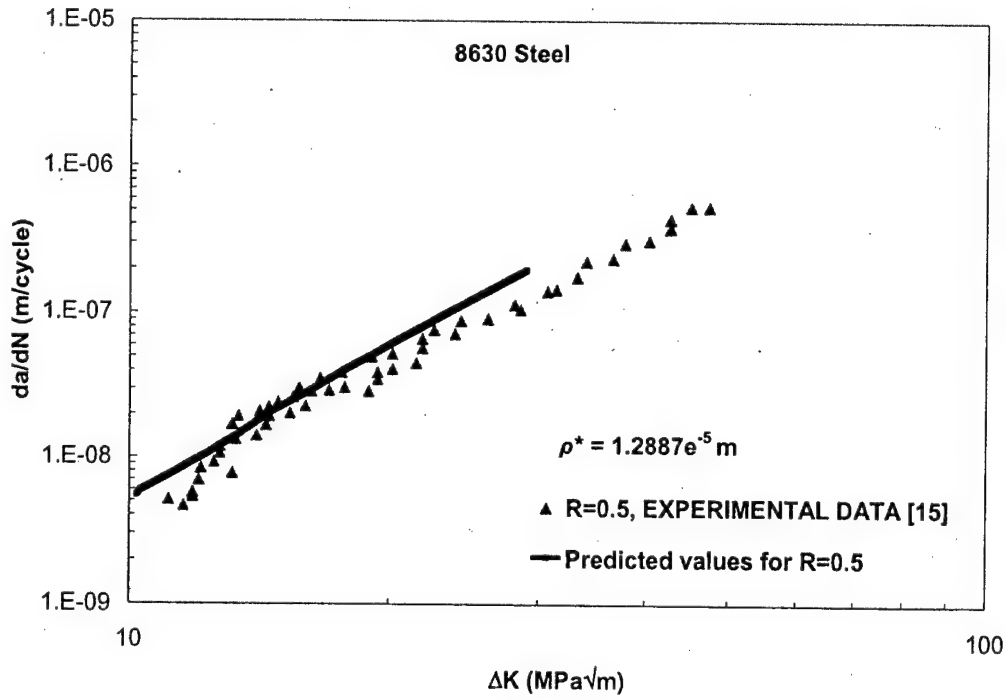

Figure A28. Predicted vs. experimental data for R=0.5, 8630 cast steel [15].

APPENDIX B

WEIGHT FUNCTION CONSTANTS FOR DIFFERENT GEOMETRIES

The crack geometries and the associated expressions for M_1, M_2 and M_3 used for the weight function calculation are given.

Center crack specimen

$$M_1 = 0.06987 + 0.40117\alpha - 5.5407\alpha^2 + 50.0886\alpha^3 - 200.699\alpha^4 + 395.552\alpha^5 - 377.939\alpha^6 + 140.218\alpha^7$$

$$M_2 = -0.09049 - 2.14866\alpha + 22.5325\alpha^2 - 89.6553\alpha^3 + 210.599\alpha^4 - 239.445\alpha^5 + 111.128\alpha^6$$

$$M_3 = 0.24721 + 2.56001\alpha - 29.6349\alpha^2 + 138.4\alpha^3 - 347.255\alpha^4 + 457.128\alpha^5 - 295.882\alpha^6 + 68.1575\alpha^7$$

where $\alpha = \frac{a}{w} = \frac{\text{crack length}}{\text{specimen width}}$

Double-edge crack specimen

$$M_1 = 0.08502 - 0.02230\alpha - 1.41028\alpha^2 + 4.64559\alpha^3 + 19.6924\alpha^4 - 148.266\alpha^5 + 336.837\alpha^6 - 336.591\alpha^7 + 127.009\alpha^8$$

$$M_2 = 0.2234 - 0.6146\alpha + 11.1687\alpha^2 - 56.5326\alpha^3 + 151.937\alpha^4 - 182.634\alpha^5 + 86.4731\alpha^6$$

$$M_3 = 0.4983 + 0.75121\alpha - 10.5597\alpha^2 + 47.9251\alpha^3 - 115.933\alpha^4 + 131.976\alpha^5 - 59.8893\alpha^6$$

where $\alpha = \frac{a}{w} = \frac{\text{crack length}}{\text{specimen width}}$

Edge crack specimen

$$M_1 = \frac{(-0.029207 + \alpha(0.213074 + \alpha(-3.02955 + \alpha(5.901933 + \alpha(-2.6578)))))}{(1 + \alpha(-1.2597 + \alpha(-0.048475 + \alpha(0.48125 + \alpha(-0.5267 + \alpha(0.34501))))))}$$

$$M_2 = \frac{(0.45116 + \alpha(3.4624 + \alpha(-1.07846 + \alpha(3.55857 + \alpha(-7.55353)))))}{(1 + \alpha(-1.4966 + \alpha(0.7646 + \alpha(-0.65931 + \alpha(0.2585 + \alpha(0.114568))))))}$$

$$M_3 = \frac{(0.427195 + \alpha(-3.730114 + \alpha(16.2763 + \alpha(-18.7999 + \alpha(14.11211)))))}{(1 + \alpha(-1.12919 + \alpha(0.033758 + \alpha(0.192114 + \alpha(-0.65824 + \alpha(0.55466))))))}$$

where $\alpha = \frac{a}{w} = \frac{\text{crack length}}{\text{specimen width}}$

APPENDIX C

MATLAB SUBROUTINES

Subroutine to calculate the ρ^* parameter

```
% --- Executes on button press in calc_dstar.
function calc_dstar_Callback(hObject, eventdata, handles)
% hObject    handle to calc_dstar (see GCBO)
% eventdata  reserved - to be defined in a future version of MATLAB
% handles    structure with handles and user data (see GUIDATA)

E =  str2double(get(handles.edit1,'String'))*1000000000;  % Units = Pa
sy = str2double(get(handles.edit2,'String'))*1000000;     % Units = Pa
n = str2double(get(handles.edit3,'String'));
SF = str2double(get(handles.edit4,'String'))*1000000;     % Units = Pa
eps = str2double(get(handles.edit5,'String'));
c = str2double(get(handles.edit6,'String'));
b = str2double(get(handles.edit7,'String'));
Dk =  str2double(get(handles.edit14,'String'))*1000000;   % Units = Pa
dadnch = str2double(get(handles.edit15,'String'));
%.............................................................
setappdata(gcbf, 'E', E);
setappdata(gcbf, 'sy', sy);
setappdata(gcbf, 'n', n);
setappdata(gcbf, 'SF', SF);
setappdata(gcbf, 'eps', eps);
setappdata(gcbf, 'c', c);
setappdata(gcbf, 'b', b);

% getting applied R Ratio from applied condition
Ratio = str2double(get(handles.edit13,'String'));
kmax = (Dk/(1-Ratio));
kmin = Dk-kmax;
clear Ratio;

% MY METHOD FOR FINDING DSTAR BY USING THE KNEE POINT RELATION THAT
% BOTH ELASTIC SWT AND PLASTIC SWT ARE SATISFIED THERE, SO EQUATING
% BOTH EQUATIONS FOR CONSTANT da/dN RHO* CAN BE FOUND OUT.

exp1 = (1/(1+n));
exp2 = (n/(1+n));
exp3 = (1/(b+c));
exp4 = (2/(b+c));
exp5 = (1/(2*b));
exp6 = (1/(exp5-exp3));
prt1 = (((4^exp1)*(1+n)*pi*E*SF*eps)^exp3);
prt2 = (((kmax*Dk)/(4*pi*(SF^2)))^exp5);
prt3 = (((kmax^exp2)*(Dk^exp1))^exp4);
Dstar =(((prt1*prt2)/(prt3))^exp6);
%-------------------------------------------------------------

setappdata(gcbf, 'Dstar',Dstar);
dstar = num2str(Dstar);
set(handles.edit16,'String',dstar);
set(handles.edit16,'enable','on');

%+++++++++++++++++++++++++++++++++++++++++++++++++++++++++++++++
```

Subroutine for the calculation and plotting of the SWT table

```
% --- Executes on button press in SWT_calc.
function SWT_calc_Callback(hObject, eventdata, handles)
% hObject    handle to SWT_calc (see GCBO)
% eventdata  reserved - to be defined in a future version of MATLAB
% handles    structure with handles and user data (see GUIDATA)

% ================================================================
%      GENERATING SWT TABLE
% ================================================================
% In the SM table 1st Column should be the Product (min. to max.), 2nd
% column should be Nf (max. to min.)....Input from user can be taken in
any way
%=================================================================
% MAKING SM TABLE BY USING KNEE POINT AND ELASTIC AND PLASTIC PART

Dstar = getappdata(gcbf,'Dstar');
n = getappdata(gcbf,'n');
sy = getappdata(gcbf,'sy');
E = getappdata(gcbf,'E');
b = getappdata(gcbf,'b');
c = getappdata(gcbf,'c');
SF = getappdata(gcbf,'SF');
eps = getappdata(gcbf,'eps');
DkKnee = str2double(get(handles.edit14,'String'))*1000000;
dadnKnee = str2double(get(handles.edit15,'String'));
RRat = str2double(get(handles.edit13,'String'));
kmx = DkKnee/(1-RRat);  %-kres;
kmn = (DkKnee-kmx);     %-kres;

xnum = 2;
clear RRat;
[maxstrs,minstrs,minstrn,maxstrn] = rice(xnum,Dstar,kmx,kmn,n,E,sy);
maxstrs = maxstrs(1);
minstrs = minstrs(1);
maxstrn = maxstrn(1);
minstrn = minstrn(1);
dstrs = (maxstrs-minstrs);
dstrn = (maxstrn-minstrn);
rb = minstrs/maxstrs;
prd = (dstrs*dstrn)/(2*(1-rb));
clear DkKnee;
clear minstrs;
clear maxstrs;
clear minstrs;
clear maxstrn;
clear minstrn;
clear dstrs;
clear dstrn;
clear rb;
```

```
% TABLE IS FOR Nf from 1e -5 to 1e 13, (1e-5 to x) "plastic part", (x to
1e15) "elastic part".

SM(1,2) = 1e15;
SMel = ((SF^2)/E)*((2*SM(1,2))^(2*b));
SMpl = (SF*eps)*((2*SM(1,2))^(b+c));
SM(1,1) = SMel; % + SMpl; % ELASTIC PART
SM(2,1) =  prd;
SM(2,2) = (Dstar/dadnKnee);
SM(3,2) = 1e-5;
clear SMel;
clear SMpl;
SMel = ((SF^2)/E)*((2*SM(3,2))^(2*b));
SMpl = (SF*eps)*((2*SM(3,2))^(b+c));
SM(3,1) = SMpl;  % + SMel;  % PLASTIC PART
clear dadnKnee;
setappdata(gcbf,'SM',SM);
set(handles.edit29,'string',SM(:,1));
set(handles.edit30,'string',SM(:,2));
hold on;
axes(handles.axes3);

% Plotting equation and the three point solution on the GUI
% SM1 is the variable with 100 point calculated equation
% SM is the three point SWT table with a knee point

loglog(SM(:,2),SM(:,1),':ok');
N = logspace(15,-5,100)';
lim = length(N);
for i = 1:lim
 RHS(i,1) = (SF^2)/E)*((2*N(i,1))^(2*b))+(SF*eps)*((2*N(i,1))^(b+c));
end
SM1(1:lim,1)=RHS(1:lim,1);
SM1(1:lim,2)=N(1:lim,1);
loglog(SM1(:,2),SM1(:,1),'-b');

%+++++++++++++++++++++++++++++++++++++++++++++++++++++++++++++++++
```

Main subroutine for the overall calculations and control of the program

```
%==================================================================
% --- Executes on button press in Runcalc.
function Runcalc_Callback(hObject, eventdata, handles)
% hObject    handle to Runcalc (see GCBO)
% eventdata  reserved - to be defined in a future version of MATLAB
% handles    structure with handles and user data (see GUIDATA)


w = str2double(get(handles.edit8,'String'));        % Units = m
af = str2double(get(handles.edit19,'String'));
Dstar = str2double(get(handles.edit16,'String'));   % Units = m
setappdata(gcbf, 'Dstar', Dstar);
sy = getappdata(gcbf, 'sy');
n = getappdata(gcbf, 'n');
ai = str2double(get(handles.edit10,'String'));
no = round((af-ai)/Dstar);      % total no. of elements in the
                                  specimen rounded off to nearest
                                  integer
setappdata(gcbf, 'no', no);
E = getappdata(gcbf, 'E');
geom = get(handles.Listbox_Geometry,'value');
ldc = getappdata(gcbf,'ldc');
Dkth = getappdata(gcbf, 'Dkth');
b = getappdata(gcbf,'b');
c = getappdata(gcbf,'c');
tempxnum = str2double(get(handles.edit31,'String'));  % from GUI
setappdata(gcbf,'tempxnum',tempxnum);

DAM = zeros((no+300),1);
DAMAGE = zeros(1,10);
LNGTH = zeros(10,1);
CYC = zeros(10,1);
KR = zeros((no+100),1);  % KR will be used as K res
setappdata(gcbf,'KR',KR);
retard = 0;
cnt = 0;
no_el_offset = 0;
init = 1;

for iter1 = 1:no
    LNGTH(iter1,1) = ai+ iter1*Dstar;     %  Storing end points of all
                                             elements in memory
end

ov = 0;
%-------------------------------------------------------------
% MAIN FOR LOOP OF CALCULATION STARTS
%-------------------------------------------------------------
for p = 1:no
%   ovpercent = str2double(get(handles.edit17,'String'))/100;
%   determines at what % of (af  ai) to apply overload
%   chk = round(ovpercent*no);
```

```
        ovbrokenels = 0;
        ovcl = 0;

      %-------------------------------------------------------------
      % THIS IF-LOOP APPLIES OVERLOAD (calls the Overload subroutine)
      %-------------------------------------------------------------

          if ov == 0  % if ov is 1 then overload is not applied
              a = ai+((p-1)*Dstar);
              al = a/w;
              if a >= 0.0254
                clear DeltaKt;

 [DAM,CYC,ovbrokenels,savedstrs,DeltaKt] =
                        overloaddam(a,al,p,DAM,no,LNGTH,Kmax,Kmin,CYC);
 % STORES DAMAGE FOR OVERLOAD 1 CYCLE

                  if ovbrokenels >= 1
                      da = (ovbrokenels*Dstar);
                      number = ovbrokenels-1;
                      for it4 = p:p+number
                          DADNA(it4,1) = a+da;
                          DADNDK(it4,1) = DeltaKt/1000000;
                          DADNDK(it4,2) = (da/1);
                          DADNA(it4,2) = DADNDK(it4,2);
                      end
                  end

                  p = p+ovbrokenels;
                  a = ai+((p-1)*Dstar);

%####################K RESIDUAL METHOD ############################
% ##########Calls the weight function subroutine #################

             [K_res] = calculateKres(a,savedstrs,n,E,Dstar,sy);

             clear Kres;
             clear XX;
             pb = p-1;

             for it9 = 1:length(K_res)
                 KR(it9+pb,1) = K_res(it9,1);
             end
             setappdata(gcbf,'KR',KR);
             clear K_res;


             ovcl = 1;
             ov = 1;
             retard = 1;
% controls if loop for applying the retardation by shifting range
             %cnt = 1;
         end
     end
     %-------------------------------------------------------------

     a = ai+((p-1)*Dstar);
```

```
al = a/w;


clear K_max;
clear K_min;
clear applDK;

if ldc == 0
    K_max = str2double(get(handles.edit12,'String'))*1000000;
    K_min = str2double(get(handles.edit11,'String'))*1000000;
    setappdata(gcbf, 'K_max', K_max);
    setappdata(gcbf, 'K_min', K_min);

elseif ldc == 1
    S_max = str2double(get(handles.edit12,'String'))*1000000;
    S_min = str2double(get(handles.edit11,'String'))*1000000;
    DS = S_max-S_min;
    [DeltaK,DeltaKt] = getDeltaK(a,al,DS,Dkth,geom);
    RR = (S_min/S_max);
    K_max = (DeltaK/(1-RR));
    K_min = K_max - DeltaK;
    setappdata(gcbf, 'K_max', K_max);
    setappdata(gcbf, 'K_min', K_min);

end

applDK = K_max-K_min;
K_max = K_max + KR(p,1);
K_min = K_min + KR(p,1);
if K_min < 0
    K_min = 0;
end

setappdata(gcbf,'K_max',K_max);
setappdata(gcbf,'K_min',K_min);

rp = (1/((1+n)*pi))*((K_max/sy)^2);
clear xnum;
xnum = round(rp/Dstar);
% No. of elements ahead of tip within Plastic zone
x0 = Dstar;
%-------------------------------------------------------

if p == 230
    stopppp = 1;
end

clear Kmax;
clear Kmin;
Kmax = K_max;
Kmin = K_min;

if Kmin < 0
    Kmin = 0;
end
setappdata(gcbf,'Kmax',Kmax);
setappdata(gcbf,'Kmin',Kmin);
```

```
Kmax = getappdata(gcbf,'Kmax');
Kmin = getappdata(gcbf,'Kmin');
R = Kmin/Kmax;

%-------------------------------------------------------
DADNDK(p,1) = applDK/1000000;
% Storing unmanipulated DK but working on the manip. DK
%-------------------------------------------------------

rp = 2*(1/((1+n)*pi))*((Kmax/sy)^2);

% CRACK IS ARRESTED IF THE rp < Dstar
if rp < Dstar
    errordlg('Crack cannot grow further','No crack growth','on');
    uiwait;
end
clear xnum;
xnum = round(rp/Dstar);
% No. of elements ahead of tip within Plastic zone
setappdata(gcbf, 'xnum', xnum);
xmin = Dstar;
xmax = xnum*Dstar;
xnu = xnum-1;
x0 = Dstar;
EL = zeros(xnum,2);
%-------------------------------------------------------
na = n;
%-------------------------------------------------------
% getting the maxstrs minstrs maxstrn minstrn from RICE + Elastic
%-------------------------------------------------------
clear rpmel;
clear rpcel;
[maxstrsr,minstrsr,minstrnr,maxstrnr,lngth,rpmel,rpcel] =
                                rice(xnum,x0,Kmax,Kmin,n,E,sy);
%-------------------------------------------------------
xnum = length(maxstrsr);
for ita = 1:xnum
    maxstrs(ita,1) = maxstrsr(ita);
    minstrs(ita,1) = minstrsr(ita);
    minstrn(ita,1) = minstrnr(ita);
    maxstrn(ita,1) = maxstrnr(ita);
end
clear maxstrsr;
clear minstrsr;
clear maxstrnr;
clear minstrnr;

for v = 1:xnum
    EL(v,1) = maxstrs(v,1);    % max strs associated to each element
    EL(v,2) = minstrs(v,1);    % min strs associated to each element
end

SM = getappdata(gcbf, 'SM');
SF = getappdata(gcbf, 'SF');

% if EL(1,1) < SF
```

```
    for it2 =1:xnum
        destrs = EL(it2,1)-EL(it2,2);
        destrn = maxstrn(it2,1)-minstrn(it2,1);
        rbar = (EL(it2,2)/EL(it2,1));
        fit(it2,1) =  ((destrs*destrn)/(2*(1-rbar)));
        % Δsigma * Δepsilon prod to find Nf
    end
    clear it2;
    life = gettingNf(fit);
    % Interpolated values of Life for the 'fit'..on SM table curve

    ni = (1-DAM(p,1))*life(1,1);  % ni for current element to fail
    pa = p-1; % just subtracting 1 from p

    if ni < 1
        ni = 1;
    end
    lt = length(life);
    for it2 =1:lt
        DAM((pa+it2),1) = (ni/life(it2,1))+ DAM((pa+it2),1);
% stores the damage value of element upto current element broken
    end
    clear it2;

    brokenels = length(find(DAM(p:(pa+lt)) >= 0.99999999));
% Finding the no. of broken elements to calculate the crak growth rate

    %     for it3=p:no
    %         CYC(it3,1) = ni + CYC(it3,1);
    % Stores the total no of cycles for element p at or after breaking
    %     end

    number = brokenels-1;
    if number < 0
        number = 0;
    end

    da = (Dstar + (number)*Dstar);
    DelK = DADNDK(p,1);
    for it = p:p+number
        DADNA(it,1) = a+da;
        DADNDK(it,1) = DelK;
        DADNDK(it,2) = (da/(ni+ovcl));
        DADNA(it,2) = DADNDK(it,2);
    end

    p = p+number;
    ovcl = 0;

    p = p+1;
```

```
 if p == round(init*no/100);
        string = ['calculation is ',num2str(init),'% complete'];
        wb = waitbar(0,string);
        waitbar(p/no);
        close(wb);
        init = init+1;
        if init == 95;
            hhh=1;
        end
    end

end
setappdata(gcbf,'DADNA', DADNA);
setappdata(gcbf,'DADNDK', DADNDK);
hold on;
DADNDK = getappdata(gcbf,'DADNDK');
axes(handles.axes1);

if ldc == 1
 loglog(DADNDK((1:round(no/20):no),1),DADNDK((1:round(no/20):no),2),'-
                                                                    .*r');
    set(handles.edit20,'string',DADNDK(1:no,1));
    set(handles.edit21,'string',DADNDK(1:no,2));

elseif ldc == 0
 plot(DADNA((1:round(no/20):no),1)*1000,DADNA((1:round(no/20):no),2),'-
                                                                    .*b');
    set(handles.edit20,'string',DADNA(1:no,1)*1000);
    set(handles.edit21,'string',DADNA(1:no,2));
end
setappdata(gcbf,'count', 1);

% ++++++++++++++++++++++++++++++++++++++++++++++++++++++++++++++++++++++
```

Subroutine for the application of the overload or block load change

```
%==================================================================
% THIS FUNCTION CALCULATES THE DAMAGE DUE TO OVERLOAD
%==================================================================

function[DAM,CYC,ovbrokenels,savedstrs,DeltaKt] =
                  overloaddam(a,al,p,DAM,no,LNGTH,Kmax,Kmin,CYC);

E = getappdata(gcbf, 'E');
sy = getappdata(gcbf, 'sy');
n = getappdata(gcbf, 'n');
SF = getappdata(gcbf, 'SF');
eps = getappdata(gcbf, 'eps');
Dstar = getappdata(gcbf,'Dstar');
Dkth = getappdata(gcbf,'Dkth');
SM = getappdata(gcbf, 'SM');
oldkmax = Kmax;
oldkmin = Kmin;
Kmax = Kmax*2;
Kmin = Kmin;
R = Kmin/Kmax;
ep = getappdata(gcbf, 'ep');
DeltaKt = Kmax-Kmin;

%-----------------------------------------------------------------
rp = 2*(1/((1+n)*pi))*((Kmax/sy)^2);

if rp < Dstar
    errordlg('Crack cannot grow further','No crack growth','on');
    uiwait;
end
clear xnum;
xnum = round(rp/Dstar);
% No. of elements ahead of tip within Plastic zone
setappdata(gcbf, 'xnum', xnum);
xmin = Dstar;
xmax = xnum*Dstar;
xnu = xnum-1;
x0 = Dstar;
EL = zeros(xnum,2);

b = getappdata(gcbf,'b');
c = getappdata(gcbf,'c');
na = n;
%-----------------------------------------------------------------
% getting the maxstrs minstrs maxstrn minstrn from RICE + Elastic
%-----------------------------------------------------------------
[maxstrsr,minstrsr,minstrnr,maxstrnr] = rice(xnum,x0,Kmax,Kmin,n,E,sy);

for ita = 1:xnum
    maxstrs(ita,1) = maxstrsr(ita);
    minstrs(ita,1) = minstrsr(ita);
    minstrn(ita,1) = minstrnr(ita);
```

```
    maxstrn(ita,1) = maxstrnr(ita);
end
clear maxstrsr;
clear minstrsr;
clear maxstrnr;
clear minstrnr;

savedstrs = zeros(xnum,1);
savedstrs(:,1) = minstrs(:,1);

EL(1:xnum,1) = maxstrs(1:xnum,1);
% max strs associated to each element
EL(1:xnum,2) = minstrs(1:xnum,1);
% min strs associated to each element

for it2 =1:xnum
    destrs = EL(it2,1)-EL(it2,2);
    destrn = maxstrn(it2,1)-minstrn(it2,1);
    rbar = (EL(it2,2)/EL(it2,1));
    fit(it2,1) =  ((destrs*destrn)/(2*(1-rbar)));
    % Δsigma * Δepsilon prod to find Nf

end

life = gettingNf(fit); % Getting Nf values from the SM table

ni = 1;            % ni = 1 for one cycle overload
pa = p-1; % just subtracting 1 from p
for it2 =p:(xnu+p)
    DAM(it2,1) = (ni/life(it2-pa,1))+ DAM(it2,1);
% stores the damage value of element upto current broken
end
% CHECKS FOR HOW MANY ELEMENTS THE DAMAGE GOES ABOVE 1
ovbrokenels = length(find(DAM(p:(xnu+p))>=0.99999999));
% for it3=p:no
%     CYC(it3,1) = ni + CYC(it3,1);    % Stores the total no of cycles
for element p at or after breaking
% end

%+++++++++++++++++++++++++++++++++++++++++++++++++++++++++++++++++++++
```

Subroutine to calculate stress profiles ahead of the crack using Rice and Elastic solution.

```
%==================================================================
%              RICE AND ELASTIC SOLUTION SUBROUTINE
%==================================================================

function [maxstrs,minstrs,minstrn,maxstrn,lngth,rpmel,rpcel] =
                                    rice(xnum,x0,Kmax,Kmin,n,E,sy);
ey = sy/E;

if xnum <= 1
    xnum = 10;
end
for i = 1:xnum
    lngth(i,1) = i*x0;
end
pow = n/(1+n);
spow = 1/(1+n);

for it = 1:xnum
    S(it,1)  = sy*((Kmax^2)/((1+n)*pi*(sy^2)*lngth(it,1)))^pow;
    EP(it,1) = ey*((Kmax^2)/((1+n)*pi*(sy^2)*lngth(it,1)))^spow;
end

rpmel = length(find(S(:,1) >= sy));
if rpmel == 0
   xm = ((Kmax/sy)^2)*(1/pi)*((1/(1+n))-0.5);
%offset for the elastic solution to be continuous at r_m
else
  for it1 = 1:rpmel
    maxstrs(it1) = S(it1,1);
    maxstrn(it1) = EP(it1,1);
  end
  xm = ((Kmax/sy)^2)*(1/pi)*((1/(1+n))-0.5);
end

% elastic solution passing through same point has to be found
for it2 = rpmel+1:xnum
    maxstrs(it2) = Kmax/(sqrt(2*pi*(lngth(it2,1)-(xm))));
    maxstrn(it2) = maxstrs(it2)/E;
end

%-----------------------------------------------------
%   FINDING DELTA SOLUTION
%-----------------------------------------------------
DK = Kmax-Kmin;

for it3 = 1:xnum
    DS(it3,1) =  2*sy*((DK^2)/(4*(1+n)*pi*(sy^2)*lngth(it3,1)))^pow;
    DEP(it3,1) = 2*ey*((DK^2)/(4*(1+n)*pi*(sy^2)*lngth(it3,1)))^spow;
end
```

```
rpcel = length(find(DS(:,1) >= 2*sy));
if rpcel == 0
    xc = ((DK/sy)^2)*(1/(4*pi))*((1/(1+n))-0.5);
%offset for the elastic solution to be continuous at rc
else
  for it4 = 1:rpcel
    deltastrs(it4) = DS(it4,1);
    deltastrn(it4) = DEP(it4,1);
  end
    xc = ((DK/sy)^2)*(1/(4*pi))*((1/(1+n))-0.5);
end

% elastic solution passing through same point has to be found

for it5 = rpcel+1:xnum
    deltastrs(it5) = DK/(sqrt(2*pi*(lngth(it5,1)-(xc))));
    deltastrn(it5) = deltastrs(it5)/E;
end

%-------------------------------------------------------------
%  MINIMUM STRESS PROFILE and MINIMUM STRAIN PROFILE
%-------------------------------------------------------------
for it6 = 1:xnum
    minstrs(it6) = (maxstrs(it6) - deltastrs(it6));
    minstrn(it6) = (maxstrn(it6) - deltastrn(it6));
end

%+++++++++++++++++++++++++++++++++++++++++++++++++++++++++++++++++++++
```

Subroutine to calculate the Residual SIF associated with the elements using the Weight Function solution

```
%=====================================================================
% This function takes input from the Overload affecting loop to
% calculate the residual stress difference profile, and then goes
% on to calculate the weight function associated with it
%=====================================================================

function [K_res] = calculateKres(a,savedstrs,n,E,Dstar,sy);

numm = length(savedstrs);

for it6 = 1:numm;
LL(it6,1) = a + (Dstar*it6);  % end points of the elements
end

clear it6;
crk_ln = a;

YY(1,1) = savedstrs(1,1);
XX(1,1) = a;
for it = 2:numm+1
   YY(it,1) = savedstrs((it-1),1);
   XX(it,1) = LL(it-1);
end

lnt = length(XX);

for it2 = 2:lnt
% it2 represents the position of the imaginary crack tip
    clear u;
    clear crk;
    clear M1;
    clear M2;
    clear M3;


    crk = XX(it2,1);

    for it3 = 1:it2
        u(it3)=XX(it3,1)/crk;
    end

    clear it3;
    K_temp = 0;
    alpha = (crk/0.5);
```

```
% Calculation of M1,M2 and M3 for the edge crack plate

    M1 = ((-0.029207+alpha*(0.213074+alpha*(-3.029553+alpha*(5.901933+
          alpha*(-2.657820)))))/
         (1+alpha*(-1.259723+alpha*(-0.048475+alpha*(.48125+alpha*(-
          .526796+alpha*(.345012))))))));
    M2 = ( (.451116+alpha*(3.462425+alpha*(-1.078459+alpha*(3.558573+
         alpha*(-7.553533)))))/
         (1+alpha*(-1.496612+alpha*(.764586+alpha*(-.659316+alpha*(
          0.258506+alpha*(.114568))))))) );
    M3 = ( (.427195+alpha*(-3.730114+alpha*(16.276333+alpha*(-
          18.799956+alpha*(14.112118)))))/
         (1+alpha*(-1.129189+alpha*(.033758+alpha*(.192114+alpha*(-
          0.658242+alpha*(.554666))))))) );


    F1 = 0;
    F2 = 0;

    for in=1:(it2-1)
        A= ((YY(in+1,1)-YY(in,1))/(u(in+1)-u(in)));
        B= YY(in,1)-(A*u(in));
        test = A*crk+B;

    F1= (crk/((2*pi*crk).^0.5)).*(A*((-4*(1-u(in+1)).^0.5)-(2*M1*(1-
     u(in+1)))+(4/3*(1-u(in+1)).^1.5)-(4/3*M2*(1-u(in+1)).^1.5)...
     +(M1*(1-u(in+1)).^2)-(M3*(1-u(in+1)).^2)+(4/5*M2*(1-
     u(in+1)).^2.5)+(2/3*M3*(1-u(in+1)).^3))-B*((4*(1-u(in+1)).^0.5)+
     (2*M1*(1-u(in+1)))+(4/3*M2*(1-u(in+1)).^1.5)+(M3*(1-u(in+1)).^2)));

    F2= (crk/((2*pi*crk).^0.5)).*(A*((-4*(1-u(in)).^0.5)-(2*M1*(1-
      u(in)))+(4/3*(1-u(in)).^1.5)-(4/3*M2*(1-u(in)).^1.5)...
      +(M1*(1-u(in)).^2)-(M3*(1-u(in)).^2)+(4/5*M2*(1-
      u(in)).^2.5)+(2/3*M3*(1-u(in)).^3))-B*((4*(1-u(in)).^0.5)...
      +(2*M1*(1-u(in)))+(4/3*M2*(1-u(in)).^1.5)+(M3*(1-u(in)).^2)));

        if ((isnan(F1)) | (isnan(F2)))
            F1 = 0;
            F2 = 0;
        end

        K_temp(in)=F1-F2;

     end

    % total stress intensity factor is
    alt = it2-1;

   K_res(alt,1) = sum(K_temp);
    clear K_temp;
    clear alt;

end

%+++++++++++++++++++++++++++++++++++++++++++++++++++++++++++++++++++++++
```

Subroutine to calculate the SIF solution for the applied loading

```
%=====================================================================
%  RETURNS THE DeltaK VALUES BACK TO THE CALL
%=====================================================================
function[DeltaK,DeltaKt] = getDeltaK(a,al,DS,Dkth,geom)

switch geom
  case 1   % CENTRE CRACK
     F = (1-(0.5*al)+(0.326*(al^2)))/sqrt(1-al);
% F Solution from Norman Dowling
        DeltaKt = F*DS*sqrt(pi*a);

  case 2   % EDGE CRACK
     F = (0.265*(1-al)^4)+((0.857+0.265*al)/(1-al)^1.5);
% F solution from Norman Dowling
        DeltaKt = F*DS*sqrt(pi*a);

  case 3   % DOUBLE EDGE CRACK
     F = 1+(0.122*(cos(pi*al/4))^4))*(sqrt((2/(pi*al))*tan(pi*al/2)));
% F solution from Norman Dowling
        DeltaKt = F*DS*sqrt(pi*a) ;

end
%-------------------------------------------------------------
if DeltaKt <= Dkth
    err = 'Delta K is less than threshold value = ';
    Delt = num2str(DeltaKt/1000000,3);
    errd = strcat(err,Delt);
    errordlg(errd,'Application halted','on');
    uiwait;
end

% If any adjustment or correction is needed it can be applied to this
% extra variable "DeltaK" here which is equal to DeltaKt normally
DeltaK = DeltaKt;


%++++++++++++++++++++++++++++++++++++++++++++++++++++++++++++++++++++
```